Politecnico di Torino

Master of Science in Automotive Engineering
A.a. 2022/2023
Graduation session March 2023

# Development and Implementation of a Model for Predicting NO Oxidation in a Diesel Oxidation Catalyst of a Heavy-Duty Engine

Academic tutors:
prof. Federico MILLO
prof. Luciano ROLANDO
Company tutors:
ing. Chris Jr. BITSIS
ing. Pruthvi BACHU
ing. Prathik MERUVA

Candidate
Niccolò SOTTILE

# Abstract

*English version*

The work presents the development of a model for the prediction of oxidation of NO within a diesel oxidation catalyst used in a heavy-duty engine.

Two different approaches were studied for the development of the model: one based on conversion tables and the other based on global kinetics. The latter was chosen for its higher precision. To reduce the model complexity, the energy balance equation was not considered, and the measurements of three thermocouples were used instead to estimate the temperature distribution inside the catalyst.

Specifically in this work, the Global Kinetic model was developed in parallel on two simulation environments: GT-Power and MATLAB. Using GT-Power, a preliminary model was built in order to calibrate the constants, and then using MATLAB, the final model was built. In this way, the speed of model creation via GT-Power was combined with the flexibility of MATLAB.

The methodology presented in this thesis, which was developed for the Diesel Oxidation Catalyst could be extended to the entire exhaust aftertreatment system.

*Versione Italiana*

Il lavoro presenta lo sviluppo di un modello per la previsione dell'ossidazione degli NO all'interno di un catalizzatore di ossidazione diesel utilizzato in applicazioni pesanti.

Per lo sviluppo del modello sono stati studiati due approcci diversi: uno basato su tabelle di conversione e l'altro sulla cinetica globale. Quest'ultimo è stato scelto per la sua maggiore precisione. Per ridurre la complessità del modello, non è stata considerata l'equazione del bilancio energetico e sono state utilizzate le misure di tre termocoppie per stimare la distribuzione della temperatura all'interno del catalizzatore.

In particolare, in questo lavoro il modello basato sulla cinetica globale è stato sviluppato in parallelo su due ambienti di simulazione: GT-Power e MATLAB. Utilizzando GT-Power, è stato costruito un modello preliminare per calibrare le costanti e, successivamente, utilizzando MATLAB, è stato costruito il modello finale. In questo modo, la velocità di creazione del modello tramite GT-Power è stata combinata con la flessibilità di MATLAB.

La metodologia presentata in questa tesi, sviluppata per il catalizzatore di ossidazione diesel, può essere inserita in un modello completo di un sistema di post-trattamento dei gas di scarico.

# Index

# List of figures

# 1. Introduction

Global warming and air pollution are a critical problem affecting the planet on a global scale. Mobility is a basic necessity to enable human activities, but it can also cause a number of negative environmental effects, including air pollution, resource consumption and the emission of greenhouse gases. Combining the need for mobility with the reduction of pollutant emissions has led to the development of stricter emission regulations, especially for a sector as fundamental to our daily lives as the transport of goods and people by road. It is in this context that the work in this thesis is set. Road transport relies almost exclusively on diesel-powered engines, and the catalytic converter is a key component of the exhaust after-treatment system to reduce harmful emissions such as nitrogen oxides (NOx), particulate matter (PM) and hydrocarbons (HC). Over the years, various catalytic converter technologies have been developed and applied to meet increasingly stringent emission standards. This work aims to provide an in-depth look at heavy-duty Diesel Oxidation Catalysts (DOC).

The need for an increasingly efficient and synergetic exhaust after-treatment system requires the use of DOC not only as a means of oxidising THC and CO emissions, but also as a converter of NO into $NO_2$ in order to improve SCR operation. Moreover, due to the exothermic nature of oxidation-reduction reactions, we have an increase in exhaust flow temperature that favours the oxidation of soot. Models capable of predicting the complex mechanisms governing diesel engine catalysts play a central role in both component design and calibration. These means can greatly reduce design time, allowing the layout to be tested virtually and verify that emission targets are met [1].

## 1.1. Diesel oxidation catalyst working principles

Diesel Oxidation Catalysts belong to the category of through-wall catalysts, in fact their structure consists of a parallel channel running from the inlet to the outlet of the brick. The external shell is usually made of thin layer of steel while the internal one can be made of ceramic or metal, this part is called *substrate*. The *substrate* is covered by a porous material called *washcoat,* where the precious metals are dispersed. The reactants, carried by the exhaust gases, diffuse towards the channel walls, where they further diffuse through the pores of the washcoat to the active site. At the active site, they can react, producing products that will retrace the reverse trajectory and eventually be released into the exhaust gas. Figure 1 illustrate the process.

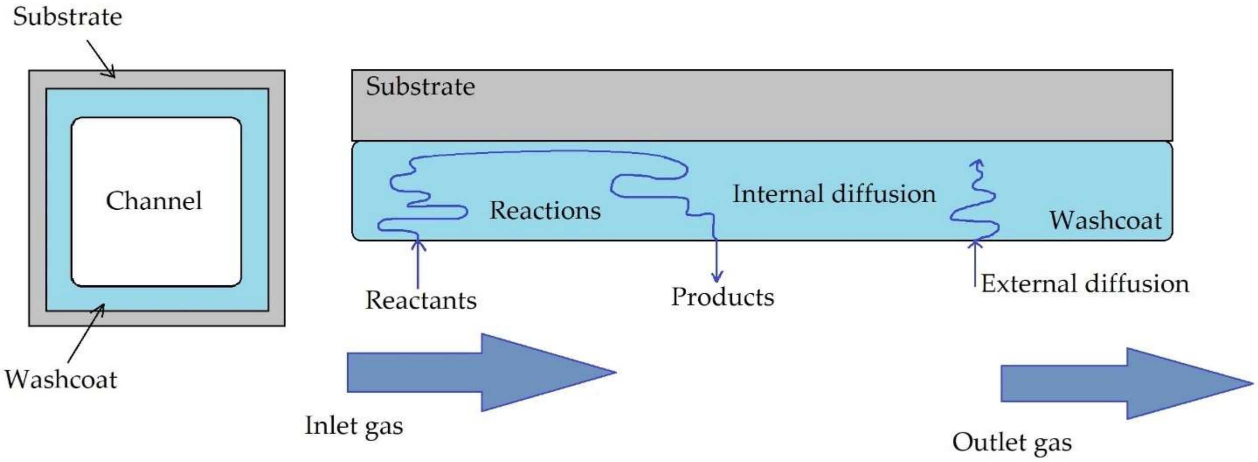

*Figure 1 Structure and process occurring inside a monolith channel*

As already mentioned, the main purpose of the DOC is the oxidation of CO and THC, the related chemical reactions are:

$$CO + \frac{1}{2}O_2 = CO_2$$

$$C_nH_m + \left(n + \frac{m}{4}\right)O_2 = nCO_2 + \frac{m}{2}H_2O$$

The unburned hydrocarbons (THC) are usually categorised in slow reactive and fast oxidizing species. Slow-oxidising HCs are usually represented with a short-chain molecule such as propane ($C_3H_6$) and decane ($C_{10}H_{22}$) is used to synthesise slower-oxidising HCs.

Oxidation of NO are strongly inhibited by the reactions of THC and CO, for this reason the most of NO is converted in $NO_2$ when THC and CO reaches the light-off temperature.

$$NO + \frac{1}{2}O_2 = NO_2$$

The reactions mentioned above are only some of those that occur within the OCD but, considering the needs of this work, are sufficient to continue the discussion.

# 2. Literature review on modelling techniques of Diesel Oxidation Catalyst

The first task of the thesis is to analyse the exiting models suitable for DOC simulation. A review of the literature has resulted in two suitable models that can describe the phenomena:

- Global kinetic model, based on publication [4]
- Look-up-table based model, based on publication [5]

To better understand the difference between the two aforementioned models, it is useful to consider the following classification:

- White box models are detailed 2D or 3D models. The phenomena studied are analysed taking into account the inhomogeneity of both the thermal and fluid fields using Computational Fluid Dynamic (CFD). The reactions are modelled taking into account the microkinetics of the studied phenomena, providing a high level of detail. Due to the complexity of the differential equations needed to solve the problem, the computational effort is high and therefore this type of modelling is used for design purposes or off-line simulation.
- Grey box models are 1D or 1+1D models, where 1+1D indicates that washcoat diffusion is considered in addition to the main dimension of the reactor. The chemistry of the process under investigation is considered by a global reaction, and several inhibition functions are used to account for the interaction between different species. The model required a medium computational effort, but is faster than the white box model and, if properly calibrated, can predict most of the conditions to which the reactor is subjected with a good degree of accuracy. This type of model is widely used to simulate the aftertreatment system of passenger cars and heavy to light duty vehicles.
- Black box models are typically 0D models. The phenomenon of interest is described by a set of reference matrices or tables that correlate the conditions of the reactor (e.g. temperature, spatial velocity, concentration, etc.) with the output being studied. It is a low computational cost model and the reliability of the results depends heavily on the data set used to construct the matrices or tables. A good mix of reactor input conditions is required to correctly predict the required outputs of a typical application.

## 2.1. Global kinetic model description

The global kinetic model is a type of model widely used to describe different types of catalytic converters in the automotive field. It is called "global" because it uses a simplified representation of the catalyst, in which it is divided into sections representing a portion of the catalyst bed. Inside the catalyst channel no inhomogeneities are considered, the evolution of the composition is calculated only along the axial dimension of the catalyst, for this reason this model is often called 1D. In some cases, the thickness of the washcoat can be taken into account and the model assumes the nomenclature of 1D+1, which means that diffusion within the washcoat is taken into account. The global kinetic model for each section considers the reaction governed by a single 'global' mechanism, which takes into account all the relevant chemical processes occurring within the catalyst. The global mechanism is typically represented as a set of differential equations describing how the concentrations of the different chemical species change over time. Different species tend to interact with each other by inhibiting or promoting certain reactions, and these phenomena are accounted for by inhibition functions.

This modelling technique requires careful calibration of reaction parameters on a large representative dataset to capture the interaction of various species at different temperatures and space-velocities. Ideally, calibration should be performed on a synthetic gas bench (SGB), with a set of constant temperature, space-velocity and well-defined input concentration. Choosing a representative test matrix, the calibration brings rate parameters capable to predict several scenarios with good precision.

### 2.1.1. Global kinetic model proposal

The authors [1] try to solve the problem of predicting the species conversion efficiency commonly found in a Diesel Oxidation Catalyst. The equations used to describe the evolution of the species concentration are a system of differential algebraic equation or DAEs shown in Eq. *1*. The system is solved for each timestep/inlet condition in order to evaluate the concentration evolution along the catalyst length. The system does not include the energy balance equation, so the temperature is set by means of thermocouple measurements and interpolating the value between them. In this work the equations have been slightly modified to use as input the mass fraction:

$$\begin{cases} \dfrac{dx_{g,i}}{dz} = -\dfrac{A}{\dot{m}} k_{m,i} S\left(x_{g,i} - x_{s,i}\right) \\ 0 = \dfrac{A}{\dot{m}}\left( k_{m,i} S\left(x_{g,i} - x_{s,i}\right) + M_i \displaystyle\sum_{j=1}^{reactions} a_j s_{ij} r_j \right) \end{cases} \qquad \text{Eq. 1}$$

To take into account the migration that species undertake from the main flux inside the channels brick to the washcoat walls, the authors proposed a simplified approach based on the asymptotic Sherwood number and the binary diffusivity of each species. This approach does not consider mass transfer from the surface of the washcoat to its inner zone, where the active sites are located. The proposed model considers the mass fraction of the species *i* in the bulk gas $x_{g,i}$, the fraction that migrates to the washcoat and settles on its surface is called $x_{s,i}$. The species can only react catalytically if they are on the surface of the washcoat. The mass transfer coefficient is:

$$k_{m,i} = \frac{Sh}{D_h} \rho_{gas} D_{i,m} \qquad \text{Eq. 2}$$

Also Eq. 2Errore. L'origine riferimento non è stata trovata. has been modified to reflect the different unit of measurement, from mole fraction to mass fraction. It is assumed that each species of interest is immersed in a mixture of nitrogen, therefore the binary diffusion coefficient is calculated using the information for the species and nitrogen. The mathematical formulation is written according to the Fuller correlation [6].

$$D_{i,m} = \frac{10^{-3}\, T^{1.75} \left(\dfrac{1}{M_i} + \dfrac{1}{M_{N_2}}\right)^{\frac{1}{2}}}{p_{avg} \left(\Sigma_i^{\frac{1}{3}} + \Sigma_{N_2}^{\frac{1}{3}}\right)^2} \qquad \text{Eq. 3}$$

The authors start by writing an initial rate of reaction then they test different variations in order to find the best formulation that gives the least difference between SGB measures and simulated values. The final formulation is:

$$r_i = \frac{k_i c_{s,i} c_{s,O_2}}{G} \qquad i = THC, CO, H_2 \qquad \text{Eq. 4}$$

$$r_{NO} = \frac{k_{NO}}{G_{NO}} \left( c_{s,NO} \sqrt{c_{s,O_2}} - \frac{c_{s,NO_2} \sqrt{c_r}}{K_{eq}} \right) \qquad \text{Eq. 5}$$

The rate of reaction has a different formulation for NO oxidation to consider its tendency of being inhibited by reducing species (CO, THC, $H_2$) present in the stream. $c_r$ is the total concentration in mol·m$^3$ at reference pressure of 1 atm. $K_{eq}$ is the equilibrium constant based on the Gibbs free energy of the NO oxidation reaction:

$$K_{eq} = 1.5e - 4\, e^{\frac{6864}{T}} \qquad \text{Eq. 6}$$

$k_i$, $k_{NO}, G_{NO}$ and $G$ are constants written in Arrhenius form, the first two are rate constants the last two are inhibition function:

$$k_i = A_i e^{\frac{E_i}{RT}} \qquad i = NO, CO, THC, H_2 \ \text{Eq. 7}$$

$$\begin{gathered} G = \left(1 + K_{CO} c_{s,CO}\right)^2 (1 + K_{NO} c_{s,NO}) \\ G_{NO} = \left(1 + K_{DF} c_{s,DF}\right)^2 \left(1 + K_{NO} c_{s,NO}\right) \end{gathered} \qquad \text{Eq. 8}$$

Where:

$$K_i = A_{ai} e^{-\frac{E_a}{RT}} \qquad i = NO, CO, THC, H_2 \ \text{Eq. 9}$$

Eq. 8 and $i = NO, CO, THC, H_2$ Eq. 9 contain the calibration parameters to be optimized to find the best value fitting the measured data. For a first calibration stage the constants that most influence the results are the pre-exponent multiplier $A_i$ and the activation energy $E_i$, then more refined investigations can include also $A_{ai}$ and $E_{ai}$ namely the inhibition constants terms.

The authors calibrate the full model presented using a representative test matrix, an extract of their results is shown in the Table *1*, this will be the starting point for the model that will be built into this work.

Table 1 - Rate constants from Sampara and Bisset publication DF stands for Diesel Fuel $C_{14.6}H_{24.8}$

| Rate constants | Value |
|---|---|
| $A_{CO}$ | $1.183 \cdot 10^{12}$ |
| $E_{CO}$ | $8.133 \cdot 10^{4}$ |
| $A_{NO}$ | $1.327 \cdot 10^{3}$ |
| $E_{NO}$ | $6.721 \cdot 10^{3}$ |
| $A_{DF}$ | $2.918 \cdot 10^{5}$ |
| $E_{DF}$ | $2.420 \cdot 10^{4}$ |
| $Aa_{CO}$ | $2.480 \cdot 10^{2}$ |
| $Ea_{CO}$ | $5.113 \cdot 10^{3}$ |
| $Aa_{NO}$ | $2.420 \cdot 10^{-1}$ |
| $Ea_{NO}$ | $-4.042 \cdot 10^{4}$ |
| $Aa_{DF}$ | $2.020 \cdot 10^{-17}$ |
| $Ea_{DF}$ | $-2.347 \cdot 10^{5}$ |

## 2.2. Map-based model proposal

The model proposed in publication [5] can be categorized as a block box model and can be divided in two main parts: the chemical one, where the effective conversion is evaluated and the thermal model, which estimate the temperature distribution along the catalyst bed. The conversion of the species is based on measured conversion map functions of catalyst bed temperature and space-velocity. As previously illustrated, the advantage of such map-based approach is that it eliminates of all the complex mathematical structure required to describe the phenomena being studied, for example it is not needed to solve differential equations that lead to a reduction in computational time. The maps can be generated both via data from Synthetic Gas Bench (SGB) or engine test bench but good mix of scenario must be included to predict with sufficient accuracy the emission from an articulated cycle like a commonly used test procedure (FTP, WLTP etc..). As for the thermal model, the authors proposed a quasi-steady approach based on the assumption that the evolution of flow rate and temperature is slower compared to the residence time range. For each time step, the catalyst bed is divided into sub-elements and for each one the heat transfer due to reactions, convection and conduction is calculated, the total heat transfer is used to evaluate the temperature evolution over time.

## 2.3. Model comparison: pros/cons

Maps-based models have the advantage of being relatively easy to implement since they rely on a set of measured conversion map functions of the catalyst bed temperature and space-velocity. This approach eliminates the need to solve complex differential equations, leading to a reduction in computational time. These maps can be generated using data from either a synthetic gas bench or engine test bench, with a good mix of scenarios necessary to predict pollutant emissions accurately over an articulated cycle like a test procedure. However, a disadvantage of maps-based models is that they require a wide range of tests (temperature and space velocity) to be able to predict complex cycles.

In contrast, a global kinetic model is more robust because the reactions are expressed by a mathematical formulation that can potentially include scenarios not directly included in the calibration matrix. This approach requires a time-consuming optimization due to the high number of parameters to calibrate, and for this reason, it cannot be executed "by hands", and it is necessary to use a searching algorithm capable of finding the set of parameters that minimize the difference between measured and simulated results. However, once developed, global kinetic models can accurately predict pollutant emissions over a wide range of operating conditions.

In summary, while maps-based models may be more straightforward to implement and require less computational time, they may not provide the adaptability needed to predict the variety of conditions a driving cycle may present compared to global kinetic models. On the other hand, while global kinetic models may require more computational resources and extensive calibration, they can provide accurate predictions over a wide range of operating conditions.

# 3. Modelling approach of Diesel Oxidation Catalyst

Both the map-based and global kinetic models were developed to assess the predictive capability of the modelling techniques. The map-based model was developed in a MATLAB environment, while the global kinetic model was based on GT-Power software for calibration purposes, while MATLAB was used to run the full model simulation.

## 3.1. Experimental data

The calibration procedure and the model development cannot be performed without a robust set of data. Ideally the calibration procedure should be based on SGB data, but unfortunately there was no possibility to have access to these instrumentations. The data pool available was acquired at the engine test bench with full Aftertreatment system at the Southwest Research Institute (SwRI) facility. The engine analysed is a Cummins X15, the engine specifications are reported in Table 2.

Table 2 Engine specification from [2]

| Parameter | Value |
|---|---|
| Configuration | In-line 6 cylinder |
| Bore x Displacement | 137 mm x 169 mm |
| Displacement | 15 l |
| Rated Power | 373 kW @ 1800 rpm |
| Peak Torque | 2500 Nm @ 1000 rpm |

The objective is to characterize the diesel oxidation catalyst (DOC), so data are acquired by taking flow conditions at the inlet and outlet of the catalyst. The inlet species composition is the same as the engine outlet since the measurements were collected with the urea injector off. Catalytic bed temperature measurements are taken with the help of 3 thermocouples, installed at the start, middle and end of the catalyst. The composition of the output species is acquired by installing instruments downstream of the catalyst outlet. Inlet and outlet exhaust flow temperature is taken using thermocouples.

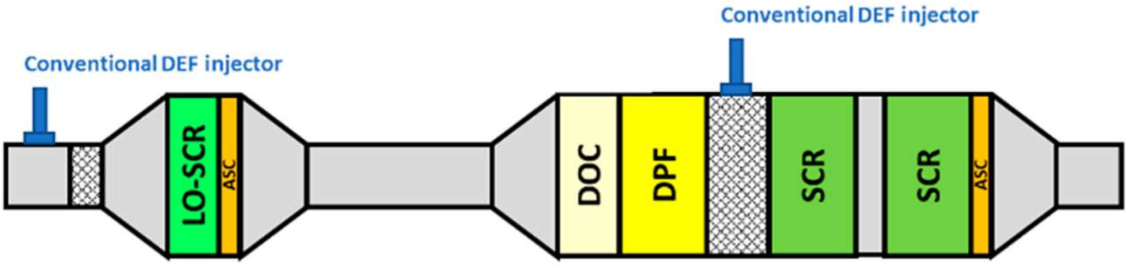

*Figure 2 Aftertreatment system layout [3]*

It is possible to estimate the temperature distribution along the catalytic bed through the data collected by 3 thermocouples. The gas composition includes the mole fractions of CO and NOx expressed in ppm and the mole fraction of oxygen, expressed as a percentage. At this point a distinction must be made between two types of tests carried out: the calibration test and the test cycles required to validate the model.

- Steady-state tests are carried out under stationary engine conditions by averaging the data collected. The results are 49 measurements across all the engine map, each point can be considered representative of the engine point. This dataset does not have information on individual species of NOx, the value of NO and NO2 is estimated by calculating the NO2/NOx before the light-off temperature, namely below 250°C.
- Test cycles are representative of a mission in which the engine can undergo during its use. The data are highly dynamic in terms of both load and temperature, for this reason they can be used to validate the calibrated model. An example could be the Federal Test Procedure (FTP). The measures also contain information on each NOx separately, in fact information about NO, NO2 and N2O are included in the spreadsheet.

Table 3 Diesel Oxidation catalyst specification [2]

| DOC characteristic | Value |
|---|---|
| Diameter x length | 33 cm x 13 cm |
| CPSI | 400 |
| Volume | 11 l |
| Active site density | 9.12 mole-site/m$^3$ |

The steady-state data used for the calibration of both the map-based model and the global kinetic model are reported in Table *4*. The average value of $NO_2/NO_x$ below 250°C for the test matrix is 0.363. $T_1$, $T_2$ and $T_3$ are respectively the inlet, mid and outlet temperature of the catalyst brick.

Table 4 Steady-state test matrix

| Test n. | Space-velocity | $T_1$ | $T_2$ | $T_3$ | $y_{NOx}$ in | $y_{NO}$ out | $y_{NO2}$ out |
|---|---|---|---|---|---|---|---|
| - | 1/h | °C | °C | °C | ppm | ppm | ppm |
| 1 | 3.116E+04 | 344.52 | 345.21 | 345.41 | 534.562 | 158.06 | 340.2 |
| 2 | 3.385E+04 | 352.38 | 353.09 | 353.28 | 458.969 | 143 | 283.97 |
| 3 | 2.558E+04 | 284.96 | 285.96 | 286.01 | 358.682 | 94.84 | 241.27 |
| 4 | 2.002E+04 | 229.69 | 230.33 | 230.5 | 105.005 | 32.2 | 65.24 |
| 5 | 1.640E+04 | 205.64 | 206.31 | 206.46 | 80.827 | 32.41 | 43.56 |
| 6 | 2.146E+04 | 228.92 | 229.38 | 229.44 | 111.56 | 39.08 | 63.71 |
| 7 | 3.605E+04 | 233.72 | 234.25 | 234.41 | 345.632 | 181.23 | 141.68 |
| 8 | 3.634E+04 | 227.02 | 227.59 | 227.81 | 304.18 | 166.29 | 119.62 |
| 9 | 3.636E+04 | 226.45 | 227 | 227.17 | 305.43 | 168.5 | 118.18 |
| 10 | 4.165E+04 | 281.4 | 282.01 | 282.14 | 563.661 | 232.26 | 283.77 |
| 11 | 4.204E+04 | 234.54 | 235.09 | 235.25 | 318.158 | 167.52 | 128.89 |
| 12 | 3.465E+04 | 337.82 | 338.58 | 338.68 | 450.398 | 142.65 | 266.81 |
| 13 | 4.250E+04 | 382.54 | 383.18 | 383.32 | 532.513 | 239.35 | 230.08 |
| 14 | 4.860E+04 | 407.27 | 408.03 | 408.11 | 550.922 | 303.3 | 182.16 |
| 15 | 6.536E+04 | 438.24 | 439.17 | 439.23 | 682.083 | 438.22 | 165.07 |
| 16 | 1.075E+05 | 441.89 | 442.79 | 442.85 | 710.327 | 452.59 | 186.16 |
| 17 | 8.395E+04 | 384.55 | 385.49 | 385.63 | 799.025 | 386.68 | 333.98 |
| 18 | 9.600E+04 | 363.74 | 364.67 | 364.85 | 739.325 | 340.45 | 332.78 |
| 19 | 9.847E+04 | 368.75 | 369.59 | 369.71 | 637.733 | 291.83 | 285.62 |
| 20 | 1.111E+05 | 432.84 | 433.75 | 433.84 | 601.754 | 364.11 | 178.35 |
| 21 | 7.700E+04 | 357.26 | 358.17 | 358.35 | 817.276 | 358.78 | 373.19 |
| 22 | 5.841E+04 | 359.66 | 360.59 | 360.84 | 791.32 | 325.5 | 382.11 |
| 23 | 6.150E+04 | 321.17 | 321.94 | 322.13 | 622.393 | 249.32 | 313.74 |
| 24 | 7.739E+04 | 309.58 | 310.34 | 310.5 | 598.886 | 272.2 | 278.07 |
| 25 | 9.428E+04 | 307.24 | 307.97 | 308.13 | 514.853 | 247.14 | 222.97 |
| 26 | 4.716E+04 | 322.81 | 323.63 | 323.82 | 671.601 | 244.25 | 360.37 |
| 27 | 7.315E+04 | 280.03 | 280.76 | 280.92 | 511.329 | 250.27 | 223.46 |
| 28 | 7.861E+04 | 255.64 | 256.3 | 256.44 | 367.748 | 200.12 | 147.12 |
| 29 | 5.408E+04 | 286.18 | 286.81 | 286.92 | 536.254 | 231.92 | 259.84 |
| 30 | 7.808E+04 | 331.74 | 332.55 | 332.74 | 664.759 | 282.16 | 339.28 |

| | | | | | | | |
|---|---|---|---|---|---|---|---|
| 31 | 9.771E+04 | 386.07 | 386.97 | 387.14 | 746.444 | 358.95 | 313.47 |
| 32 | 1.069E+05 | 421.48 | 422.4 | 422.54 | 709.552 | 400.67 | 237 |
| 33 | 5.811E+04 | 405.4 | 406.33 | 406.53 | 734.238 | 381.55 | 265.62 |
| 34 | 8.709E+04 | 317.16 | 318.02 | 318.18 | 603.88 | 289.11 | 262.36 |
| 35 | 5.252E+04 | 350.06 | 350.95 | 351.2 | 1215.749 | 475.18 | 636.52 |
| 36 | 5.409E+04 | 260.54 | 261.23 | 261.37 | 353.187 | 161.07 | 167.16 |
| 37 | 3.348E+04 | 270.71 | 271.41 | 271.6 | 630.87 | 265.07 | 313.4 |
| 38 | 5.435E+04 | 230.67 | 231.19 | 231.37 | 278.951 | 152.59 | 109.44 |
| 39 | 5.309E+04 | 213.91 | 214.43 | 214.59 | 270.815 | 169.52 | 87.22 |
| 40 | 3.966E+04 | 214.06 | 214.59 | 214.76 | 255.22 | 146.84 | 93.66 |
| 41 | 5.490E+04 | 155.86 | 156.3 | 156.43 | 141.501 | 124.72 | 18.72 |
| 42 | 4.051E+04 | 144.15 | 144.54 | 144.65 | 156.133 | 144.75 | 13.83 |
| 43 | 3.970E+04 | 129.92 | 130.27 | 130.4 | 143.548 | 144.03 | 3.12 |
| 44 | 3.321E+04 | 289.25 | 289.87 | 289.95 | 402.13 | 114.95 | 259.08 |
| 45 | 1.263E+04 | 181.8 | 182.51 | 182.8 | 85.1 | 41.24 | 39.02 |
| 46 | 1.802E+04 | 227.59 | 228.31 | 228.39 | 347.936 | 134.43 | 192.38 |
| 47 | 6.522E+04 | 215.04 | 215.57 | 215.74 | 329.726 | 218.57 | 100.17 |
| 48 | 6.468E+04 | 169.98 | 170.4 | 170.54 | 128.107 | 110.51 | 19.31 |
| 49 | 6.332E+04 | 153.68 | 154.08 | 154.22 | 126.516 | 118.05 | 11.83 |

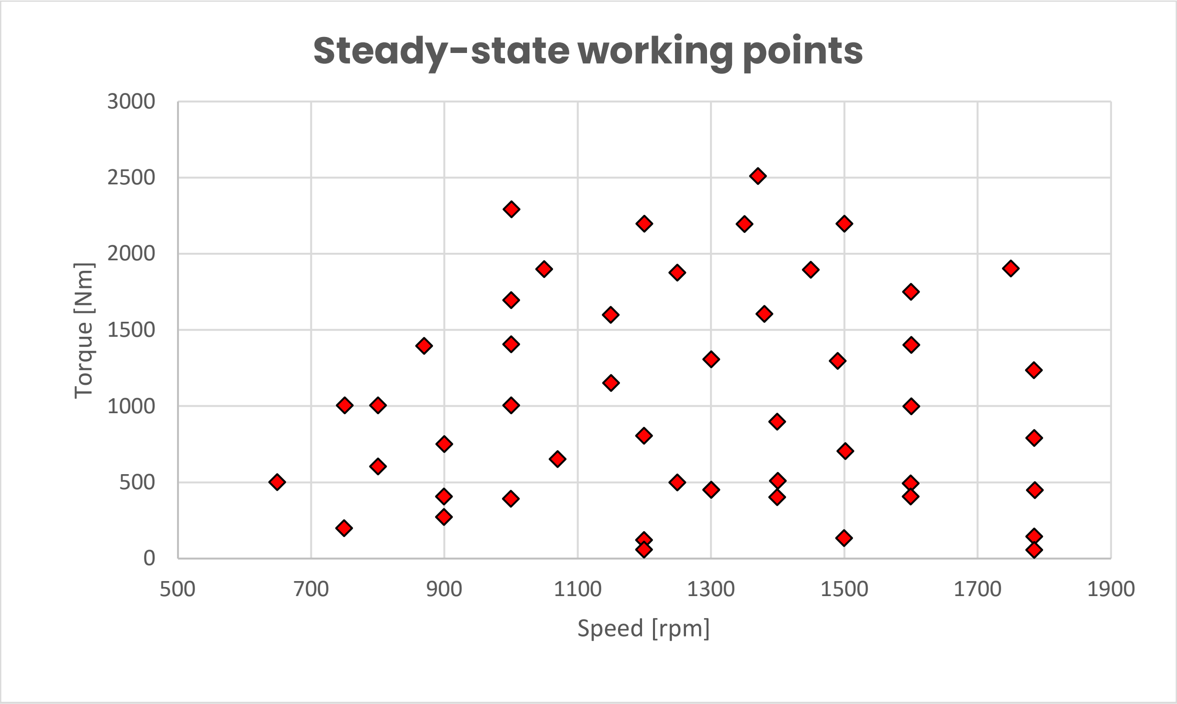

*Figure 3 Working points where the steady-state data were acquired*

The model was validated on a driven cycle provided by SwRI. The data were collected in a similar way to the steady-state data. Most of the cycles are United States Federal Test Procedure (FPT), but some of them are particular tests useful to test aftertreatment system. The available tests are:

- Cold-FTP, 2 tests available. Standard United States homologation cycle. The test requires the catalyst to start from an ambient temperature of approximately 25°C
- Hot-FTP, standard United States homologation cycle.
- Low load cycle or LLC, cycle designed to challenge the engine at low load, it is useful to assess the emissions.
- Beverage data, fast transient cycle, the average temperature is 150°C.
- StayHot, test performed to evaluate the thermal properties of the aftertreatment system.

## 3.2. Map-based model

The core of the model is the map, which is used to calculate the conversion efficiency for each input condition. To achieve a robust model, the data used to build the maps must ideally cover a wide range of engine operating points. Maps built from steady-state conditions are repeatable and constant, even if they are less representative of a real application. On the other hand, if the model is based on dynamic cycles, the map will contain a lot of signal noise, which will have a negative effect on the prediction. However, to reduce the signal noise, the transient input data should not include the driving cycle, but rather a specific transient profile designed to highlight characteristic phenomena such as light-off temperature. As Aristotle, a Greek philosopher, says "*in medio stat virtus*", so the better performance is obtained with a mix of steady-state and transient tests to capture the catalyst behaviour under different conditions. The coordinates commonly used to define the catalyst operating point are the space-velocity and the bed temperature, so these are used as input to enter the conversion map.

The $NO_2/NO_x$ map was built generating a grid of points with bed temperature as the abscissa and space-velocity as the ordinate, then the measured $NO_2/NO_x$ was interpolated for each point of the grid. The MATLAB function *meshgrid* is used to create a 2D grid of temperature and space velocity values, the mesh size of the grid is an important parameter, finer mesh generates more noise on the map while larger meshes do not capture the behaviour of the catalyst. This grid is then used to interpolate the $NO_2/NO_x$ data using the MATLAB function *griddata*, which produces a 2D matrix representing the NOx conversion map.

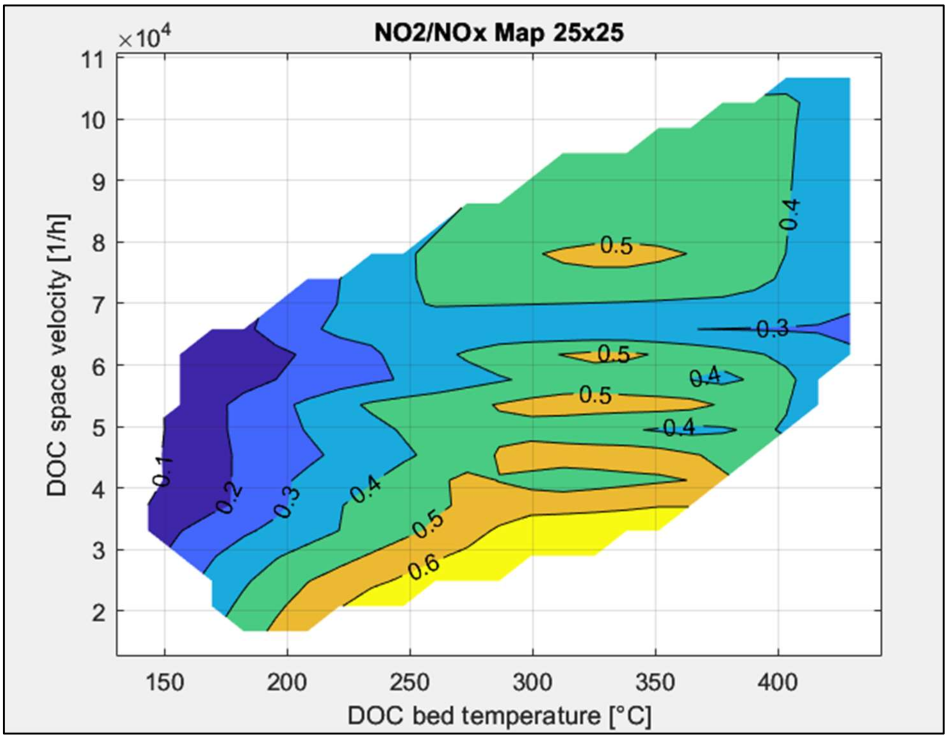

*Figure 4 NO2/NOx map generated with a 25x25 grid of points*

From Figure 4 we can see that the code is not able to interpolate the measured value for conditions not included in the input data. In fact, the map has a well-defined contour over which there is no values, as we will see later, this is represent a limit to predict the conversion for a wide range of condition like a driving cycle.

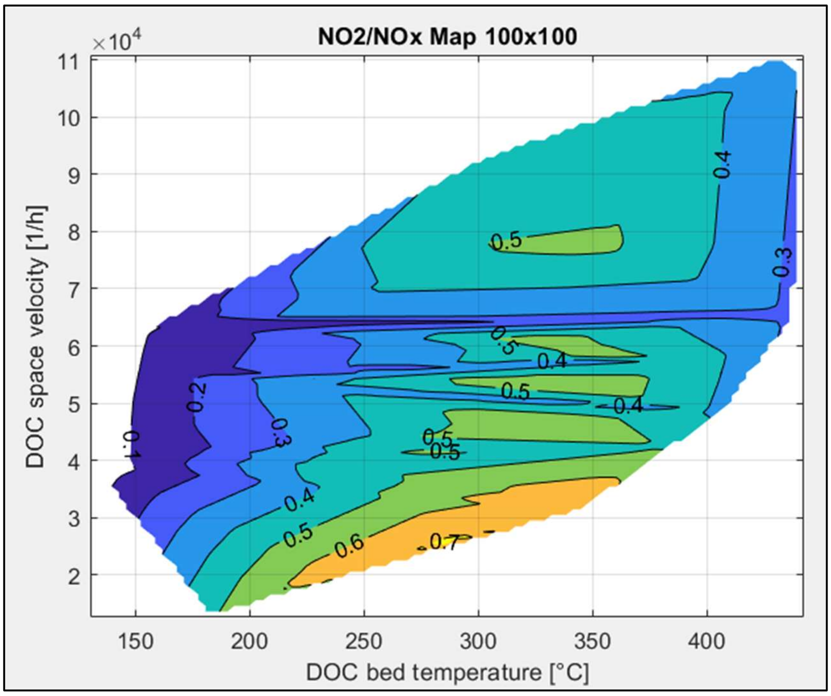

*Figure 5 NO2/NOx map generated with a 100x100 grid of points*

The difference between Figure 4 and Figure 5 is the mesh size. The first case has larger mesh translating in a less noisy contour for the same number of zones compared with the latter map.

### 3.3. Global kinetic model calibration procedure

Calibration of a global kinetic model means searching a set of reaction rate constants and inhibition terms that provide the best fit between the model output and the measurements. The simulation output should adequately predict the conversion rate of the species of interest over the temperature and space-velocity range of the application. The procedure strongly depends on the data available and on the nature of the mechanism to be analysed. As already discussed, the most desirable type of data is the SGB because it allows to calibrate the rate constant of the species separately isolating the complex interaction between species. In addition, it provides precise measures that eliminate errors and inconsistencies. Engine-out data should be performed at fixed speed and load to obtain stable measures for a first optimisation procedure. A further optimisation, selecting a representative driving cycle, can then be used to improve the model performance also in the dynamic state. Active site density is a factor used to quantitatively estimate the sites at which the catalyst species is actually active and able to react with reactants. It is usually provided by the manufacturer or can be assessed experimentally by chemisorption of CO. In this paper the CO chemisorption procedure is not discussed as the active site density was provided by SwRI.

Calibration can be carried out by iteratively changing the rate constants manually, running the model and comparing the simulated results with the measured ones. This procedure is useful to gain confidence in the effects of the different rate constants, but this technique is only feasible with SGB data and only to define an initial value. The minimisation of the error over the whole engine map is possible by using an automated algorithm capable of handling several rate constants by combining them according to a mathematical approach capable of finding the minimum. The definition of a suitable objective function, capable of guiding the optimisation solver in the right direction, plays a fundamental role in the optimisation process. There are several ways to define the objective function, more or less articulated, but the common feature among the formulations must be that if the model produces the same results of the actions, the objective function is zero. In this way, the objective of the solver is to minimise the value of the objective function across all points of interest.

Here there are two simple objective function proposal, following [7]:

$$obj_i = \left|x_{i,predicted} - x_{i,simulated}\right| \quad \text{Eq. 10}$$

$$obj_i = \left(x_{i,predicted} - x_{i,simulated}\right)^2 \quad \text{Eq. 11}$$

The proposal can be used for SGB and engine-out calibration, also for steady-state data or transient operation. Eq. 10 and Eq. 11 are referred to each species considered, in steady operation each species objective function should be sum and optionally the square root of the summatory can be done.

### 3.3.1. NO input data consistency check

The DOC performance strongly depends on NO oxidation moreover, the focus of this work is the prediction of NO and $NO_2$ for this reason a dedicated calibration is needed in order to obtain the requested performance. After the collection of the data, it is useful to plot the $NO_2/NO_x$ under steady condition against temperature, this gives a hint about the consistency of the data.

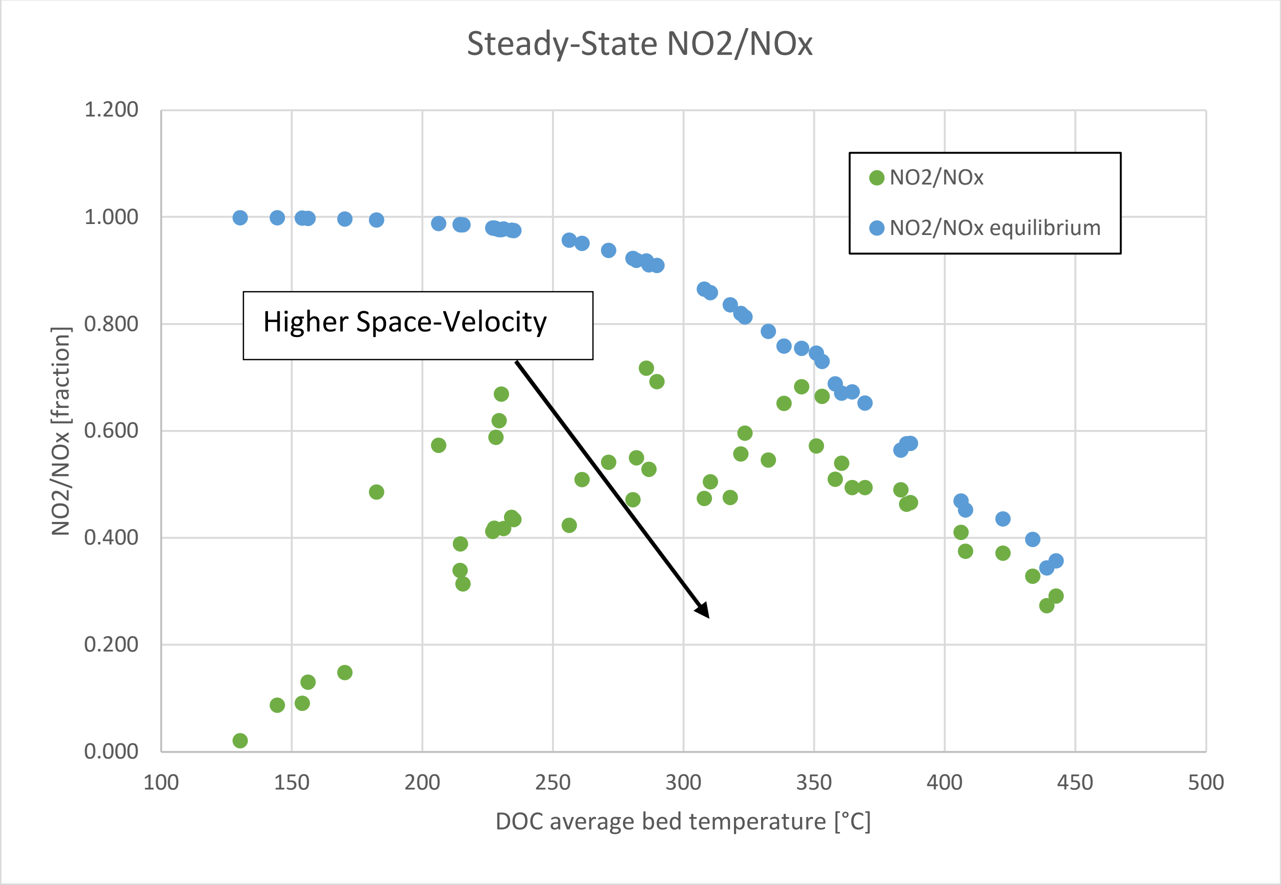

*Figure 6 NO2/NOx measured vs average bed temperature with NO oxidation equilibrium curve*

The Figure 6 shows the equilibrium curve that represents the limit of the chemical equilibrium with the measured point of the steady-state tests. The curve is obtained following the expression:

$$\left(\frac{NO_2}{NO_x}\right)_{eq} = \frac{y_{O_2}^{0.5}\, K_{eq}}{1 + y_{O_2}^{0.5}\, K_{eq}} \qquad \text{Eq. 12}$$

The Eq. *12* assumes that the NO oxidation is written as NO + 0.5 $O_2$ = $NO_2$, where $K_{eq}$ is the equilibrium constant and it is unit-less. It was already presented in Eq. 6.

This graph is only meaningful if the tests are carried out in a steady state, in our case the temperature between the first and the last section of the catalytic bed there is a gap of 2-5°C, low enough to be considered steady. We can see that the catalyst reaches reaction equilibrium at 350°C, but remains below the equilibrium points. At lower temperatures, the measured points are arranged in a bell shape because the lack of time does not allow the complete consumption of the reactant. There are some measured points farther away from the main group, this can be explained considering that the space velocity is not constant across the measurements, so the points with similar temperature but higher NO2/NOx will probably have higher space velocity that leads to more time for the reactants to be converted into products.

### 3.3.2. Rate constants optimization using Log-space

Usually, to obtain the best performance from the optimizer the rate constant should be transformed to perform the search in the Logarithmic space. This approach allows to optimize the parameters in a wider field. In this case the parameter to optimize is re-written in $10^{[power]}$, inside the square bracket there is the optimization variable. To further separate the effect of the calibration parameters this technique should be applied to few/only one parameters per species at time.

### 3.3.3. Rate constants and inhibition terms optimization

The optimization is a time-consuming process, so setting up optimisation intelligently can lead to better results in less time. To isolate the effects of different parameters, run the optimisation with fewer parameters and add them gradually to improve the overall quality of the work. Initially, the optimisation should be performed by including only the rate constants without the inhibition function parameters ($Aa_i$ and $Ea_i$). The inhibition functions are then added to the formulation to account for the mutual effects that different species have when reacting in the same volume. For example, as reported in Figure 6, at low temperatures the NO oxidation does not take place because more reactive species compete for oxygen and the available catalytic site slowing down the NO oxidation. To express this phenomenon mathematically, we are helped by the inhibition functions, as expressed in chapter 2.1.1:

$$G_i = 1 + Aa_i\, e^{-\frac{Ea_i}{RT}} c_{s,i} \qquad \text{Eq. 13}$$

Inhibition function $G_i$ can be squared and functions of different species can be combined together as shown in Eq. 14:

$$G = \left(1 + Aa_{CO}\, e^{-\frac{Ea_{CO}}{RT}} c_{s,CO}\right)^2 (1 + Aa_{NO}\, e^{-\frac{Ea_{NO}}{RT}} c_{s,NO}) \qquad \text{Eq. 14}$$

If the optimization run is not well set, the solver will vary the parameters $Aa_i$ and $Ea_i$ without significantly changing the results thus increasing the simulation time unreasonably. The inhibition function is an exponential term added to 1, thus to have an effect on the output concentration the exponential term should assume value between 0.1 and 10 at a consistent concentration level. Moreover, inhibition function depends also on temperature therefore great care must be taken when the inhibition function parameters are optimized, perhaps including specific optimizations at low and high temperatures, monitoring the value that the inhibition function takes on.

# 4. Diesel Oxidation Catalyst modelling

Considering the versatility requested to predicts the emission over a variety of cycle, the modelling technique chosen is the global kinetic that can offer, after an optimization campaign, the trade-off between computational effort and results reliability. MATLAB is the environment used to build the model while the parameters optimization is performed on GT-Power due its ease of use. Although more attention will be given to the global kinetic model, both modelling techniques will be reported for a better overview.

## 4.1. Map based model: results and discussion

The maps obtained from the steady-state data, see for example Figure 4 and Figure 5, are directly used to estimate the NO to $NO_2$ conversion. The actual model is built in the MATLAB-Simulink environment. The MATALB script is used to construct the map and calculate the coordinate of each point to be evaluated, namely the space-velocity and the average bed temperature; then Simulink discretize the input data in time format and extrapolates the point $NO_2/NO_x$ value to be multiplied by the input NOx concentration, thus obtaining the molar fraction of $NO_2$ as output. The Simulink blocks used to extrapolate the NO2/NOx value are the Interpolation *using Prelookup* coupled with *Prelookup* block. To improve the simulation accuracy, the step size was set to 0.1s even if the input data was collected every second.

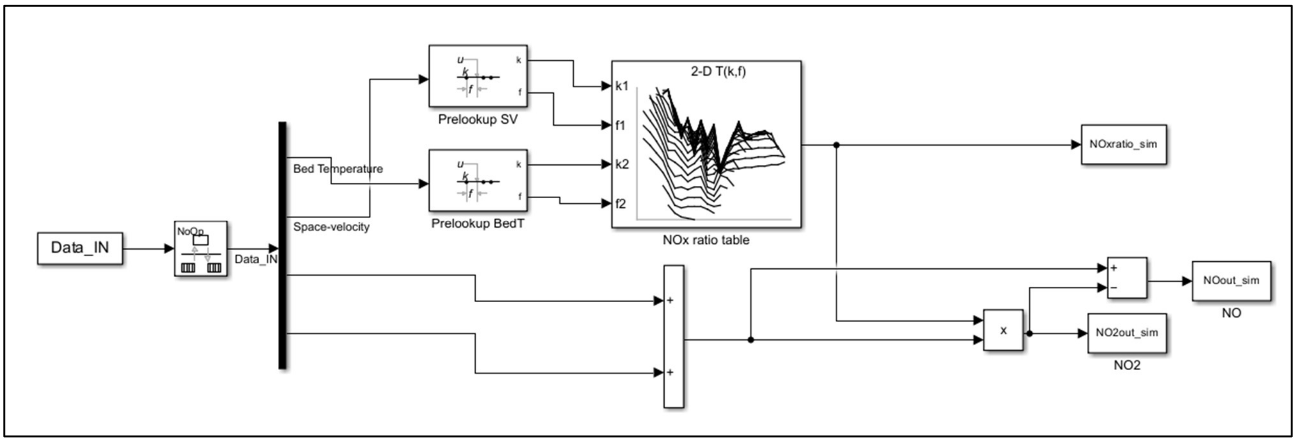

*Figure 7 Screenshot of the Simulink blocks used to calculate the NOx mole fraction in the outlet. Map Based model*

The following pages will show the most relevant driving cycles results, If the reader is interested, all the results are collected in the appendix.

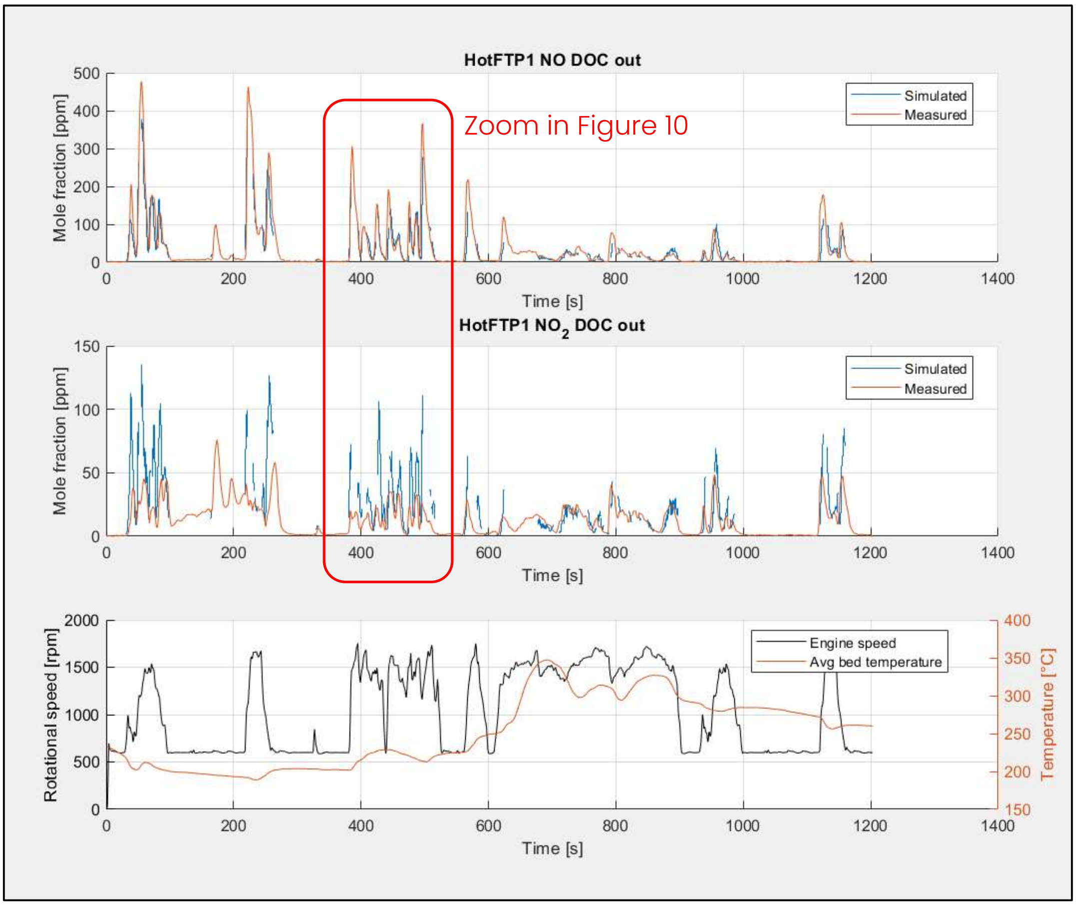

*Figure 8 NO and NO2 HotFTP cycle. Map mesh size of 25x25. Map based model*

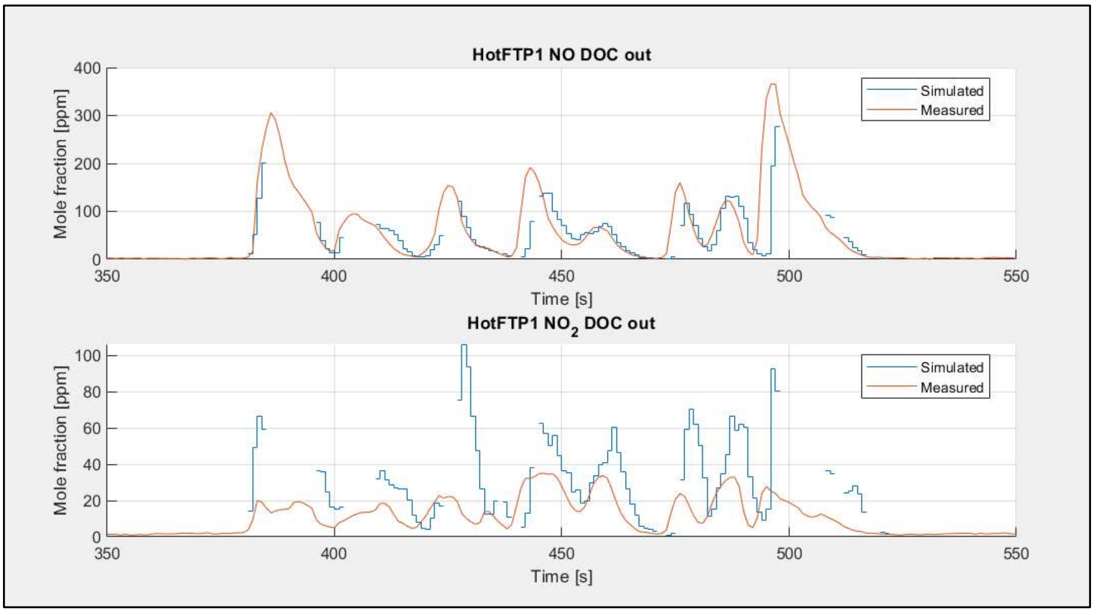

*Figure 9 Zoom of the HotFTP cycle showing NO and NO2 emission. Map based model, mesh size 25x25.*

Figure 8 shows that the model is unable to calculate NOx emissions at all points of the driving cycle.

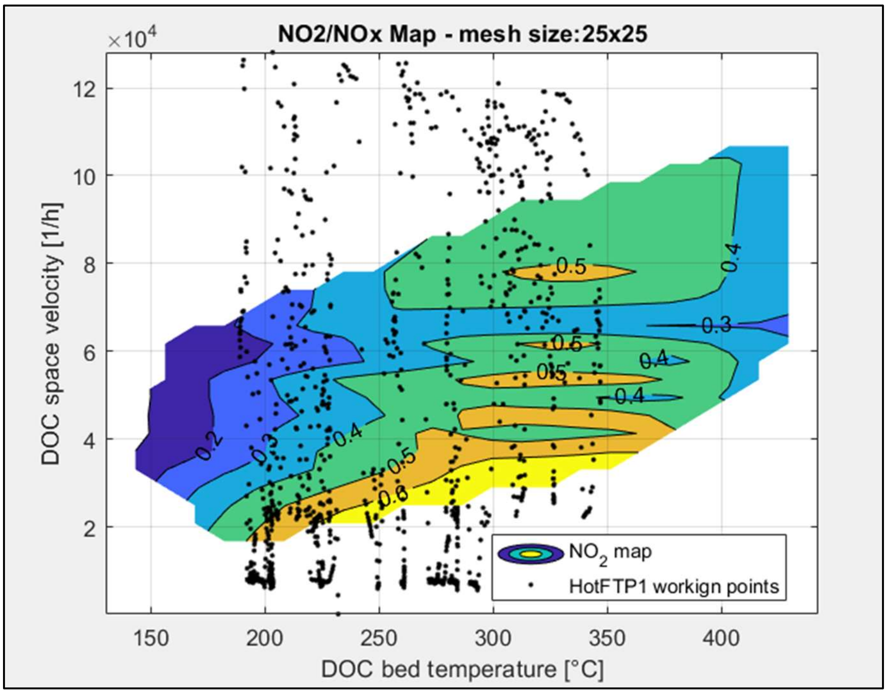

*Figure 10 HotFTP working points plotted in the NO2/NOx map, mesh size 25x25*

Looking at Figure 10, there are many points falling out the calculated map. The model shows a good level of predictions for the points inside the range of the map, see Figure 9. The prediction of NO is satisfactory, the $NO_2$ output is less precise.

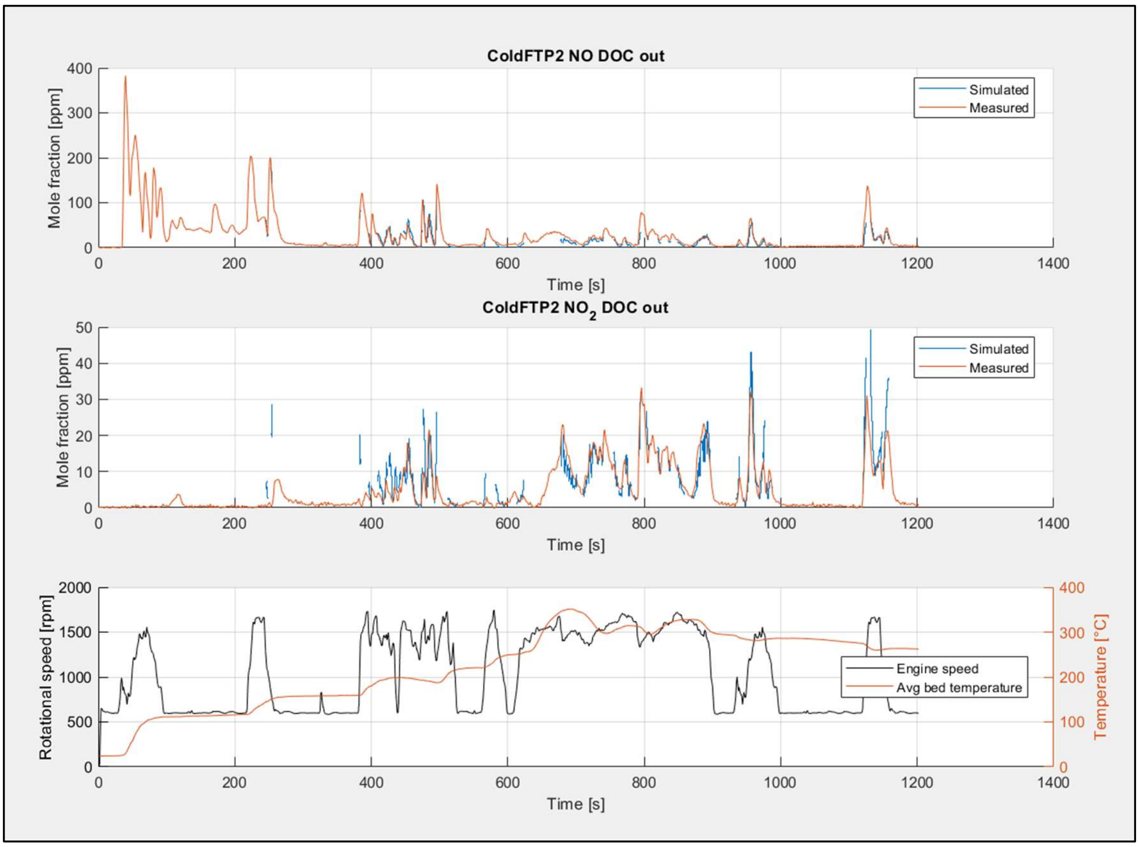

*Figure 11 NO and NO2 ColdFTP cycle. Map mesh size of 25x25. Map based model*

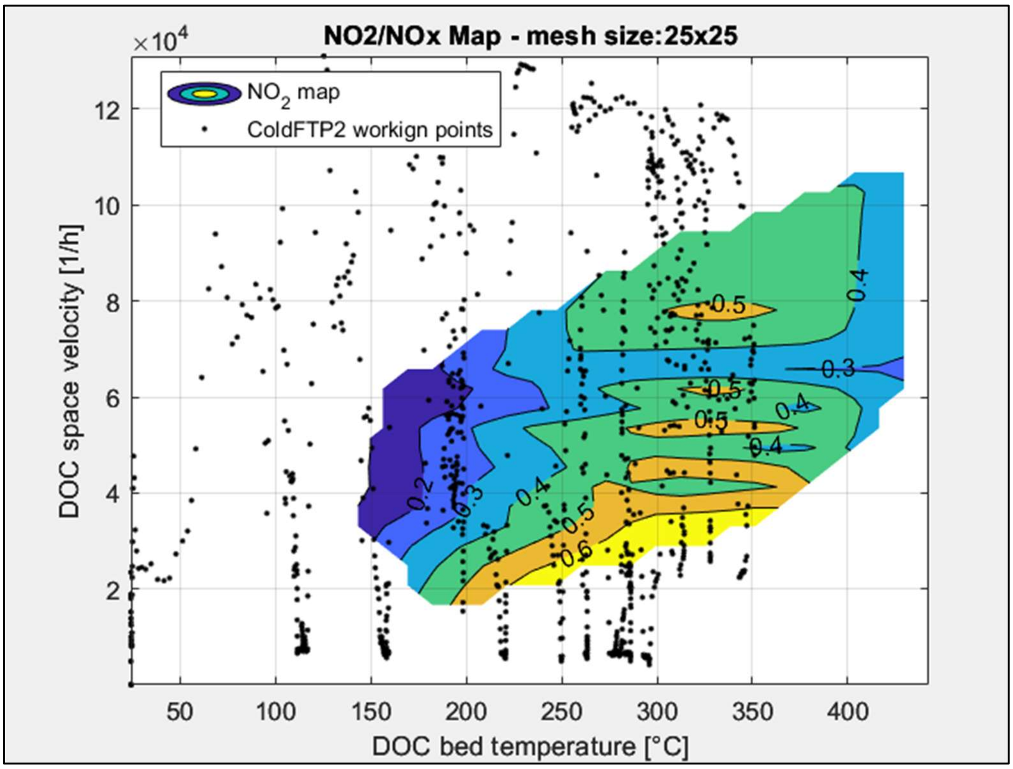

*Figure 12 ColdFTP working points plotted in the NO2/NOx map. Mesh size 25x25*

For colder cycle as reported in Figure 12 the results are worse because more points fall outside the calculated range.

The results with an increased mesh size are reported in Figure 13 and Figure 14, the accuracy remain similar.

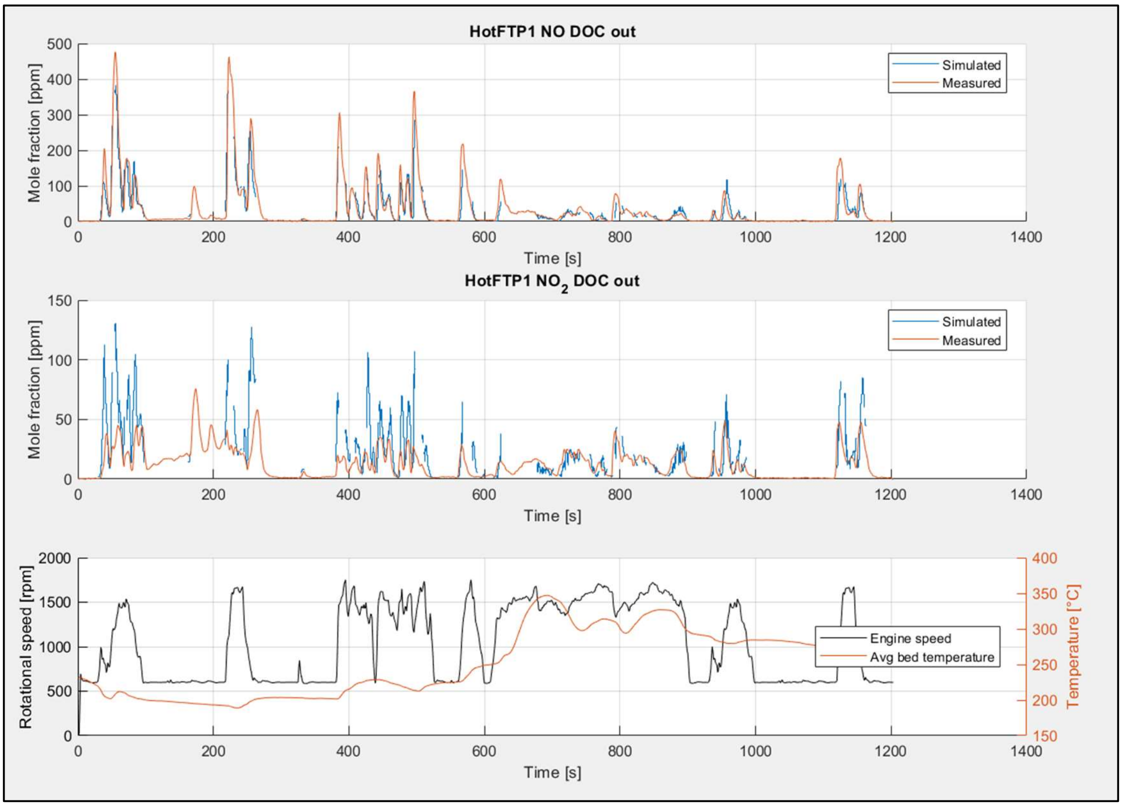

*Figure 13 NO and NO2 ColdFTP cycle. Map mesh size of 50x50. Map based model*

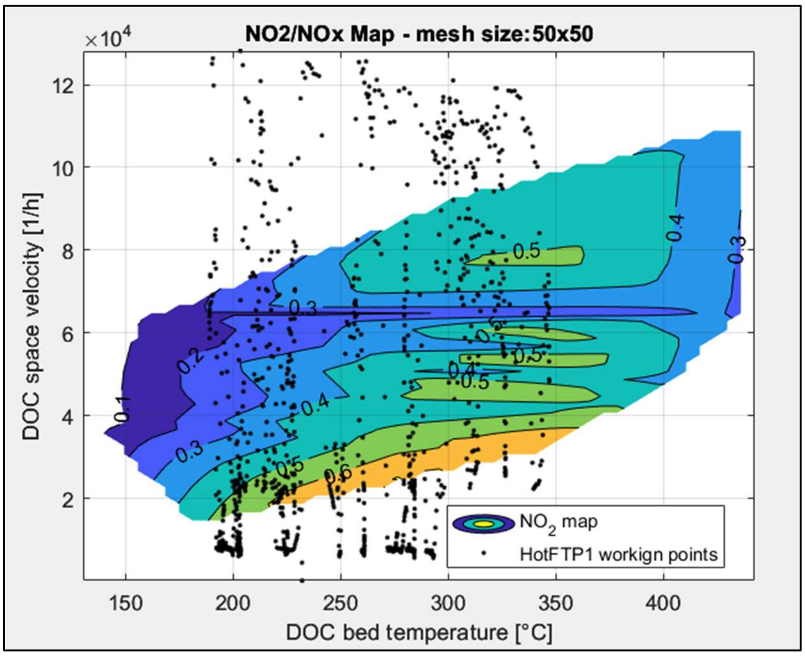

*Figure 14 HotFTP working points plotted in the NO2/NOx map. Mesh size 50x50*

## 4.2. Global kinetic model calibration

The final set of rate constants and inhibition terms is obtained following different calibration procedure, most of them were illustrated in the previous chapter. The data available strongly constrain the optimization that can be carried out, the engine-out data suitable for the optimization process include information about inlet and outlet concentration of NO, NO2 and CO. With the data provided, it is possible to calibrate the oxidation reactions of NO and CO with their inhibition functions modified to account for the available species. But considering the target and the deadline of this work, the only reaction calibrated is the NO oxidation with a modified inhibition function to account for the only species considered. The inhibition function becomes:

$$G = (1 - Aa_{NO}\, e^{-\frac{Ea_{NO}}{RT}} c_{s,NO}) \qquad \text{Eq. 15}$$

All the other parameters expressed in Table *2* Engine specification and in Table *3* Diesel Oxidation catalyst specification are entered in GT-Power software. It was created a case for each steady-state point and, in order to reach the stationary condition, each case of the simulation last 20s. Moreover, the bed temperature was imposed taking the temperature of the middle thermocouple as representative for the whole brick.

The model was calibrated following 3 different strategies:

- *Campaign 1*, following the procedure express in the previous chapter using as objective function both NO and $NO_2$ traces.
- *Campaign 2*, this calibration also follows the procedure express in the previous chapter, but the objective function uses as target the $NO_2/NO_x$. In this method small errors in NO or $NO_2$ output leads to a large error in $NO_2/NO_x$.
- *All-in one* calibration, where all the rate constants and the inhibition function terms were calibrated together. The objective function was targeting only the NO.

the first method analysed is the "Campaign 1" then we will move to the "*Campaign 2*", since the two methods have many points in common. The "*All-in one*" will be the last analysed.

### 4.2.1. Campaign 1 and 2: Log-space optimization results and discussion

The first step considered was the optimization through the Log-space. The solver's task is to minimize the objective function, written in Eq. *16*, by applying a searching method that in this case is the *Simplex Algorithm.*

$$ObjF = \sqrt{\sum_{i=1}^{NO_x} \left(x_{g,meas} - x_{g,sim}\right)^2} \qquad \text{Eq. 16}$$

The proposed objective function was chosen taking into account the available input data and the final objective of this work. Clearly a more complete calibration would include also other species, in this case, if reducing species had been considered, interactions between them and NOx through inhibition functions could have been considered, as shown 2.1.1.

Figure 15 shows the baseline objective function obtained from the model with rate constant from Table *1* and the results of the optimization. The initial model was not capable to correctly predict the NOx conversion efficiency. Despite this the optimizer was able to find a pre-exponent multiplier capable of providing an objective function lower than 4 times the initial value. Over the entire temperature range, the solver was able to reduce the objective function, resulting in a more accurate model. Note that when the objective function reaches zero, the model gives the same results as the experimental tests.

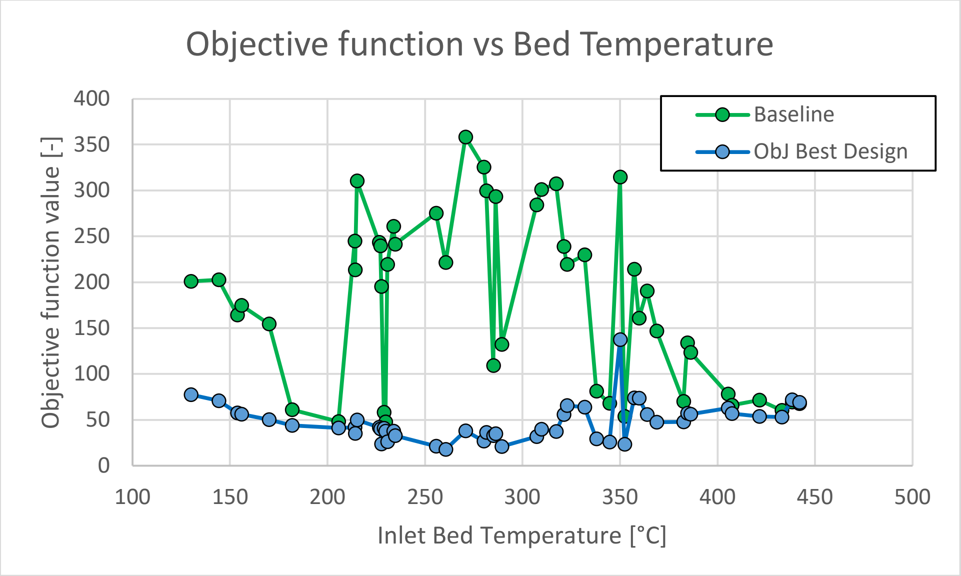

*Figure 15 Log-space optimization: baseline objective function and best design*

### 4.2.2. Campaign 1: Rate constants optimization

At this stage, the pre-exponent multiplier and the activation energy of the species of interest are optimized. Note that inhibition functions were excluded voluntarily because as explained in 3.3.3.

The second optimization step was carried out varying the pre-exponent multiplier and the activation energy in a +/- 100% the value resulting from log-space optimization, see Table *5*.

Table 5 Log-space optimization results for NO oxidation

| NO rate constant | Value |
|---|---|
| Pre-exponent multiplier $A_{NO}$ | $10^{1.445} = 27.86$ |
| Activation energy $E_{NO}$ | 6721 (value from Table *1*) |

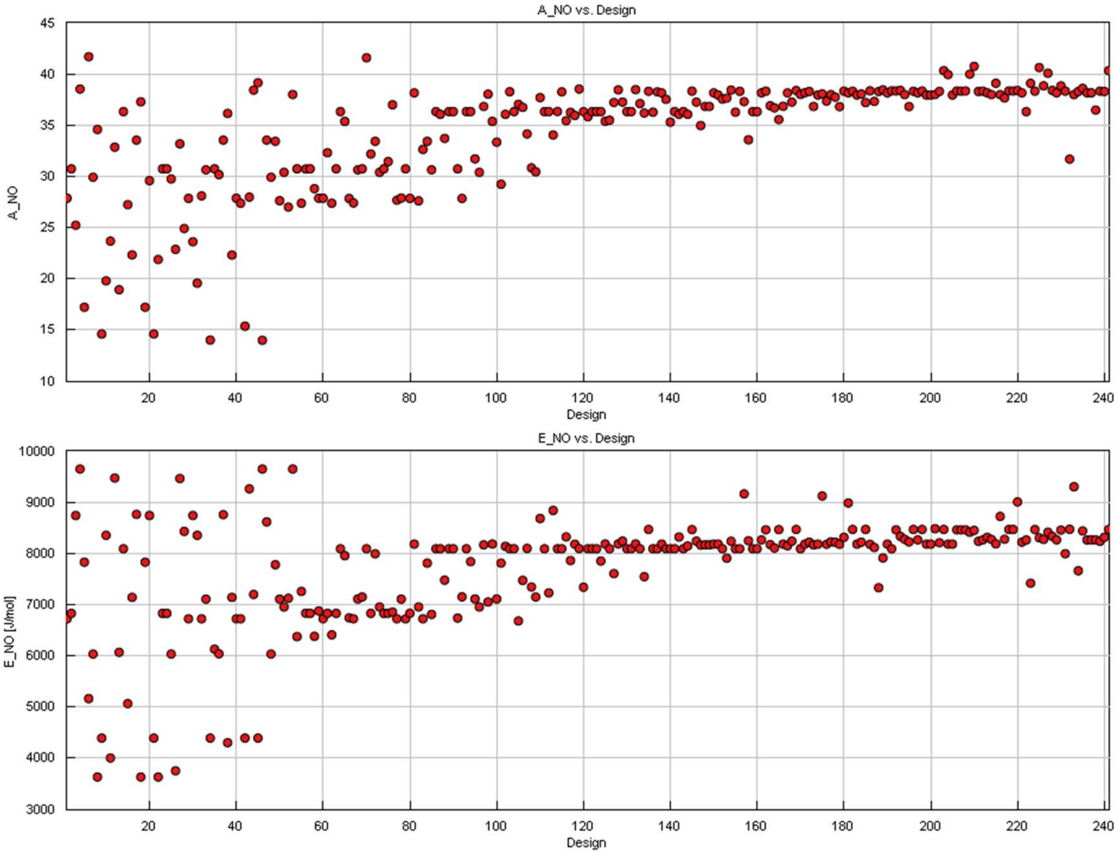

*Figure 16 Design iteration vs rate constants for second optimization of the Global Kinetic model*

Considering that for $A_{NO}$ the solver can search between 13.93 and 55.72 while for $E_{NO}$ the limits were fixed between 3360.5 and 13442 both of the results shown in Figure 16 can be considered acceptable and there is no evidence that the minimum of the objective function was out of the limits. To have a better overview of this optimization let see the actual value of the objective function in Figure 17 and Figure 18. Figure 17 shows the best design vs the starting point, the average improve of the best design is 2.6% over all the cases, it is not a huge step forward however between 150°C and 250°C the improvement is around 7-8%, see Figure 19. In Figure 18 the first red dot represents the baseline and the trend of the last designs do not make big improvement to the accuracy of the model.

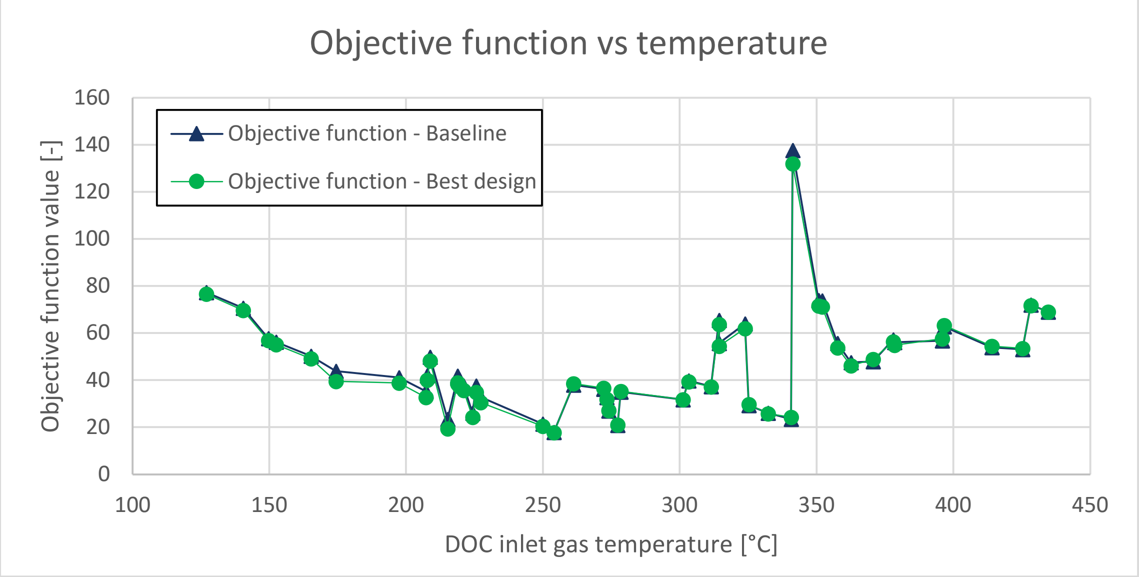

*Figure 17 Value of objective function for each steady tests vs. inlet gas temperature. Rate constants and inhibition terms optimization, campaign 1, Global Kinetic model*

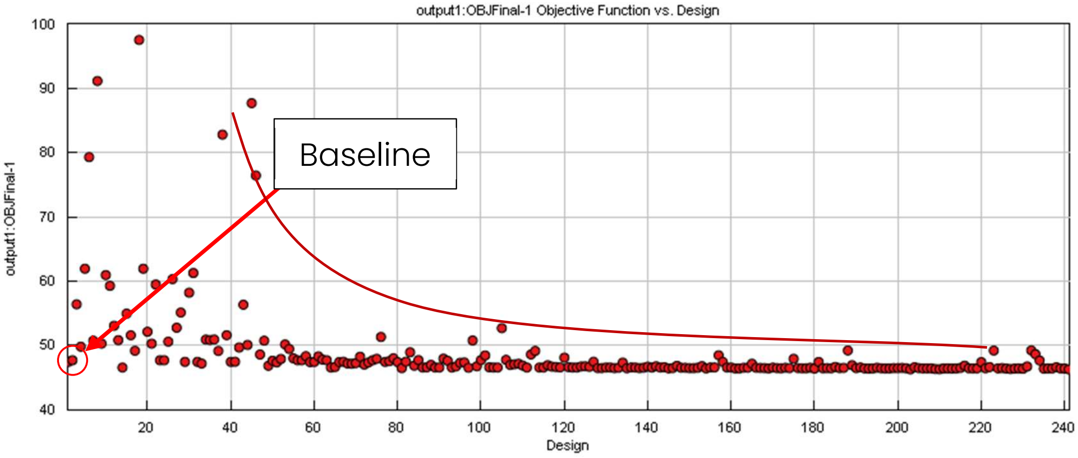

*Figure 18 Average value of the objective function for all the tested cases. Rate constants optimization, campaign 1, Global Kinetic model*

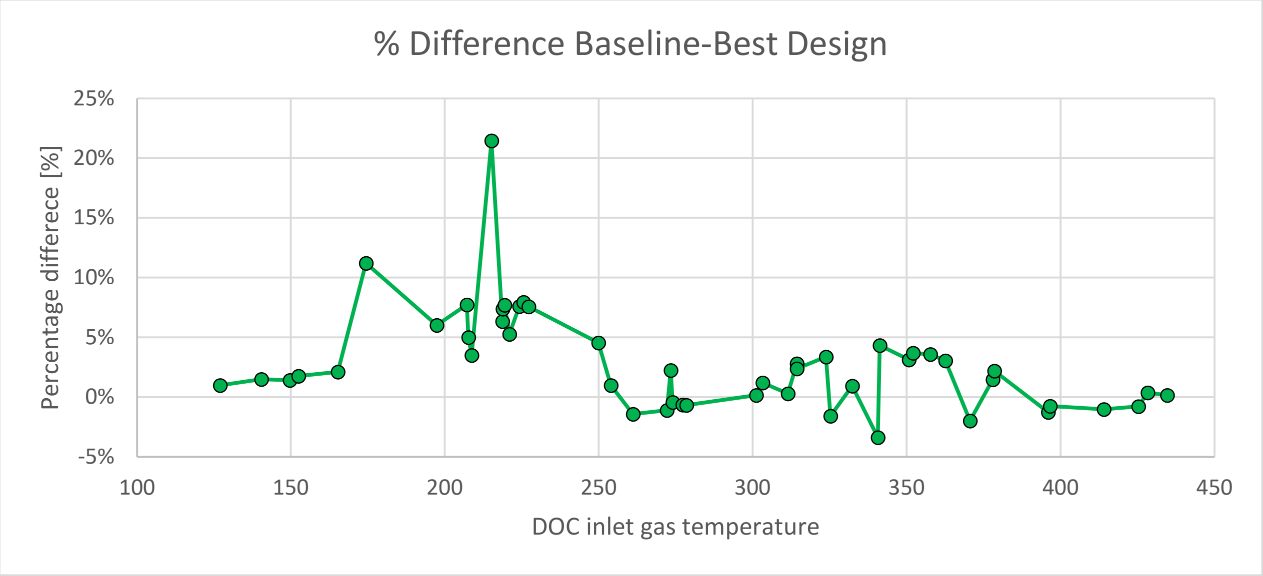

*Figure 19 Percentage difference between best design and baseline for the Global Kinetic model optimization. Only rate constants optimized*

### 4.2.3. Campaign 1: Rate constants and inhibition terms optimization

The last iteration in the optimisation process consists in optimising the rate constants and the inhibition terms. The solver settings were the same as 4.2.2 like the initial values of the parameters to optimize. The initial value and their range are reported in Table *6*, in most of the cases the lower limit is the half the nominal value while the upper limit is the double.

Table 6 Campaign 1, initial value and limits for Global Kinetic Model optimization.

| | Pre-exponent multiplier $A_{NO}$ | Activation energy $E_{NO}$ | Inhibition term $Aa_{NO}$ | Inhibition term $Ea_{NO}$ |
|---|---|---|---|---|
| Lower limit | 0 | 4233 | 0.121 | -80840 |
| Initial value | 40.32 | 8466 | 0.242 | -40420 |
| Upper limit | 80 | 16932 | 0.484 | -20210 |

This further optimization phase led to an improvement in the temperature window of 150°C to 200°C and it lowered the error present at about 350°C, Figure 20. Between 150°C to 250°C the average improvement was of 15%, as shown in Figure 21

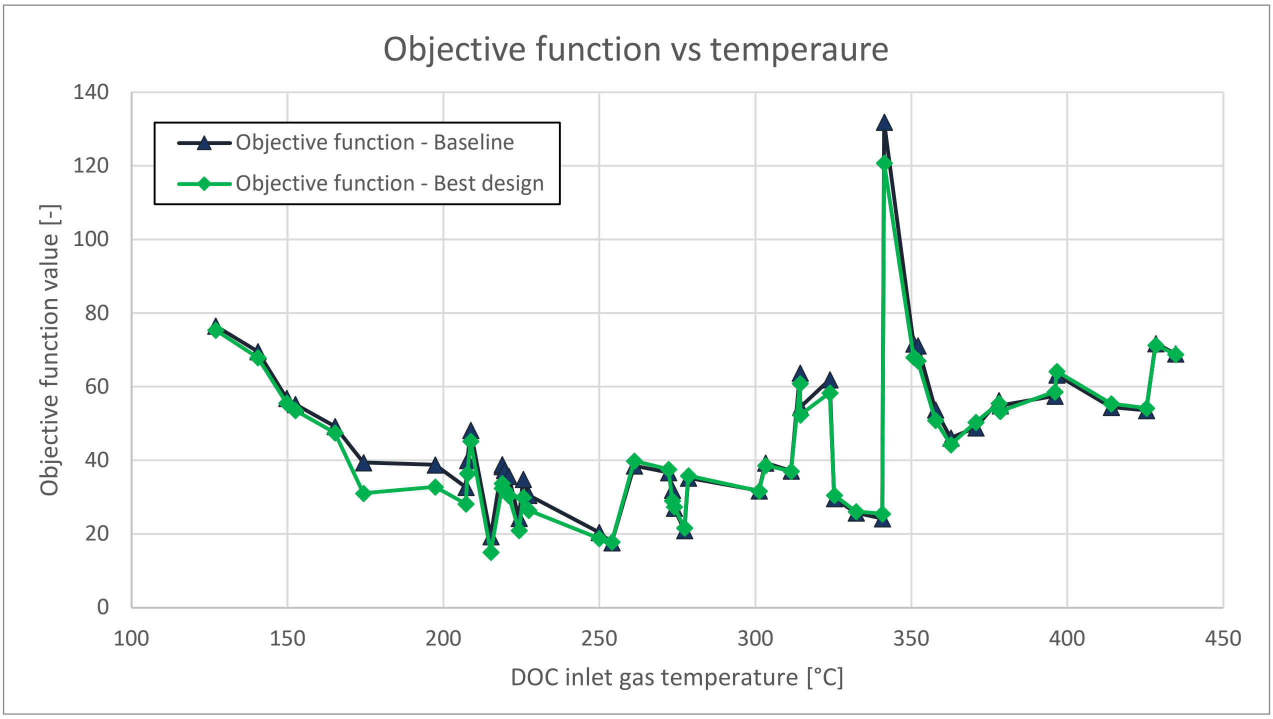

*Figure 20 Value of objective function for each steady tests vs. inlet gas temperature. Rate constants and inhibition terms optimization, campaign 1, Global Kinetic model*

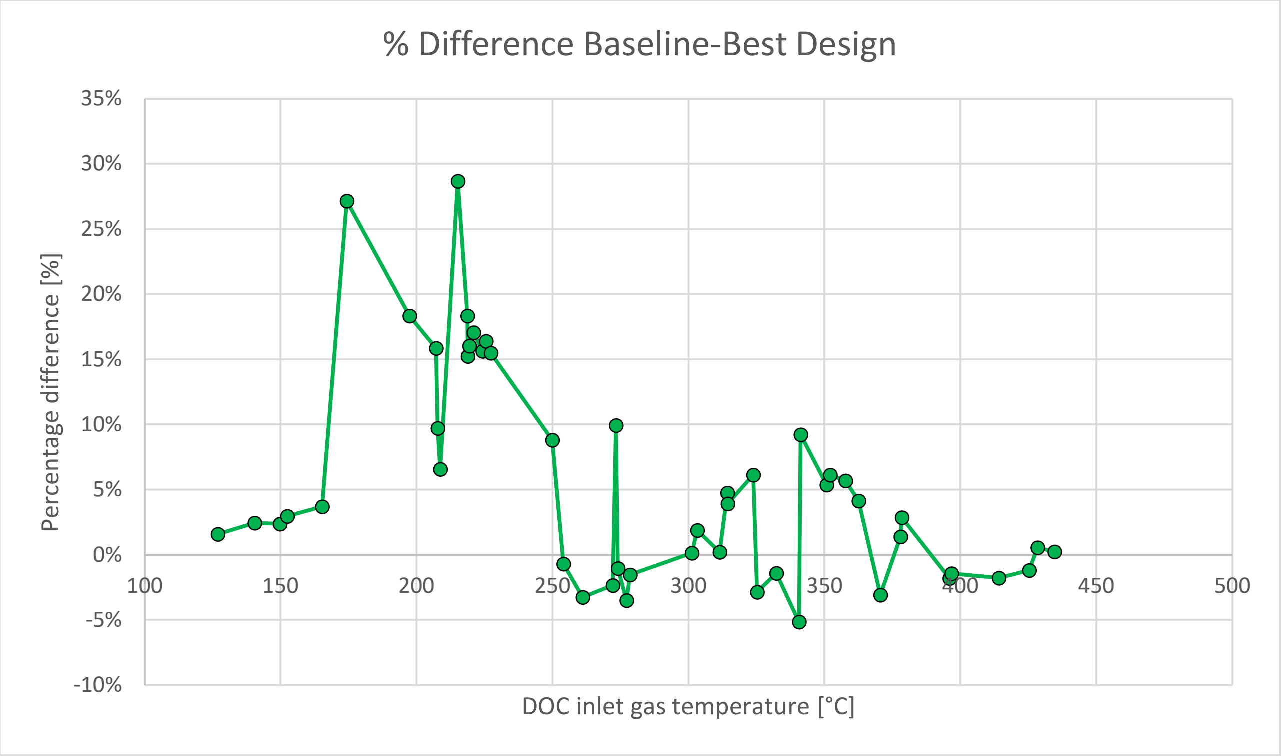

*Figure 21 Percentage difference between best design and baseline for the Global Kinetic model optimization, campaign 1, rate constants and inhibition terms optimized*

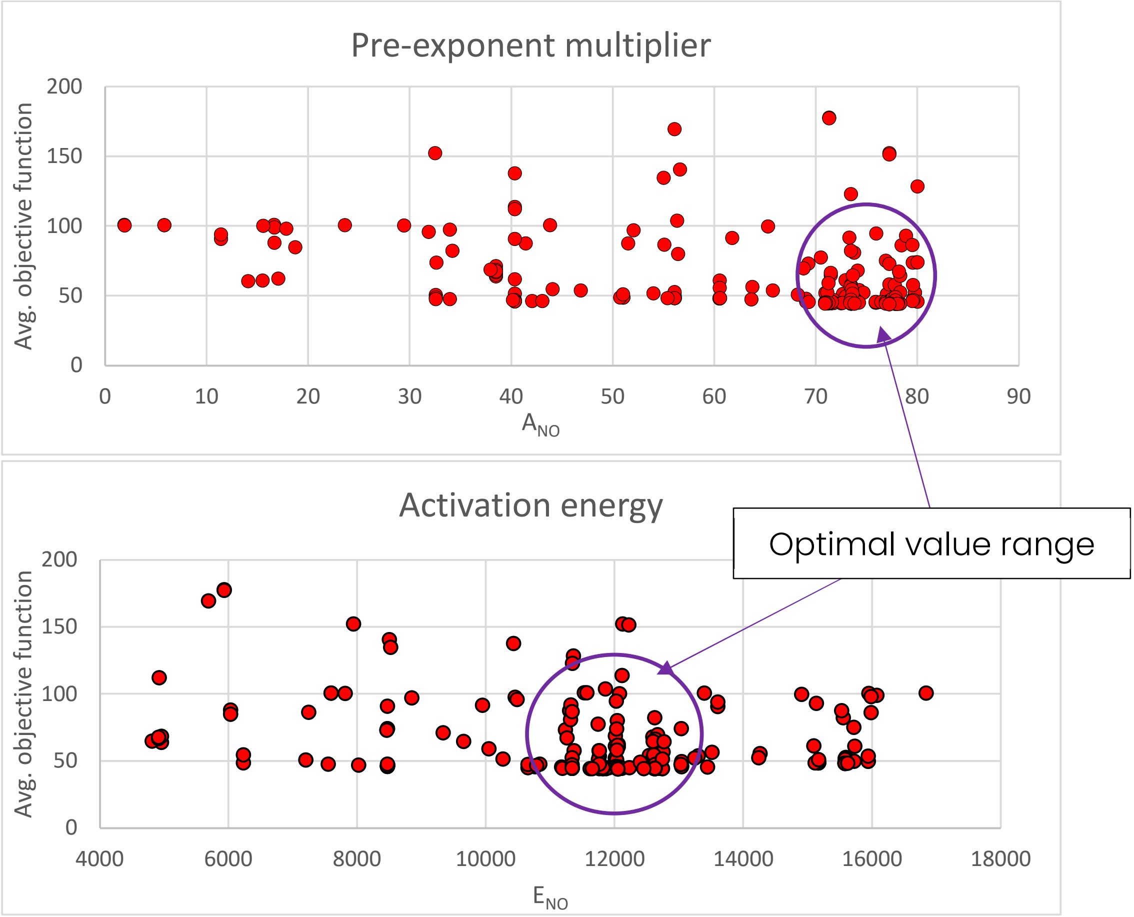

*Figure 22 Average objective function for each iteration vs rate constants values. Global kinetic model optimization, campaign 1, rate constants and inhibition terms*

The upper chart of Figure 22 shows that the optimal value for $A_{NO}$ is close to the limit of 80 while for $E_{NO}$ the limits are far from the optimal value, the limits are reported in Table 6. Despite the proximity between the optimum value and the research limits, it was agreed that is not necessarily further optimization because the point of minimum of the objective function strongly depends on the parameters to be varied during the optimization. The scope of the procedure followed aims to focuses on few parameters at time, in this iteration the focus was on the terms of inhibition function so considering that $A_{NO}$ does not overlap the limit, as far as the rate constants are concerned, the optimization is considered completed.

Looking at Figure 23, the values of $Ea_{no}$ below -50000 do not have a sensible effect on the objective function, probably this range of values generate an out of range inhibition function.

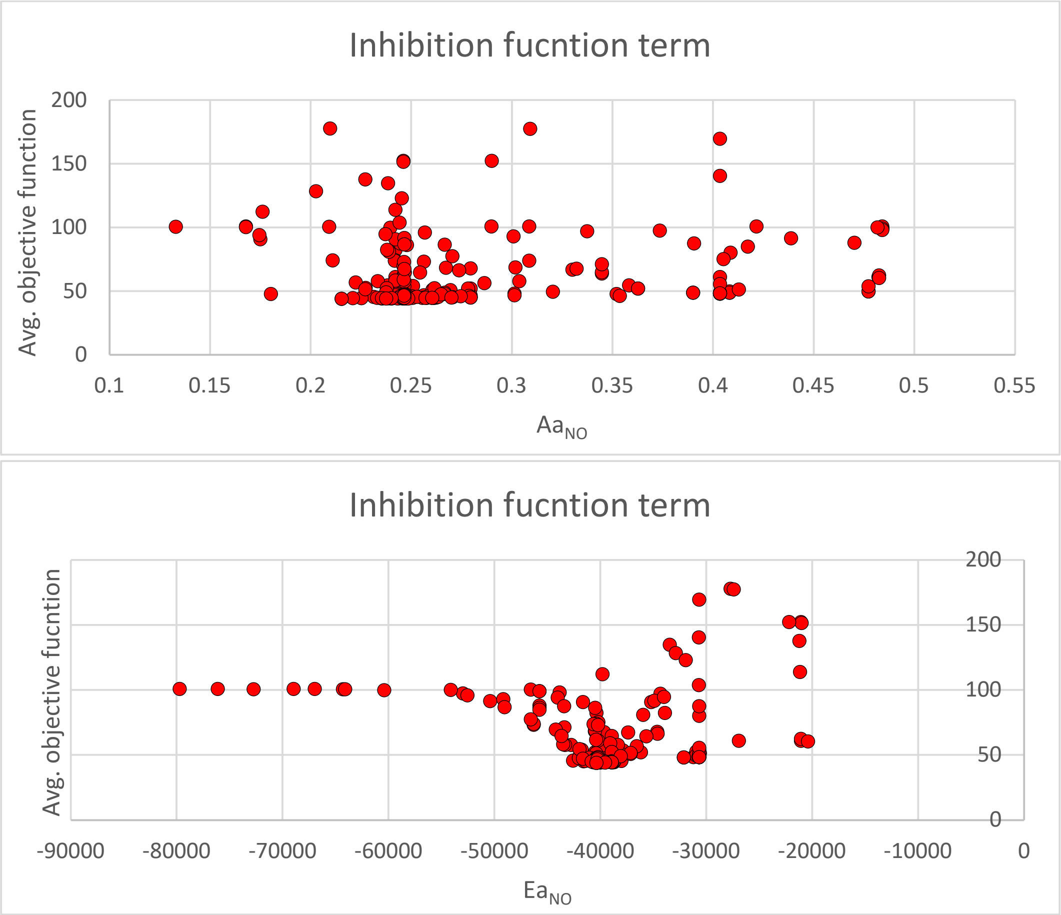

*Figure 23 Average objective function for each iteration vs inhibition terms values. Global kinetic model optimization, campaign 1, rate constants and inhibition terms*

Table 7 Final results of optimization campaign 1. Parameters calibrated are: rate constants and inhibition terms

| | Pre-exponent multiplier $A_{NO}$ | Activation energy $E_{NO}$ | Inhibition term $Aa_{NO}$ | Inhibition term $Ea_{NO}$ |
|---|---|---|---|---|
| Final results | 77.22 | 12048 | 0.215 | -40405 |

Table 7 report the final results of the last optimization. The last check must be made on the inhibition terms, we want to control if at low, mid and high temperature the inhibition function assumes a reasonable value. The temperature has been selected as follow:

- Low temperature: 150°C. At this temperature the catalyst is not able to convert any species thus we expect a high value of inhibition function so as to inhibit reactions.

- Mid temperature: 350°C. This is the temperature in which mostly all reducing species have been oxidised, we expect a lower value of inhibition function but high enough to represent the transition condition, now the catalyst start to oxidised NO at higher rate.
- High temperature: 600°C, inhibition function near 1.

To test the behaviour of the inhibition function, its value was calculated at different concentration levels with 3 different temperature values, Figure 24. The concentration level is given in mole fraction and it is representative of the minimum and maximum level that could be met during normal operation. Focusing on the graph at 150°C, the value is around 1 up to 10ppm then it increases rapidly to represent the inhibition effect. Between 100ppm and 1000ppm the inhibition function reduces the conversion by a factor of 5 and 20. The other two temperature, as expect, show a much lower inhibition term for all the concentration levels. We can conclude that the inhibition function calibration has been successfully concluded.

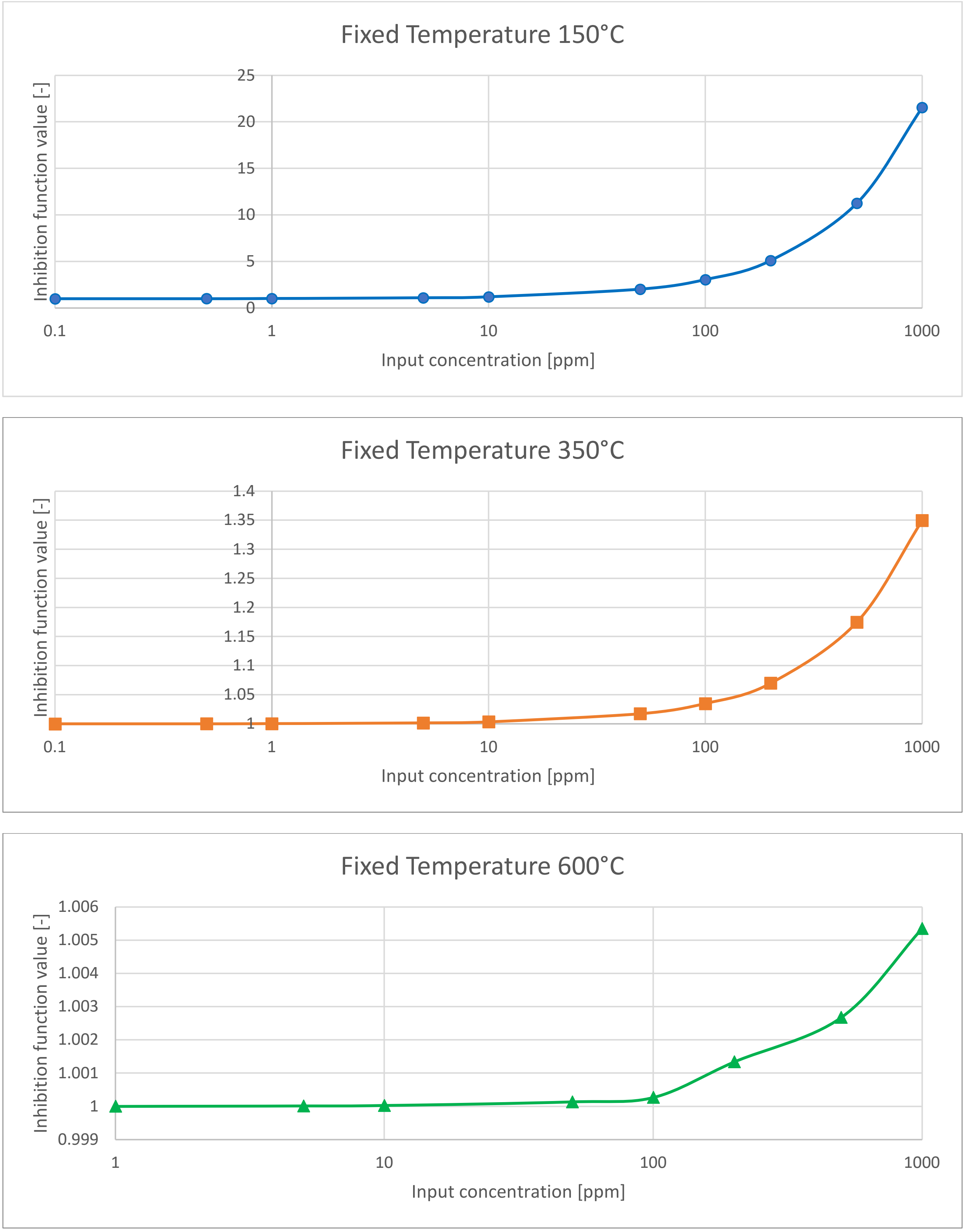

*Figure 24 Inhibition function values at different concentration. For each chart the temperature is constant and it is increased from top chart to bottom chart. In all the charts the x-axis is reported in logarithmic scale.*

### 4.2.4. Campaign 2: rate constants and inhibition terms optimization

Since the SwRI internally uses the $NO_2/NO_x$ as a verification parameter, the 2nd optimization campaign was performed by reformulating the objective function and using as target the $NO_2/NO_x$. The ratio amplifies the error hence its usage as target could generate a better result. The starting point of this calibration is the log-space optimization reported in 4.2.1, the initial values are reported in Table *5*.

To account for the characteristics of the $NO_2/NO_x$ the objective function was changed with:

$$objF = \frac{\left| \frac{NO_2}{NO_x}_{meas} - \frac{NO_2}{NO_x}_{sim} \right|}{\frac{NO_2}{NO_x}_{meas}} \qquad \text{Eq. 17}$$

This formulation takes into account that the ratio is a value between 0 and 1 so, considering the former equation, illustrated in Eq. *16*, by making the root of the difference of the ratios, the value of the objective function becomes very small causing solver issue. Moreover Eq. 17 is scaled by the measured ratio, highlighting the most critical points. This time the parameters to be optimised were not divided in two groups, namely in a first optimization with only the rate constants and then all the four, but all the four parameters were optimized together.

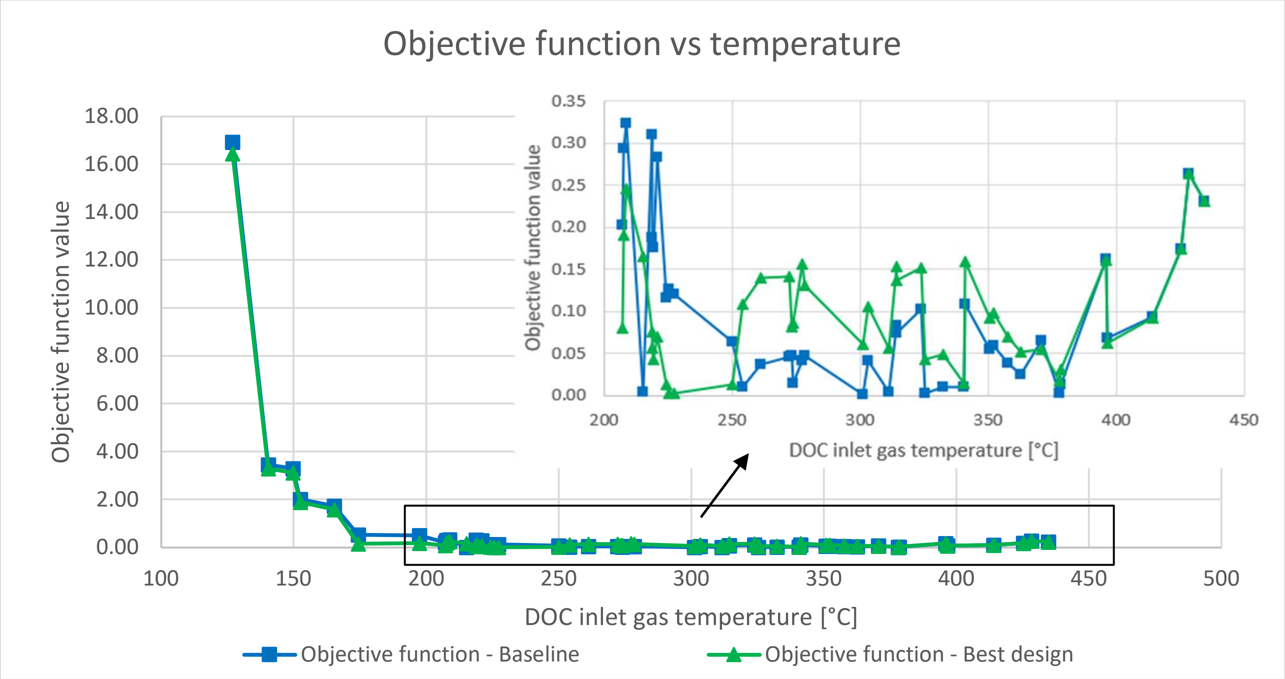

*Figure 25 Value of objective function for each steady tests vs. inlet gas temperature. Rate constants and inhibition terms optimization, campaign 2, Global Kinetic model*

Analysing Figure 25 it is clear that the prediction accuracy at low temperatures is really low. Before 200°C the predictions are wrong by a factor ranging of 2 to 18, which is clearly unacceptable. After 200°C the objective function returns to a value less than 1, which as function is formulated means that the ratio has a maximum error of about 35%, looking at zoom in Figure 25.

Only the 12% (6/49) of the total calibration cases have an unacceptable error (>100%) and for this reason no further optimizations were carried out. The final result is reported in Table *8*.

Table 8 Final results of optimization campaign 2. Parameters calibrated are: rate constants and inhibition terms

| | Pre-exponent multiplier $A_{NO}$ | Activation energy $E_{NO}$ | Inhibition term $Aa_{NO}$ | Inhibition term $Ea_{NO}$ |
|---|---|---|---|---|
| Final results | 109.7 | 11761 | 0.1358 | -46584 |

### 4.2.5. All-in one calibration

This section analyses the last type of calibration carried out to evaluate the best set of parameters for the global kinetic model. In this calibration it was assumed that all oxidised NO was converted to NO2. This assumption reduces the complexity of the inhibition function by reducing the term from NO and NO2 to NO only. Furthermore, the log-space optimisation is not considered, but several optimisation sessions have been started, changing the bounds of the parameters from time to time. This procedure can lead to a suboptimal minimum if the bounds are too close together or, if a larger range is considered, to a long simulation time..

The objective function used is:

$$objF = \left|x_{g,meas} - x_{g,sim}\right| \qquad \text{Eq. 18}$$

It was considered only NO mass fraction. After several iteration the best result is reported in Table *9*.

Table 9 Final results of optimization "*All-in one*". Parameters calibrated are: rate constants and inhibition terms

| | Pre-exponent multiplier $A_{NO}$ | Activation energy $E_{NO}$ | Inhibition term $Aa_{NO}$ | Inhibition term $Ea_{NO}$ |
|---|---|---|---|---|
| Final results | 2196 | 34315 | 0.2154 | -2701 |

## 4.3. Global kinetics model design on MATLAB environment

After the calibration procedure, the mathematical model proposed in chapter 2.1.1 has been created in MATLAB environment. The model is built with the following differential-algebraic equations system or DAE's proposed in Eq. *1*. The input data are reported in mole fraction but the equations use mass fraction and concentration [mol/m$^3$], to convert from mole fraction $y_i$ to concentration $c_{s,i}$ was used:

$$c_{s,i} = \frac{\rho_{avg}}{M_{air}} y_i \qquad \text{Eq. 19}$$

The density inside the catalyst brick was considered constant both for steady operation and for driving cycle. The molar mass of the exhaust gas was set the same as that of air, i.e., of 28.96 g/mol.

The model does not include energy equation hence the temperature must be imposed from measures. The temperature dependent parameters are divided in two categories according to whether the temperature appears in the exponent or the parameters is multiplied by temperature:

- Parameters multiplied by temperature use the average value of the 3 measured bed temperature.
- Parameters having temperature in the exponent use a second-order interpolation between the 3 measures.

This procedure has been identified in order to reduce the complexity and the simulation time. As we can see from Figure 26 the temperature difference between the inlet and the outlet temperature is very low, it is between 1°C and 2°C for all the cases. This justifies the utilization of the average temperature for parameters that have a weaker temperature dependency.

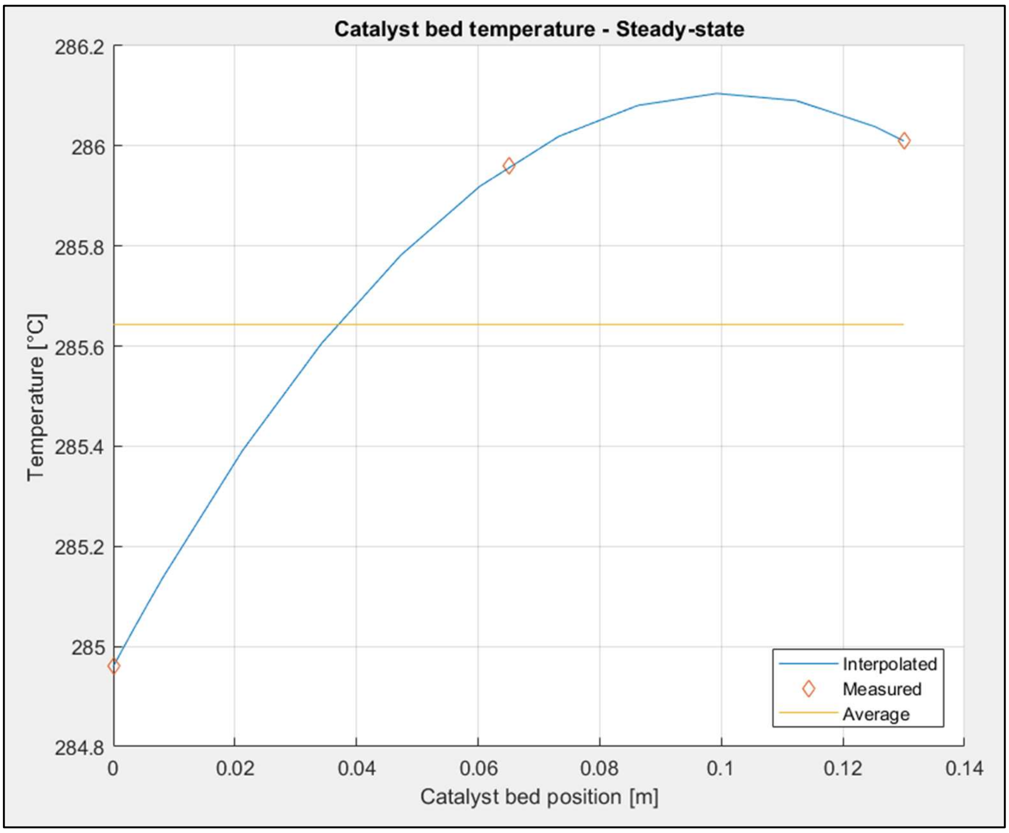

*Figure 26 Average and interpolated temperature for steady-state test n.3*

The solver used is the MATLAB *ode15s,* it is designed to solve stiff differential equations and DAE's system. The solver applies a variable integration step size to obtain a more accurate solution [8]. The solver returns the calculated mass fraction for each point in which the catalyst length is divided, namely the integration step-size.

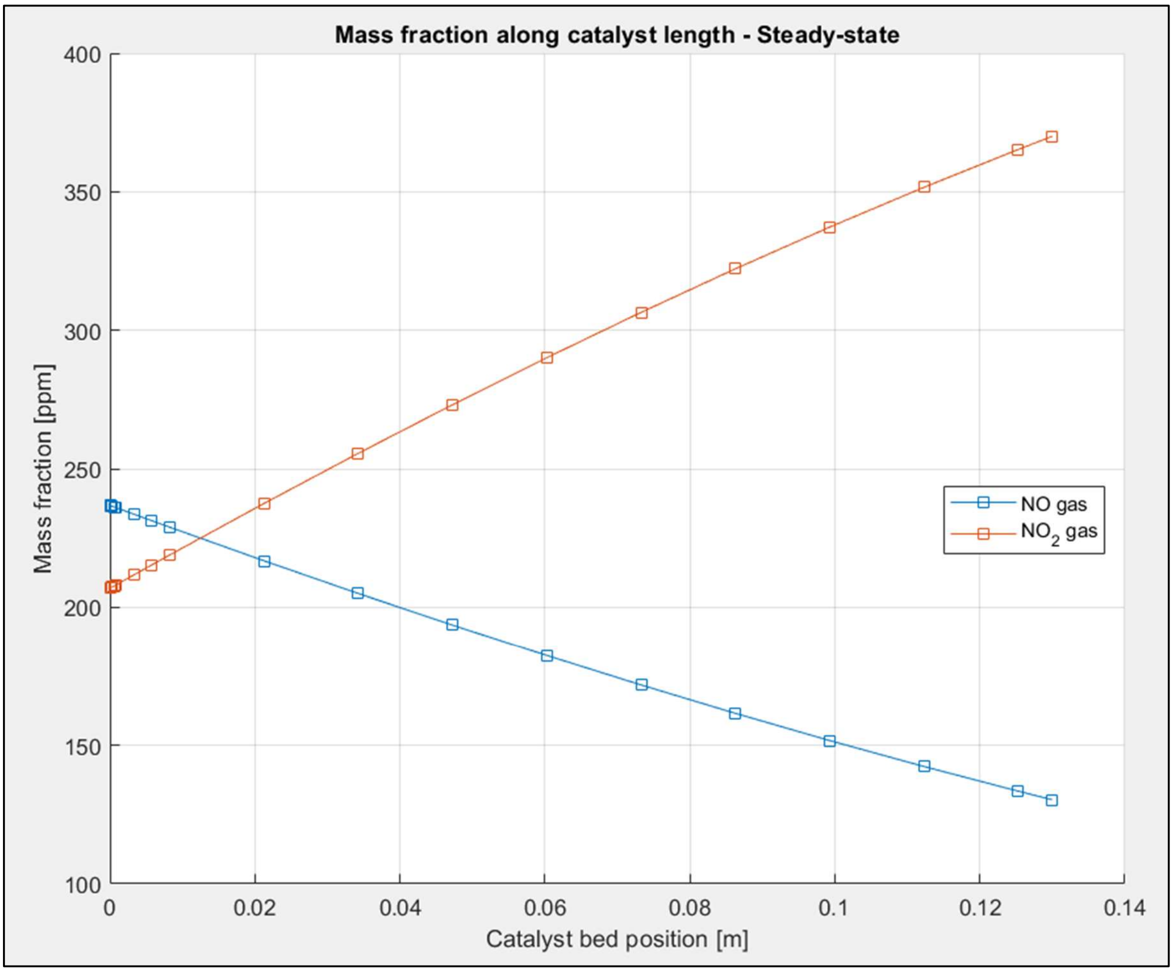

*Figure 27 Evolution of the mass fraction along the catalyst length. Steady-state test n.3*

## 4.4. Global kinetic model results and discussion

For sake of simplicity, the Table *10* reports the final results of the calibrations performed in paragraphs 4.2.1, 4.2.2, 4.2.3, 4.2.4 and finally in 4.2.5.

Table 10 Results of all the calibrations for global kinetic model

| | Pre-exponent multiplier $A_{NO}$ | Activation energy $E_{NO}$ | Inhibition term $Aa_{NO}$ | Inhibition term $Ea_{NO}$ |
|---|---|---|---|---|
| Campaign 1 | 77.22 | 12048 | 0.215 | -40405 |
| Campaign 2 | 109.7 | 11761 | 0.1358 | -46584 |
| All-in one | 2196 | 34315 | 0.2154 | -2701 |

As we can expect the first two rows' values are of the same order of magnitude, in contrary to "*all-in one*".

### 4.4.1. Campaign 1: results and discussion

The first results shown are in steady operations.

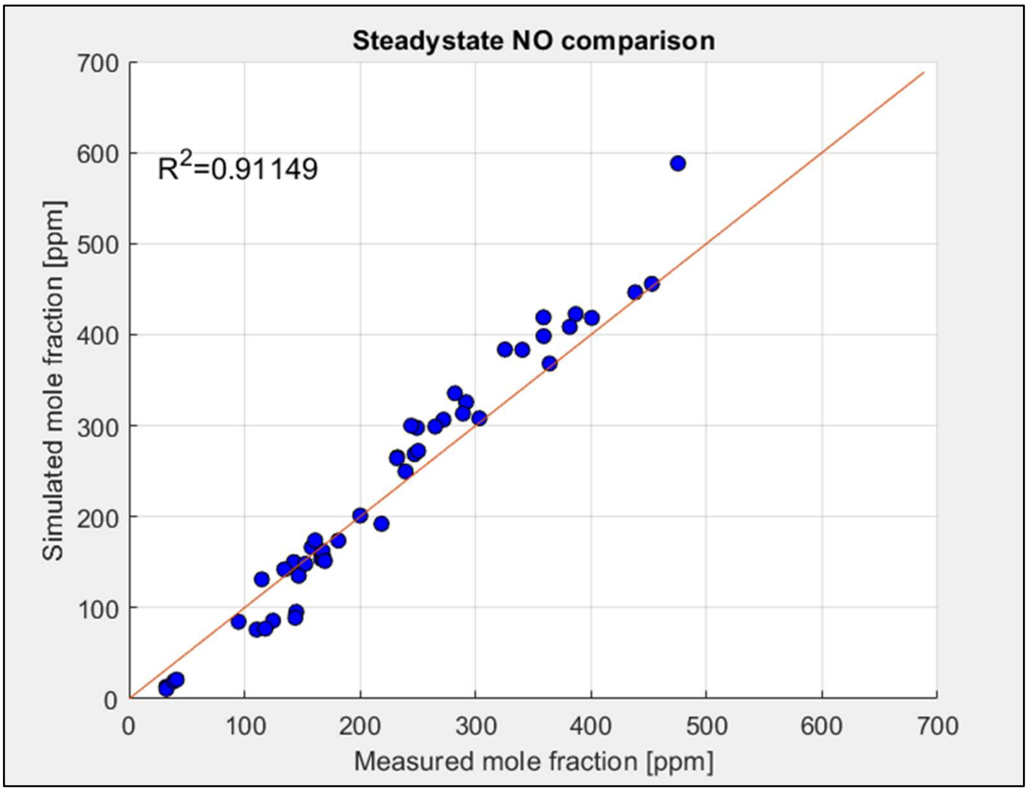

*Figure 28 Comparison between NO emission measured vs simulated. Global kinetic model, campaign 1.*

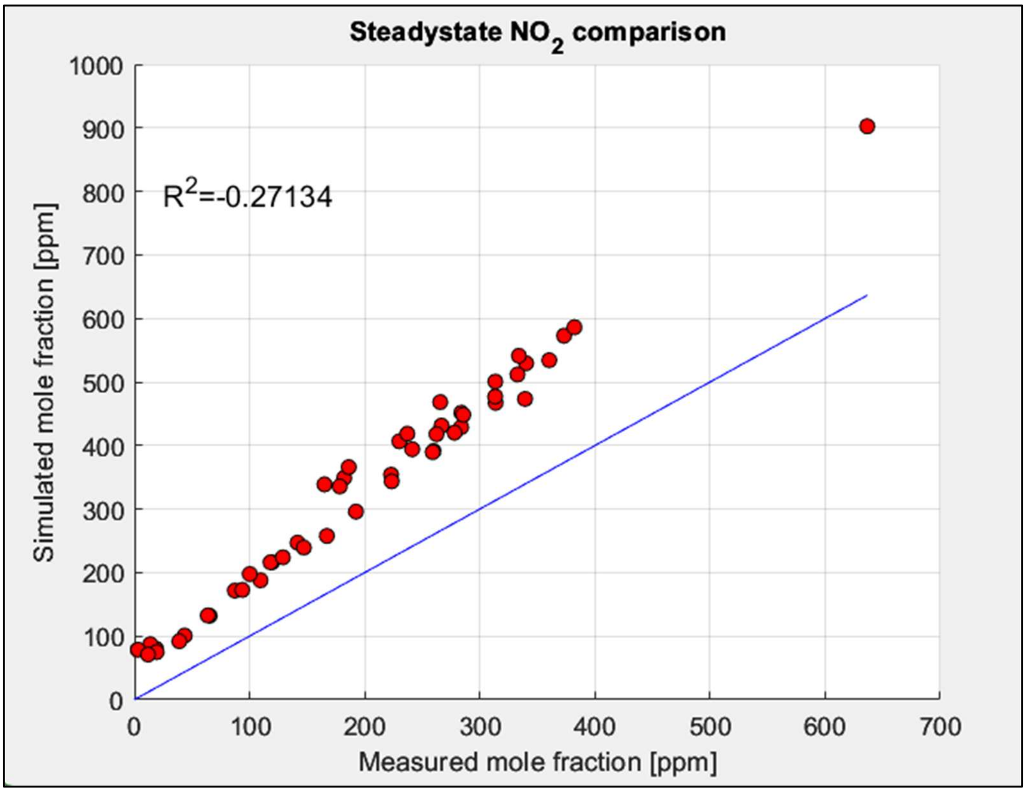

*Figure 29 Comparison between $NO_2$ emission measured vs simulated. Global kinetic model, campaign 1.*

The red bisector line in Figure 28 and the blue in Figure 29 represent a model 100% correlated to the measured data, this kind of model would be $R^2 = 1$. The $R^2$ for NO simulation is 0.911 and it is acceptable. On the contrary $NO_2$ predictions are not well correlated as suggested by the negative $R^2$, so it cannot be used.

Theoretically the NO number of mole that are oxidized should be converted in $NO_2$ so, following this assumption, the $NO_2$ emission was re-calculated based on the NO value, following Eq. *20*.

$$y_{NO_2,out,var} = y_{NO_x,in,meas} - y_{NO,out,sim} \qquad \text{Eq. 20}$$

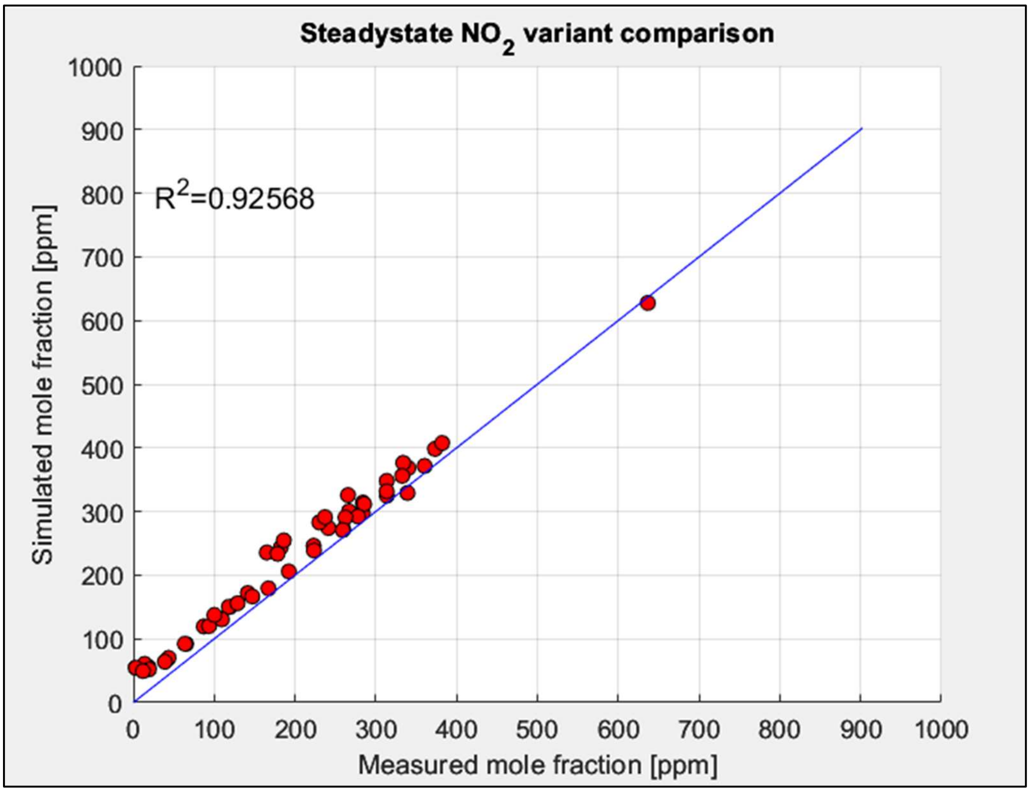

*Figure 30 Comparison between $NO_2$ emission measured vs simulated. The $NO_2$ emitted are calculated using the NO value. Global kinetic model, campaign 1.*

Using the alternative method to calculate $NO_2$ the $R^2$ obtained is much better so, to have a double-check on the method applied in Eq. *20*, the Figure 31 shows a comparison between the MATLAB (lower plot) and GT-Power (upper plot) results. Considering GT-Power results as reference, it can be seen that the alternative method expressed above gives similar results, therefore the $NO_2$ calculation will involve the method express in Eq. *20*.

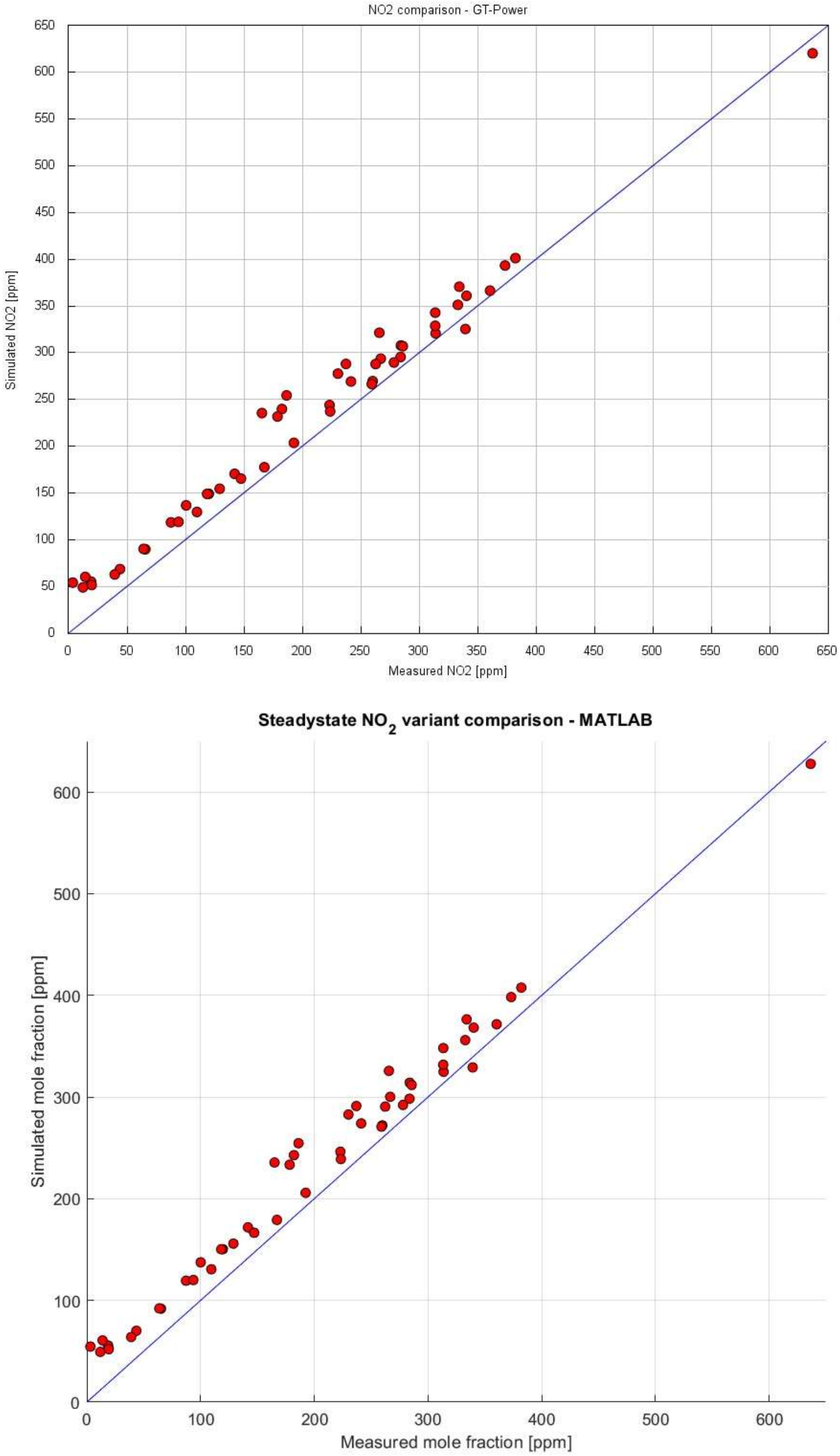

*Figure 31 Upper plot: $NO_2$ GT-Power simulation. Lower plot: $NO_2$ MATLAB simulation. Both of the model uses calibration parameters from optimization campaign 1*

As shown in Figure 32, after 250°C the relative error is less than +/-25%. On the contrary, below 250°C the relative error skyrockets with peaks higher than 100%. For this reason, it could be helpful to add to the model an inhibition function dependent on CO or HC. In fact, between 250°C and 350°C, as shown in Figure 6, the thermo-chemical theoretical limit of NO oxidation approaches its measured values. This region is the most critical to predict therefore coupling the reaction rate with an inhibition function that consider a reducing species can help to model the behaviour of the real system.

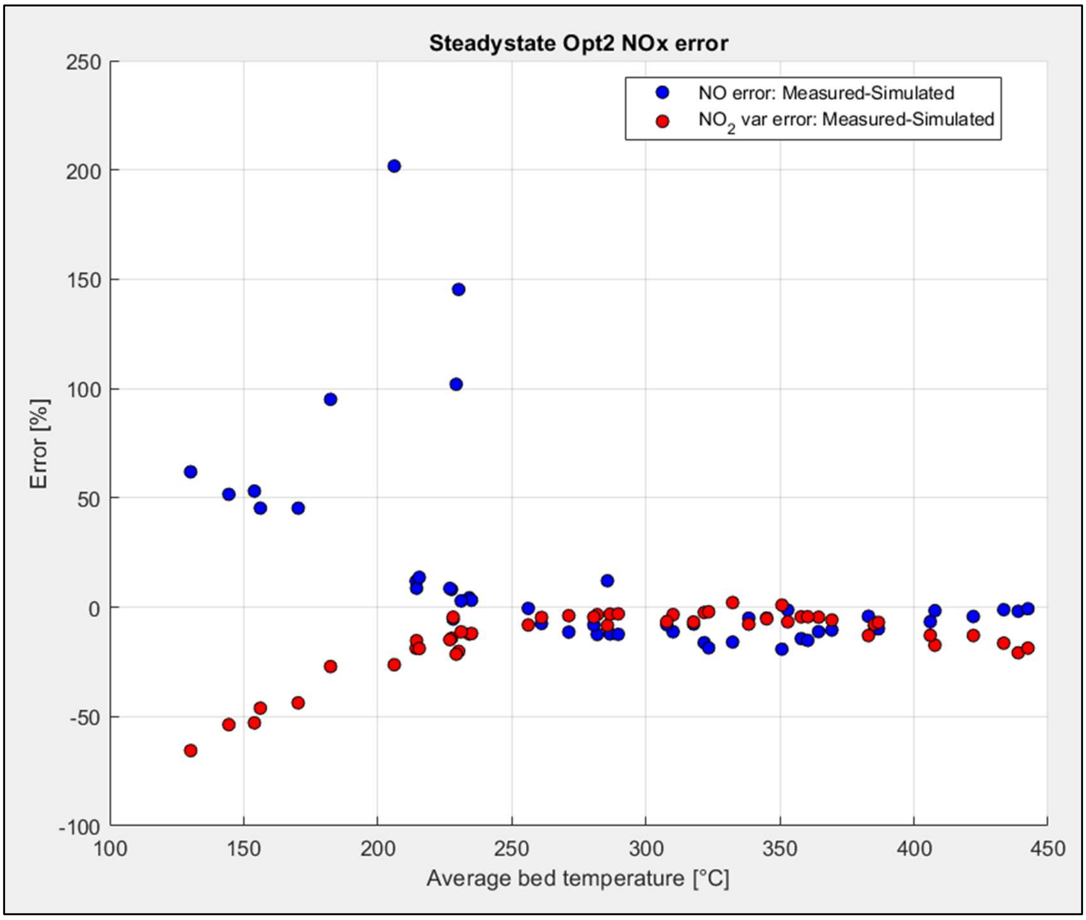

*Figure 32 Percentage error between measured and simulated NOx emission. Global kinetic model, campaign 1.*

Now we focus on the $NO_2/NO_x$. Figure 33 shows a worse behaviour than might be expected when compared with Figure 28 and Figure 30. If the $R^2$ for NO and $NO_2$ are 0.911 and 0.926 respectively, the $NO_2/NO_x$ has an $R^2$ of 0.382, which translates into a very low correlation.

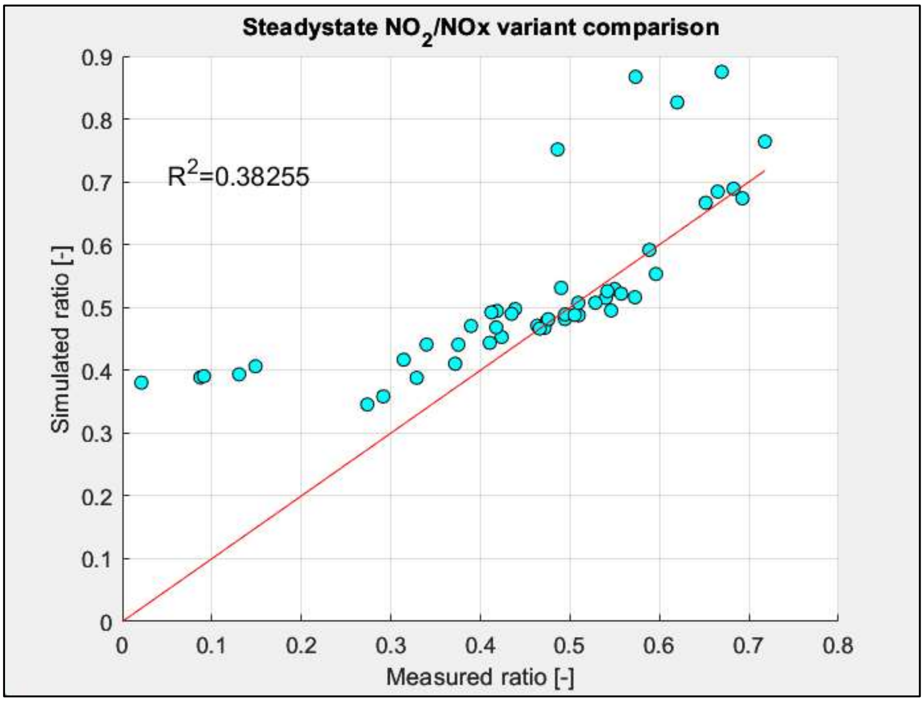

*Figure 33 Comparison between $NO_2$/NOx emission measured vs simulated. Global kinetic model, campaign 1.*

Excluding the temperature below 200°C the relative error is shown in Figure 34.

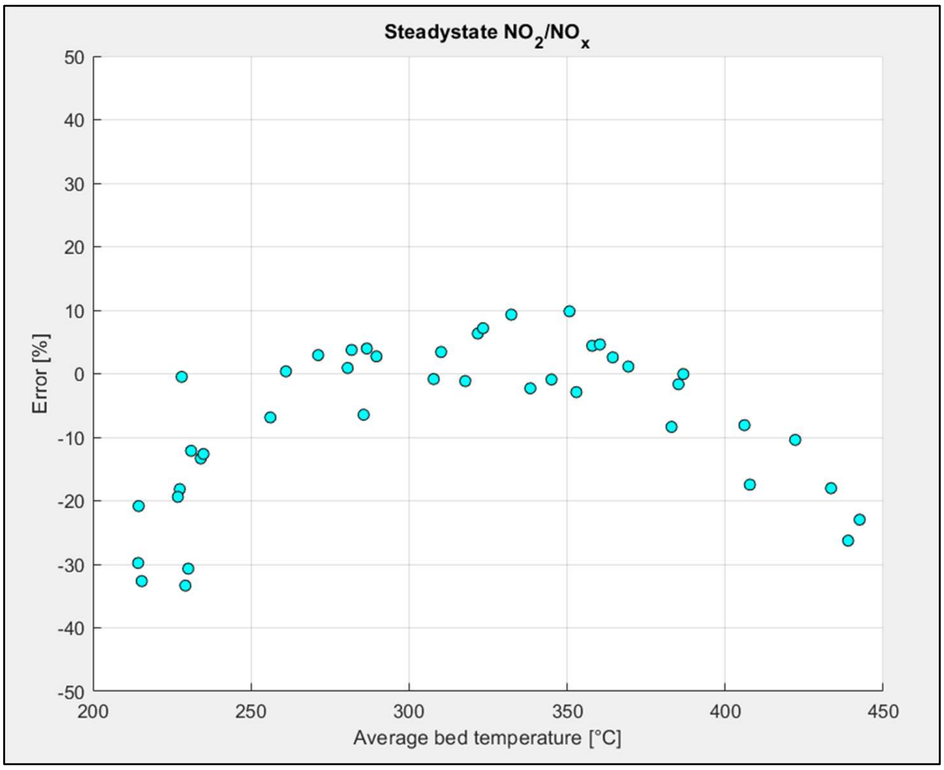

*Figure 34 Percentage error between measured and simulated $NO_2$/NOx emission. The calculation method of $NO_2$ is the "variant". Global kinetic model, campaign 1.*

Although the correlation between the measurements and the model is not satisfactory for $NO_2$/NOx, the validation procedure has been carried out anyway. The reported cycles are the most representative. The interested reader can find all the results in the appendix.

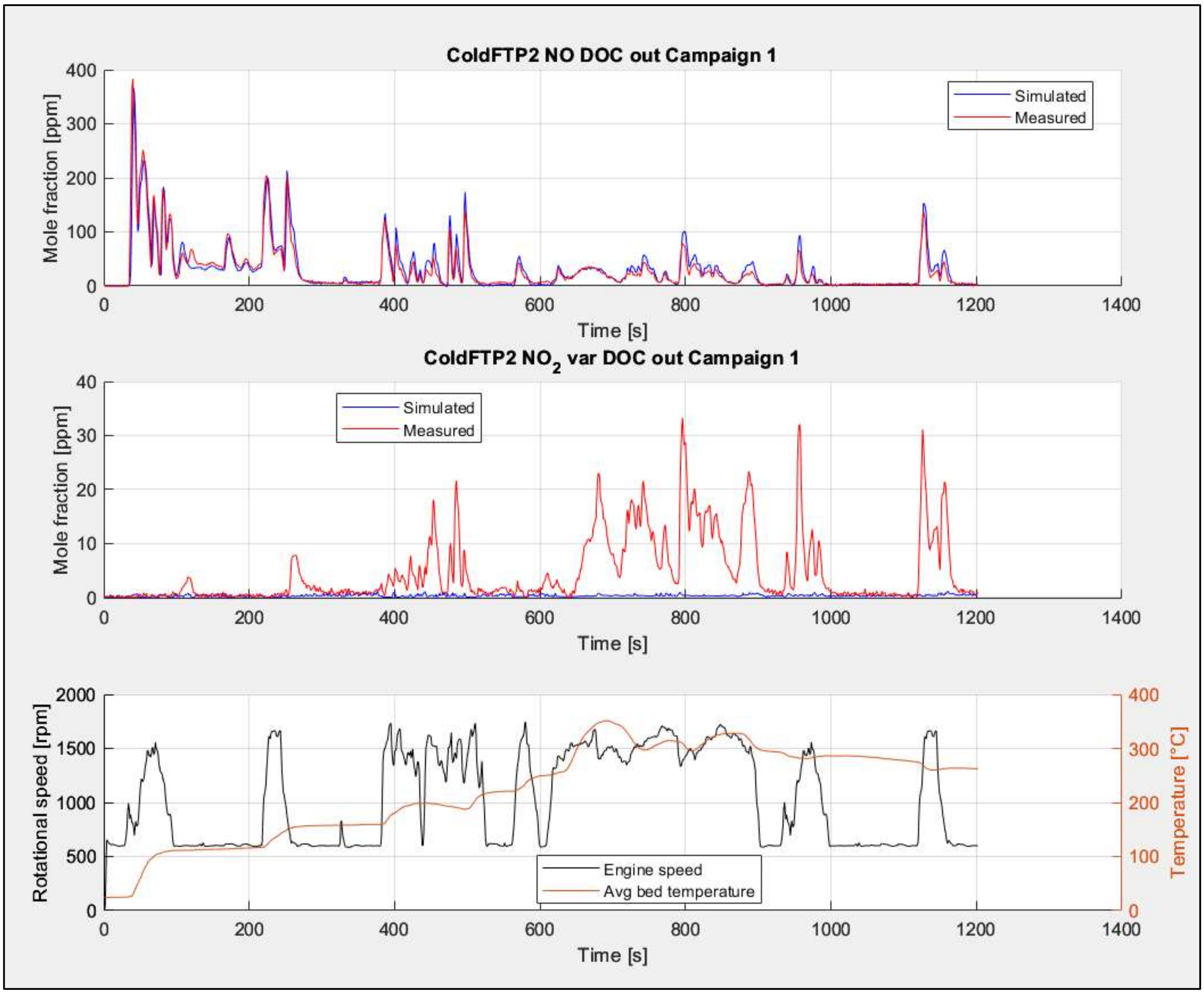

*Figure 35 NO and $NO_2$ ColdFTP cycle. Global kinetic model, campaign 1.*

The model is not able to predict the $NO_2$ emission, as the middle chart of Figure 35 illustrates. Also utilising the variant calculation method, expressed in Eq. *20* the results is similar. Probably the low amount of mole fraction does not allow to activate the inhibition function that should reduce the emitted quantity of NO. Another aspect to be considered is the combined effects of the species present in the exhaust stream; at low level of emission other species like $N_2O$ or ammonia slipped from SCR may lead to discrepancy between the simulation and the measures.

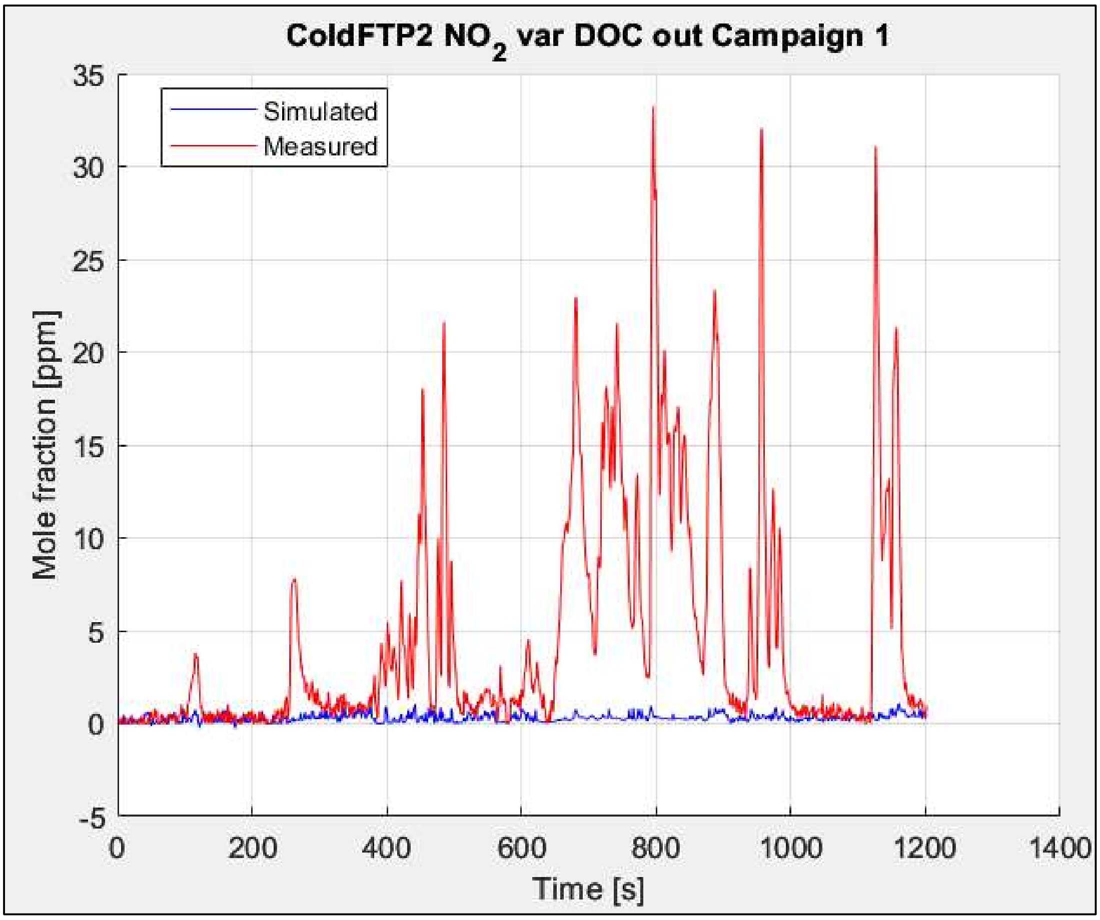

*Figure 36 NO$_2$ variant simulation output for ColdFTP cycle. Global kinetic model, campaign 1.*

For HotFTP the results are comparable, NO is predicted with sufficient accuracy while the model is unable to trace the $NO_2$ emission. As expected $NO_2/NO_x$ is also not adequate.

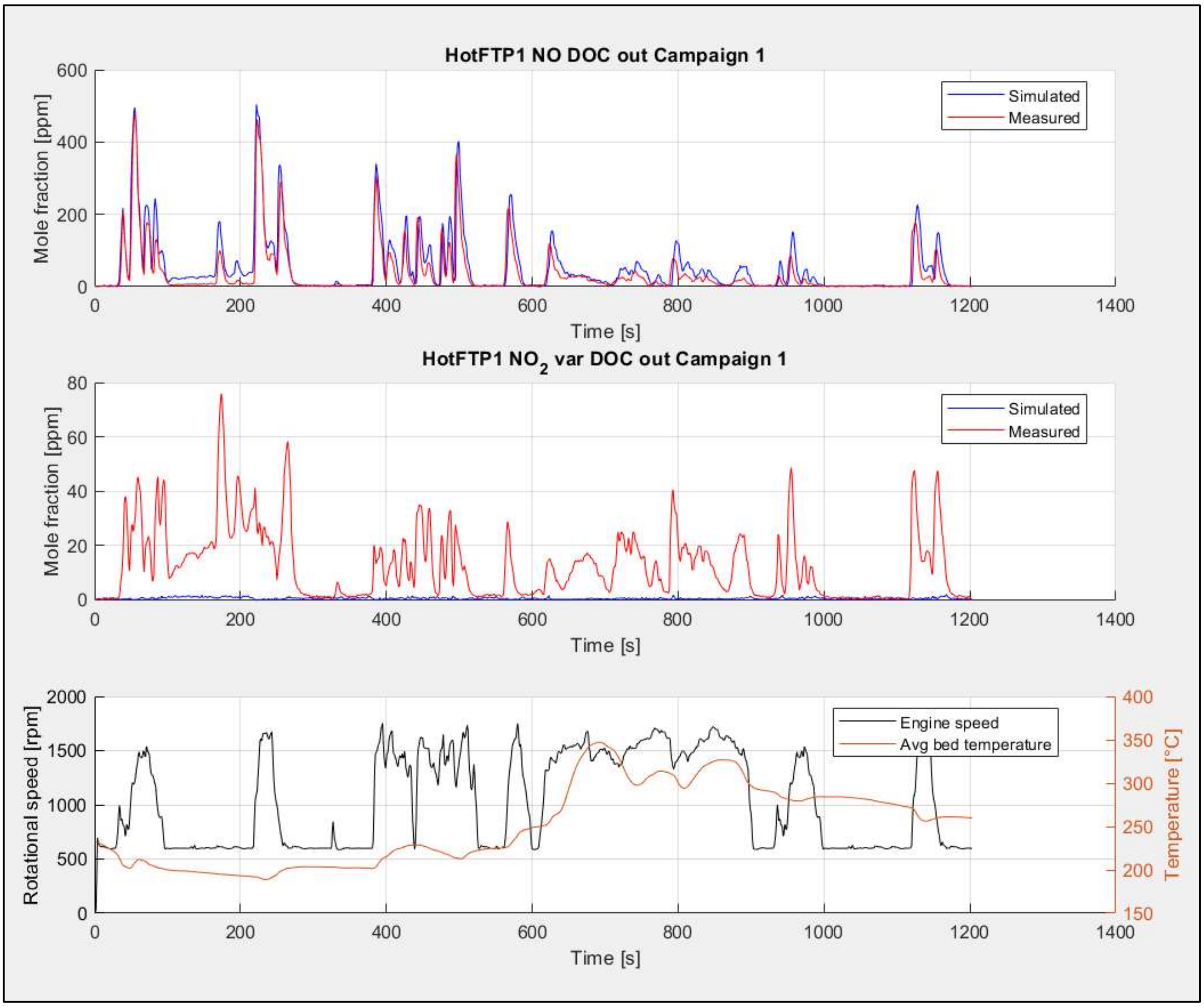

*Figure 37 NO and NO2 HotFTP cycle. Global kinetic model, campaign 1.*

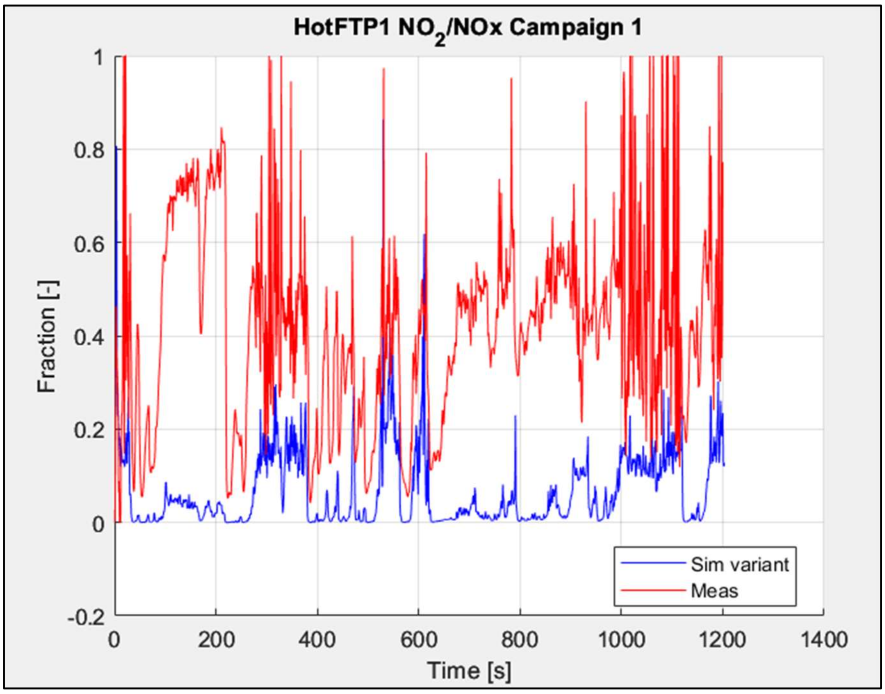

*Figure 38 NO2/NOx HotFTP cycle. Global kinetic model, campaign 1.*

### 4.4.2. Campaign 2: results and discussion

The first results reported are the steady operation.

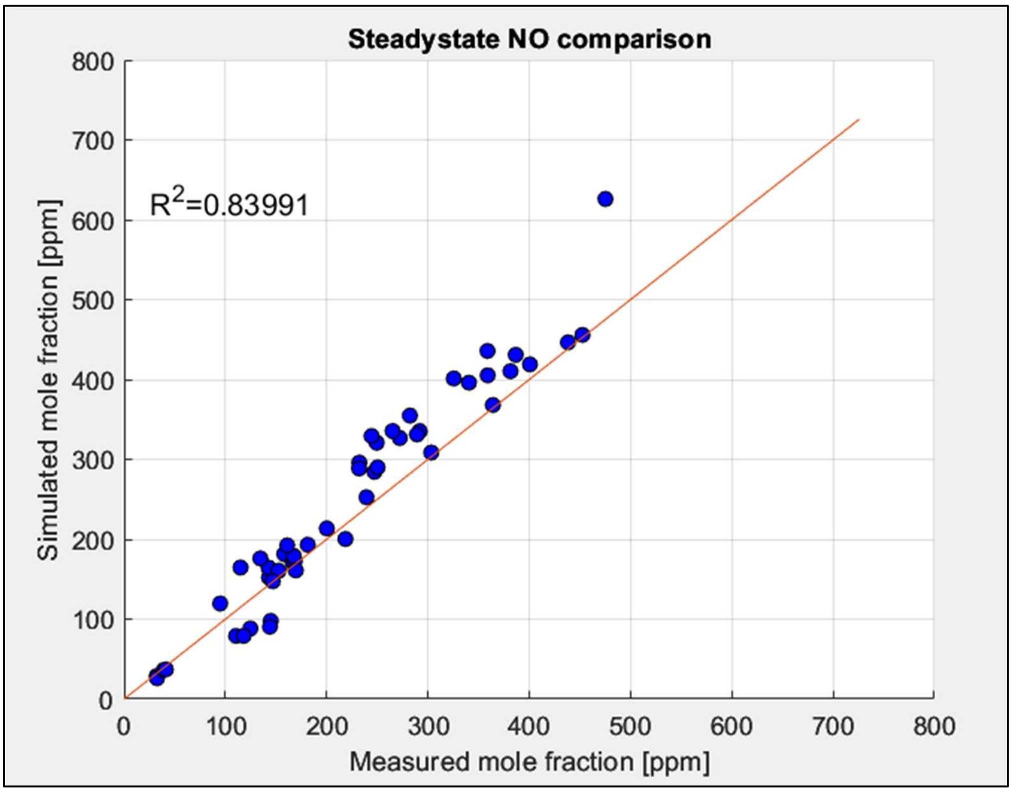

*Figure 39 Comparison between NO emission measured vs simulated. Global kinetic model, campaign 2.*

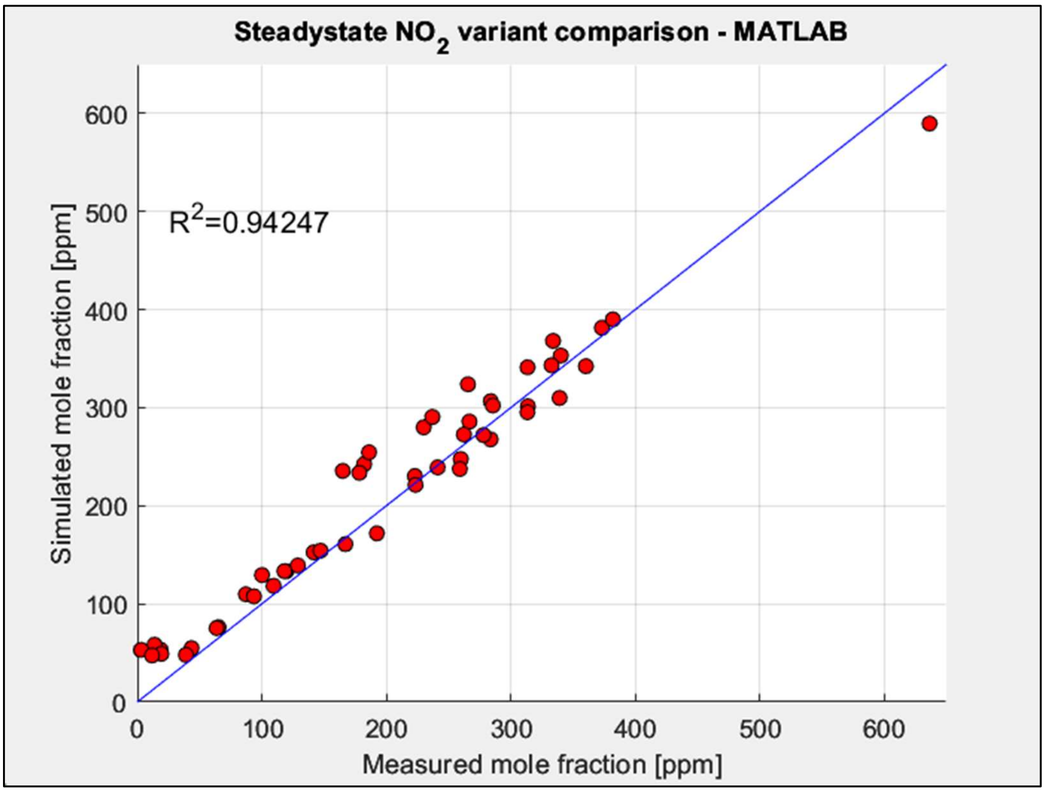

*Figure 40 Comparison between $NO_2$ emission measured vs simulated. Global kinetic model, campaign 2.*

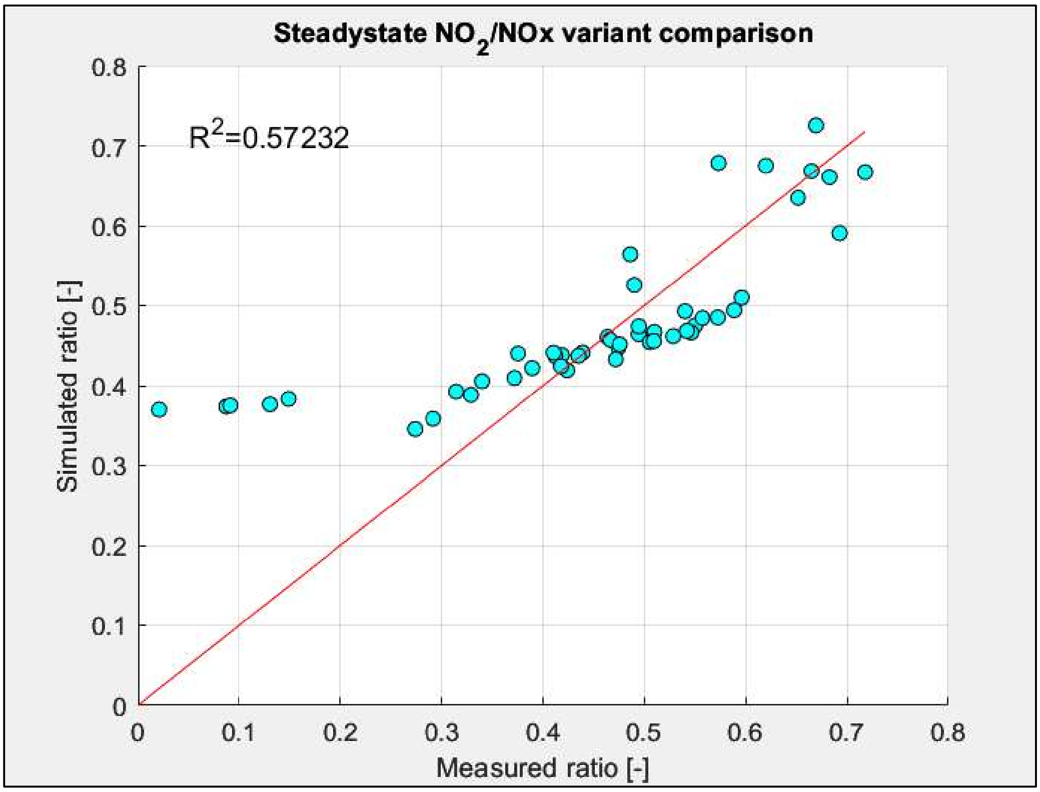

*Figure 41 Comparison between NO$_2$/NO$_x$ emission measured vs simulated. Global kinetic model, campaign 2.*

The optimization target was the NO$_2$/NO$_x$ in fact the R$^2$ of Figure 41 is lower of 33% compared with the results shown in Figure 33, 0.572 against 0.382. In both of optimization campaign 1 and 2 the largest relative error is localized at low emission levels. The largest error on NO$_2$/NO$_x$ occurs at low emitted quantities because small deviations in terms of ppm emitted result in a large relative error that is amplified by the ratio. Also, the error vs temperature trend is similar to the previous case as shown in Figure 42.

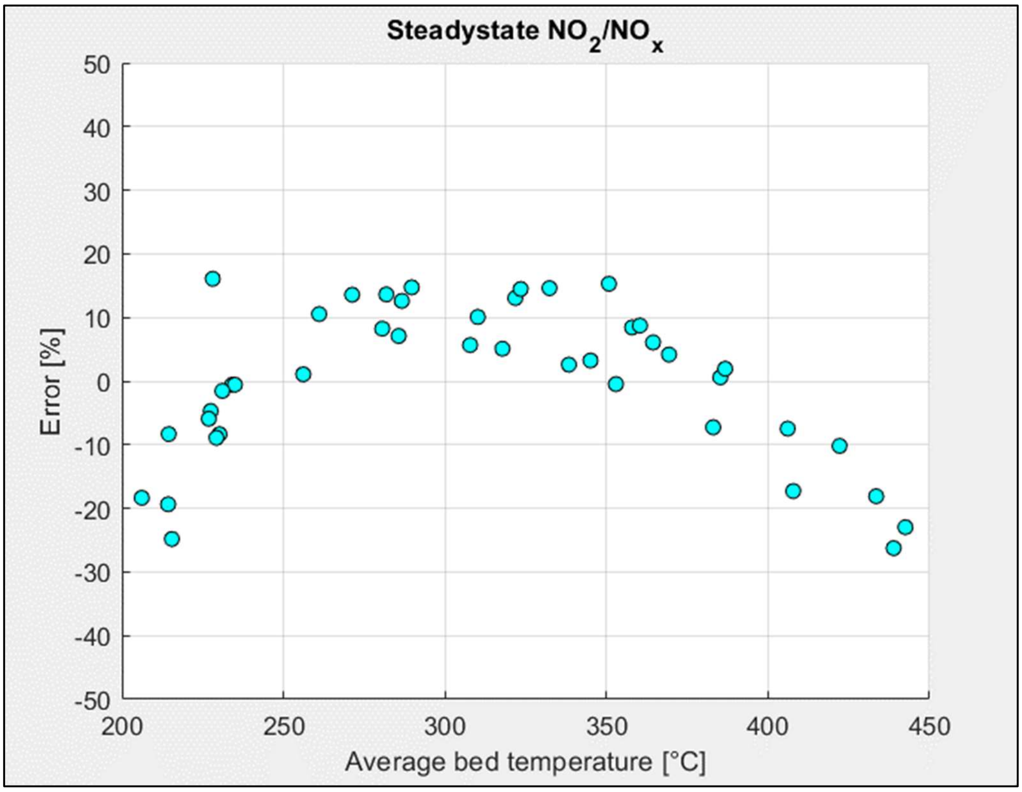

*Figure 42 Percentage error between measured and simulated $NO_2$/NOx emission. The calculation method of $NO_2$ is the "variant". Global kinetic model, campaign 2.*

Graph of the driving cycles follows, the same consideration made for the previous set of rate constant and inhibition terms can be made.

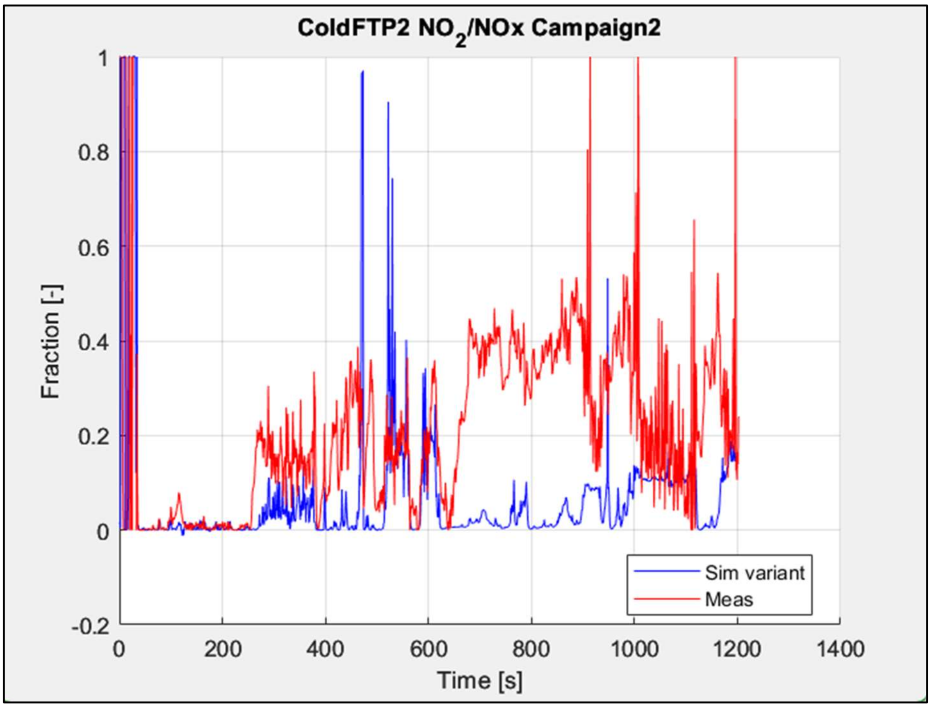

*Figure 43 NO2/NOx ColdFTP cycle. Global kinetic model, campaign 2.*

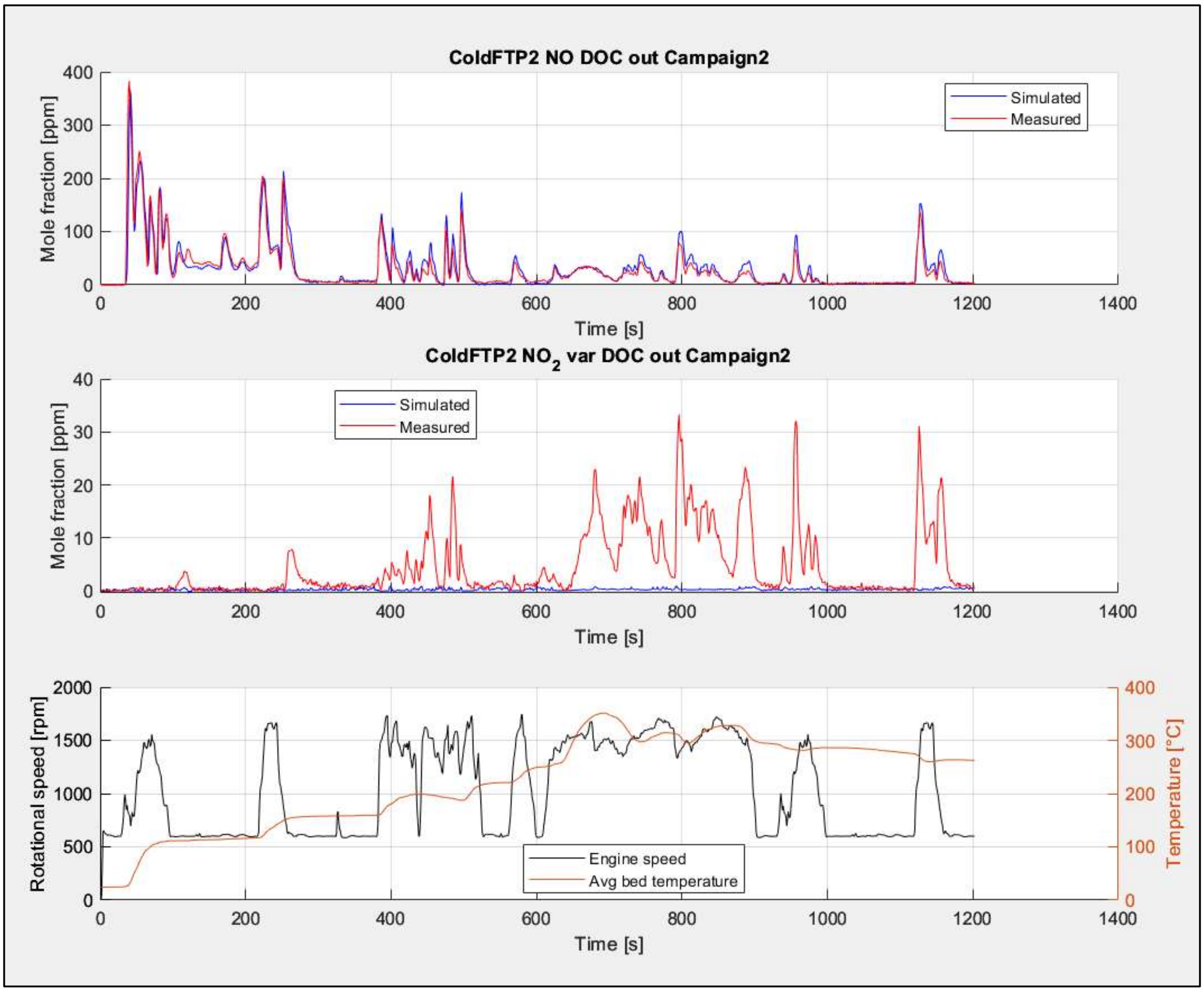

*Figure 44 NO and NO2 ColdFTP cycle. Global kinetic model, campaign 2.*

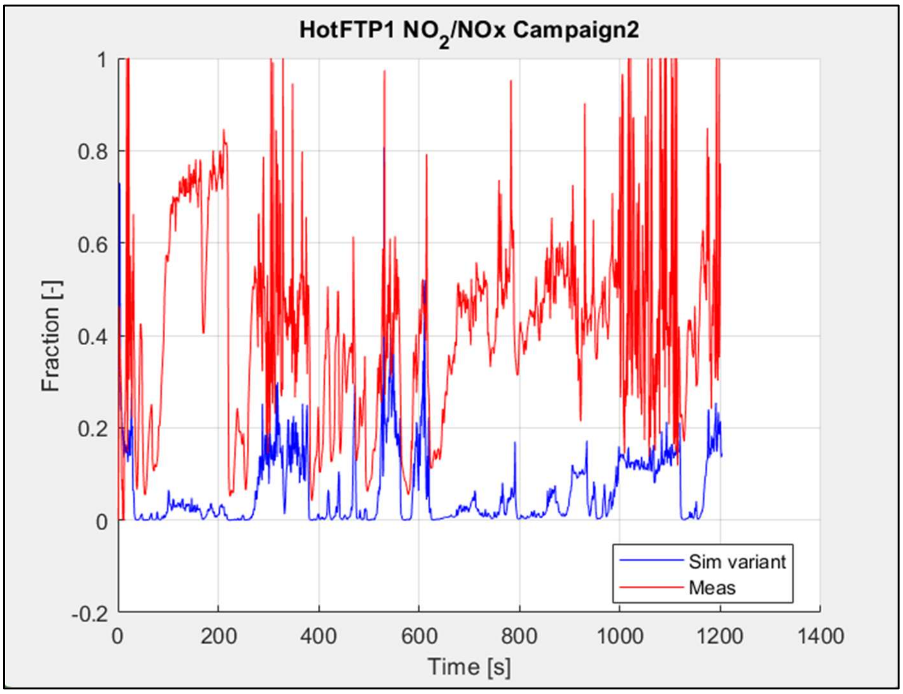

*Figure 45 NO2/NOx HotFTP cycle. Global kinetic model, campaign 2.*

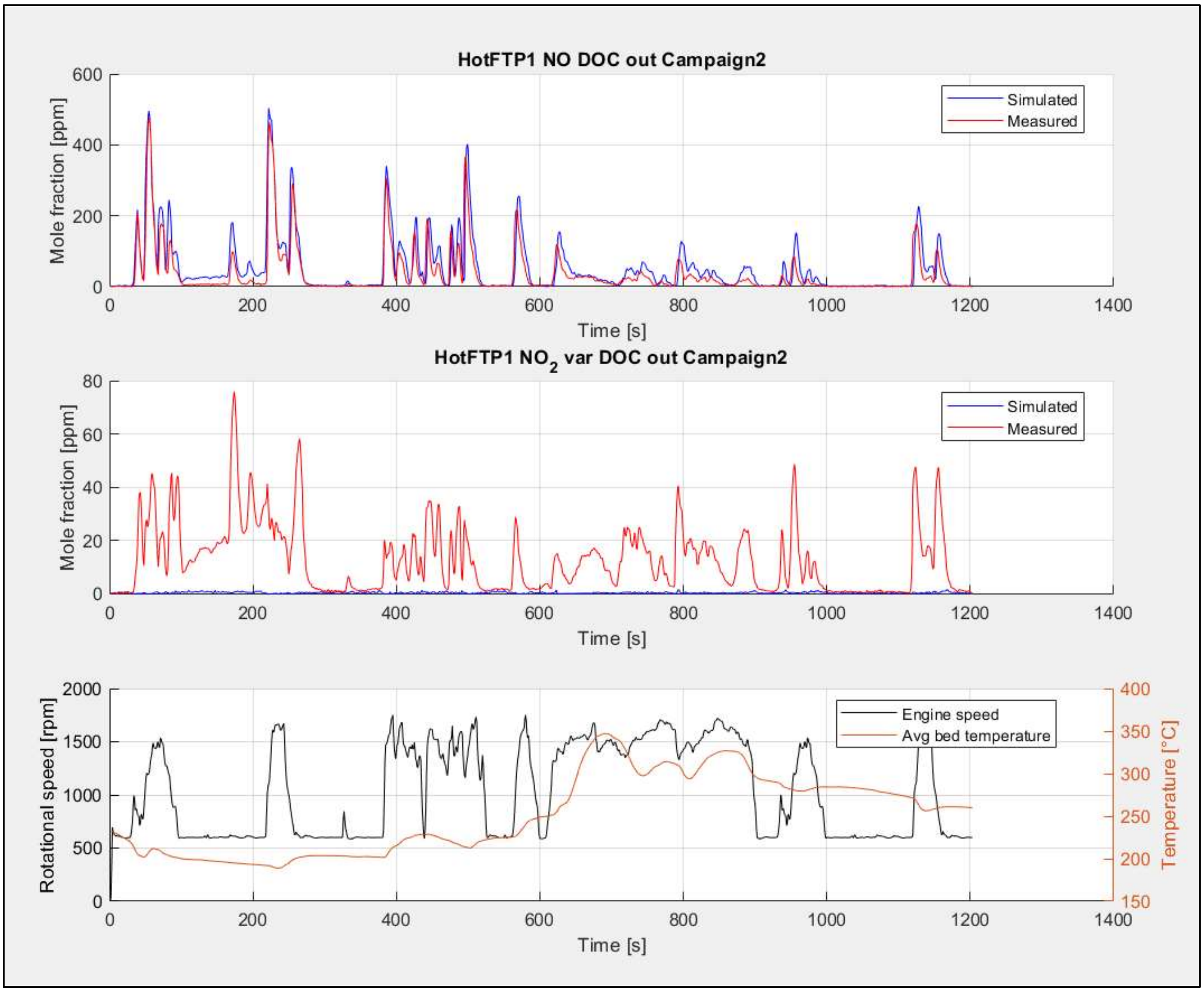

*Figure 46 NO and NO2 HotFTP cycle. Global kinetic model, campaign 2.*

### 4.4.3. *"All-in one"*: results and discussion

The time spent to achieve the *"All-in one"* parameters was about twice as long as in *campaign 1* and *campaign 2* but despite this the results is less accurate than the previous ones, as Figure 47 shows. This should suggest that the procedure to be followed is the one exposed in "Campaign 1" and "Campaign 2".

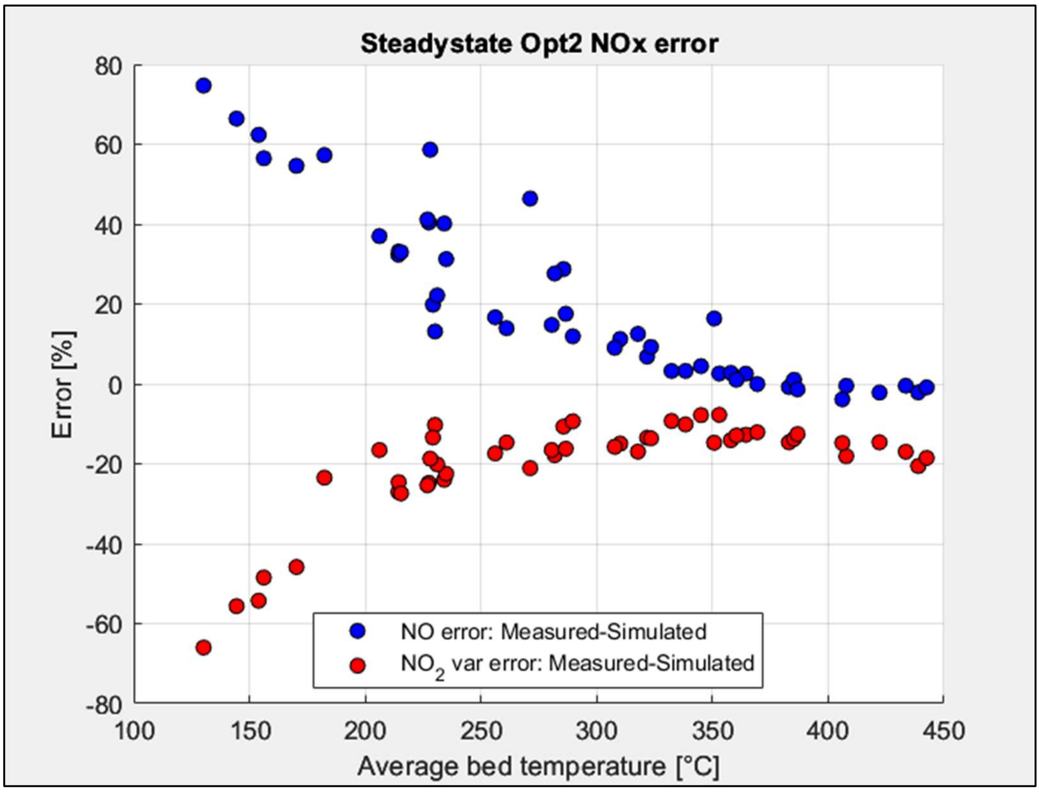

5

*Figure 47 Percentage error between measured and simulated NOx emission. Global kinetic model, "All-in one".*

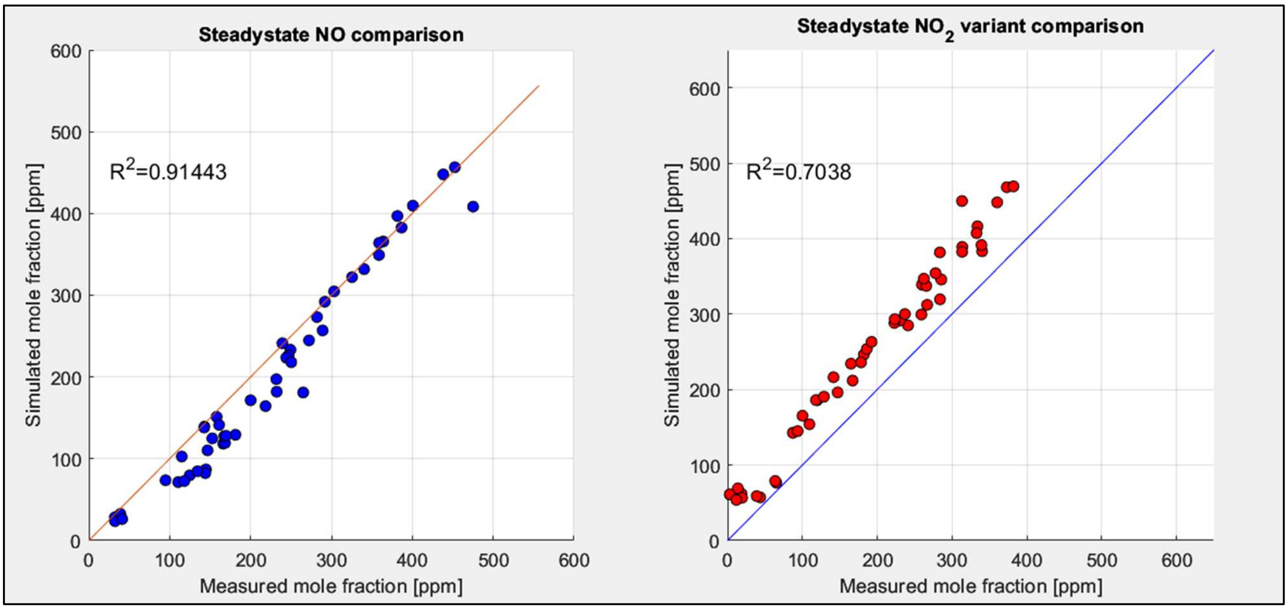

*Figure 48 Comparison plot for NO and NO₂. NO₂ is calculated using the variant methood Global kinetic model, "All-in one".*

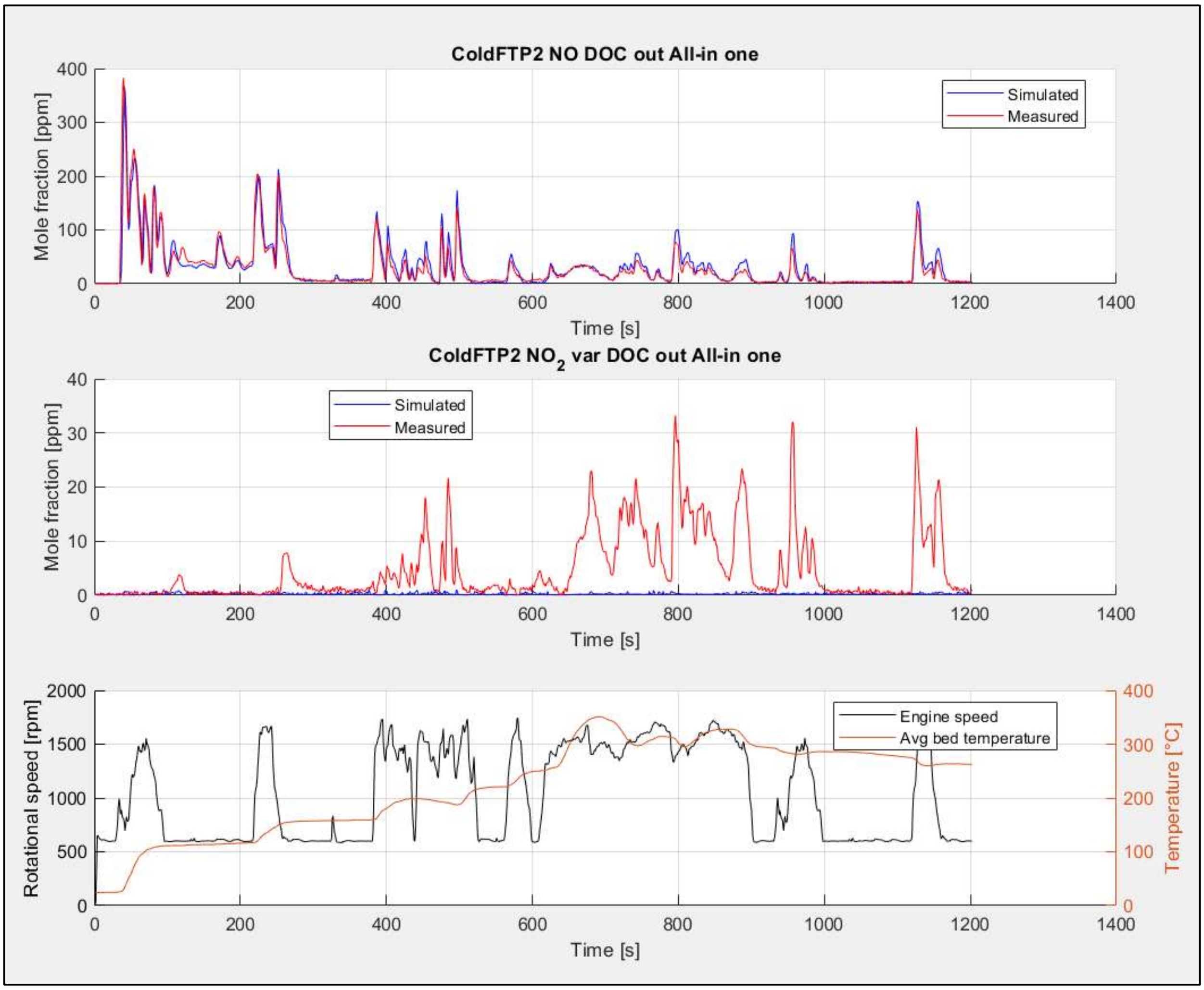

*Figure 49 NO and NO2 ColdFTP cycle. Global kinetic model, "All-in one"*

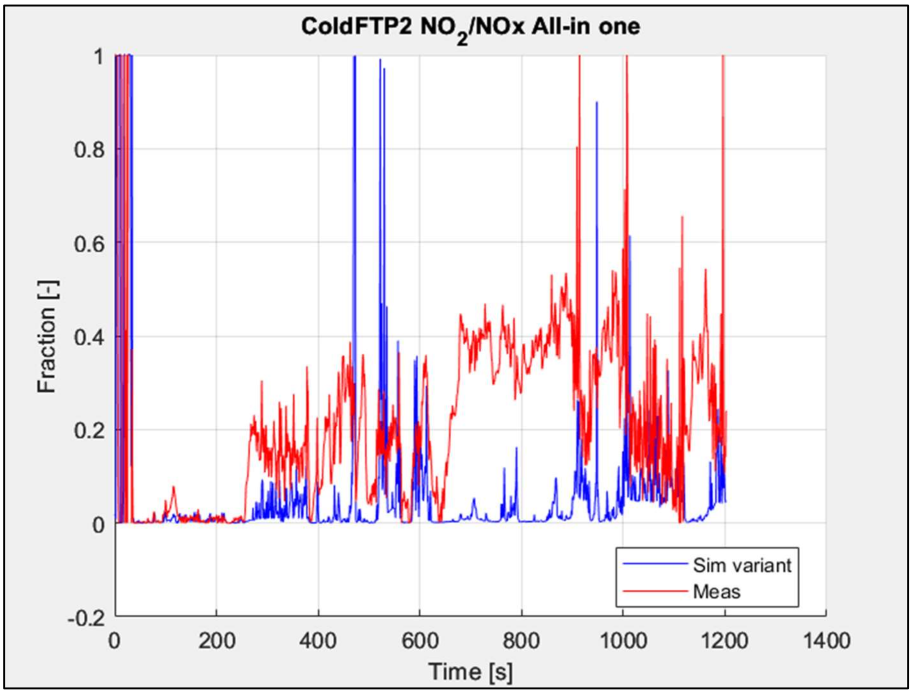

*Figure 50 NO2/NOx ColdFTP cycle. Global kinetic model, "All-in one".*

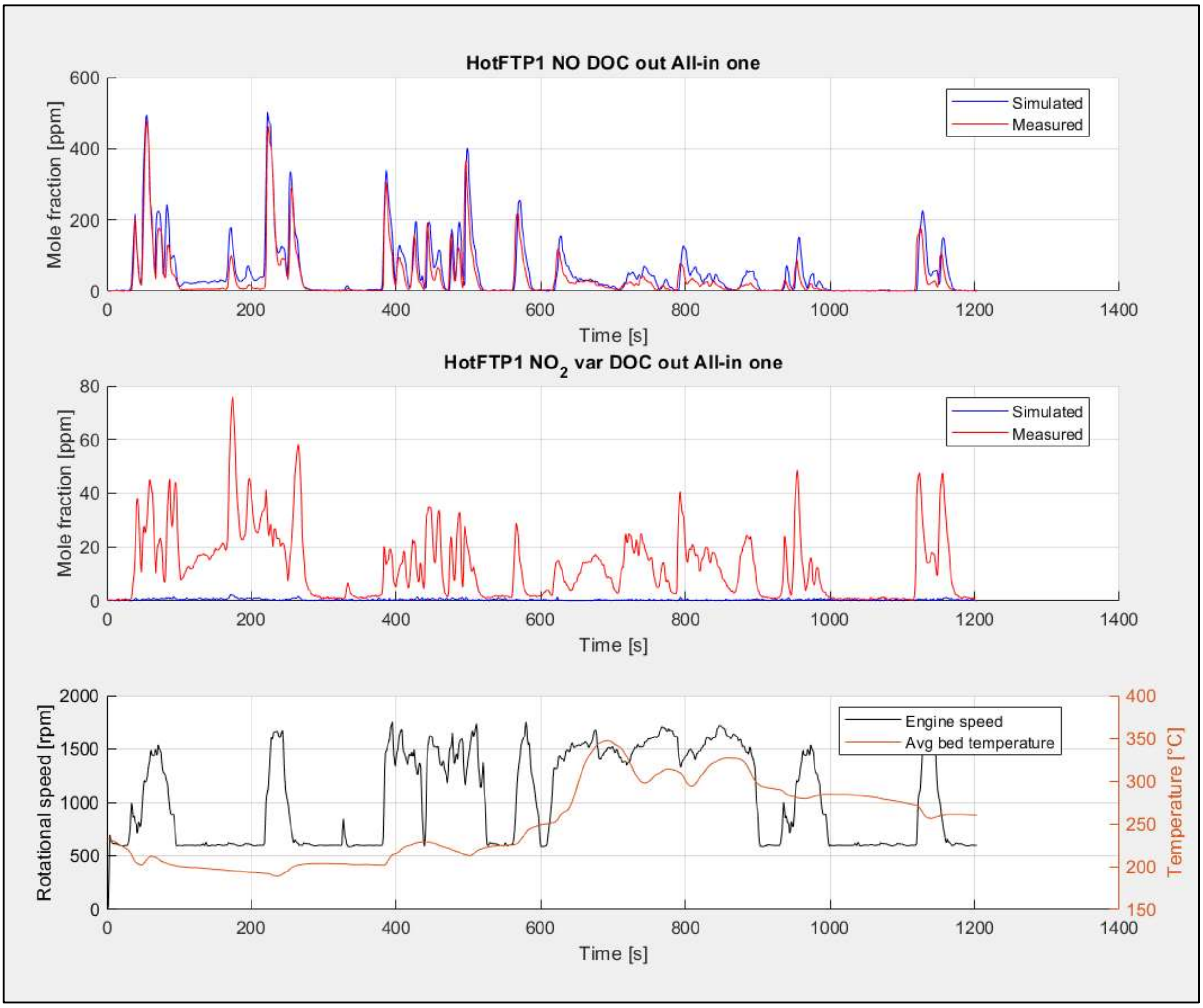

*Figure 51 NO and NO2 HotFTP cycle. Global kinetic model, "All-in one"*

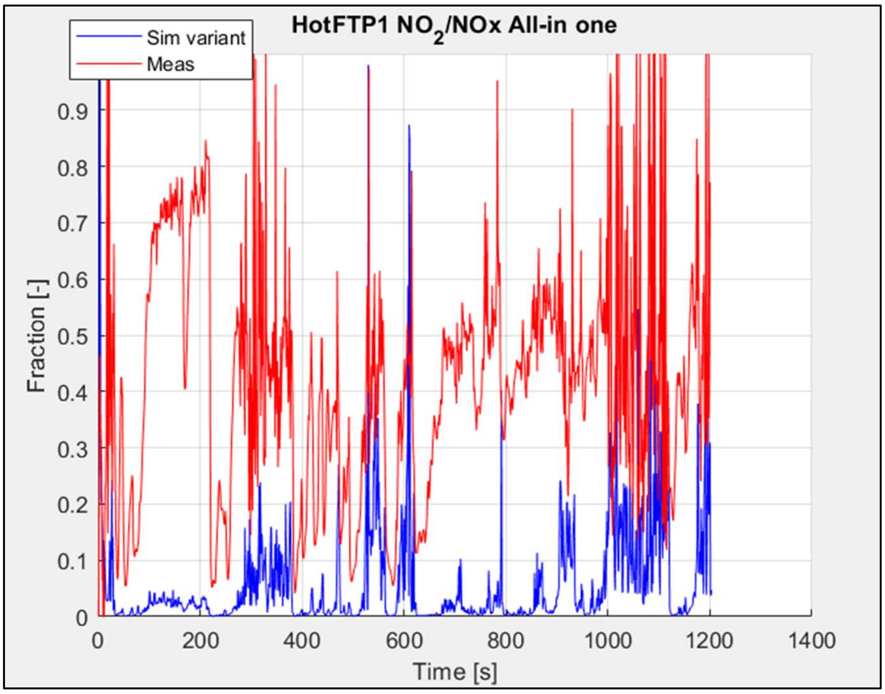

*Figure 52 NO2/NOx HotFTP cycle. Global kinetic model, “All-in one”.*

# 5. Conclusion

This work stems from SwRI's desire to test different DOC modelling techniques in order to be able to compare the benefits obtainable from each type of modelling. Having a complete model of the exhaust line makes it possible to exploit the synergy of the two components: the DOC placed upstream of the SCR is able to adjust the ratio between NO2 and NO to a level that allows the SCR to reach light-off at low temperatures. The work focuses on modelling the NO oxidation reaction that takes place in the DOC channels. In order to find the best modelling technique, two different methods were investigated:

- the model based on conversion maps
- the model based on global kinetics

The use of previously measured data to construct conversion maps offers the advantage of a model that is easy to build and has a fair degree of accuracy. On the other hand, it is necessary to rely on a wide range of data ranging over multiple combinations of space-velocity and catalytic bed temperature to obtain a model capable of predicting a driving cycle, see results in chapter 4.1

On the other hand, the model based on global kinetics is capable of predicting the NO conversion rate under a variety of conditions, provided that an accurate calibration of the kinetic parameters has been made. Precisely the calibration is the key point in order to obtain a reliable model. Specifically in this work, the Global Kinetic model was developed in parallel on two simulation environments. In this way, the features of both pf them were exploited: GT-Power and MATLAB.  Using GT-Power, a first model was built in order to calibrate the constants, and then using MATLAB environment, the final model was built. In this way, the speed of model creation via GT-Power was combined with the flexibility of MATLAB.

The performance of both models can be considered as good starting points for further development and for achieving a more accurate predict the NO2/NOx ratio, which is crucial for defining whether the conditions generated by the DOC are advantageous for the SCR. The critical issue with the map-based model is the narrow range of tests available to generate the conversion maps. This leads to limited maps that are unable to define the operating points we find in a driving cycle, generating void points in the simulation result.

The global kinetics model is able to predict NO emissions with very good accuracy in most of the cycles used for validation. The result for the NO2/NOx ratio can be improved by including dynamic tests in the calibration set to represent all those conditions that the stationary points are unable to express. A substantial difference between the stationary data used for calibration and the driving cycles lies in the emission level of the NO2 species. This in fact ranged between 100ppm and 600ppm mole fraction in the calibration data. Looking at the emission values in the driven cycles, we can see that this value is between 20ppm and 120ppm.

Although the global kinetic model cannot provide an accurate prediction on transient cycles, it provides accurate indications of NO oxidation with stationary data. Deepening the calibration procedure by including specific non-stationary data sets will probably improve the model's predictive capabilities.

# 6. References

[1] Rao, S., Sarlashkar, J., Rengarajan, S., Sharp, C. et al., “A Controls Overview on Achieving Ultra-Low NOx,” SAE Technical Paper 2020-01-1404, 2020, doi:10.4271/2020-01-1404

[2] Zavala, B., Sharp, C., Neely, G., and Rao, S., “CARB Low NOX Stage 3 Program - Aftertreatment Evaluation and Down Selection,” SAE Technical Paper 2020-01-1402, 2020, doi:10.4271/2020-01-1402.

[3] Meruva, P., Matheaus, A., Zavala, B., Sharp, C. et al., "Application of Model-Based Controller on a Heavy-Duty Dual Selective Catalytic Reduction Aftertreatment," SAE Int. J. Engines 16(5):2023 doi:10.4271/03-16-05-0040

[4] Sampara, C. & Bissett, E. & Chmielewski, M. (2007). Global Kinetics for a Commercial Diesel Oxidation Catalyst with Two Exhaust Hydrocarbons. Industrial & Engineering Chemistry Research - IND ENG CHEM RES. 47. 10.1021/ie070813x.

[5] Mallamo, F. & Longhi, S. & Millo, F.& Rolando, L. (2013). Modeling of diesel oxidation catalysts for calibration and control purpose. International Journal of Engine Research. 15. 965-979. 10.1177/1468087413492526.

[6] Diffusion of halogenated hydrocarbons in helium. The effect of structure on collision cross sections E. N. Fuller, K. Ensley, and J. C. Giddings. The Journal of Physical Chemistry 1969 73 (11), 3679-3685 DOI: 10.1021/j100845a020

[7] Gamma Technologies LLC, GT-SUITE Aftertreatment Manual, 2021.

[8] Shampine, L. F. and M. W. Reichelt, “The MATLAB ODE Suite,” SIAM Journal on Scientific Computing, Vol. 18, 1997, pp. 1–22.

# 7. Appendix

Will follow the results of the optimization campaign 1 and 2.

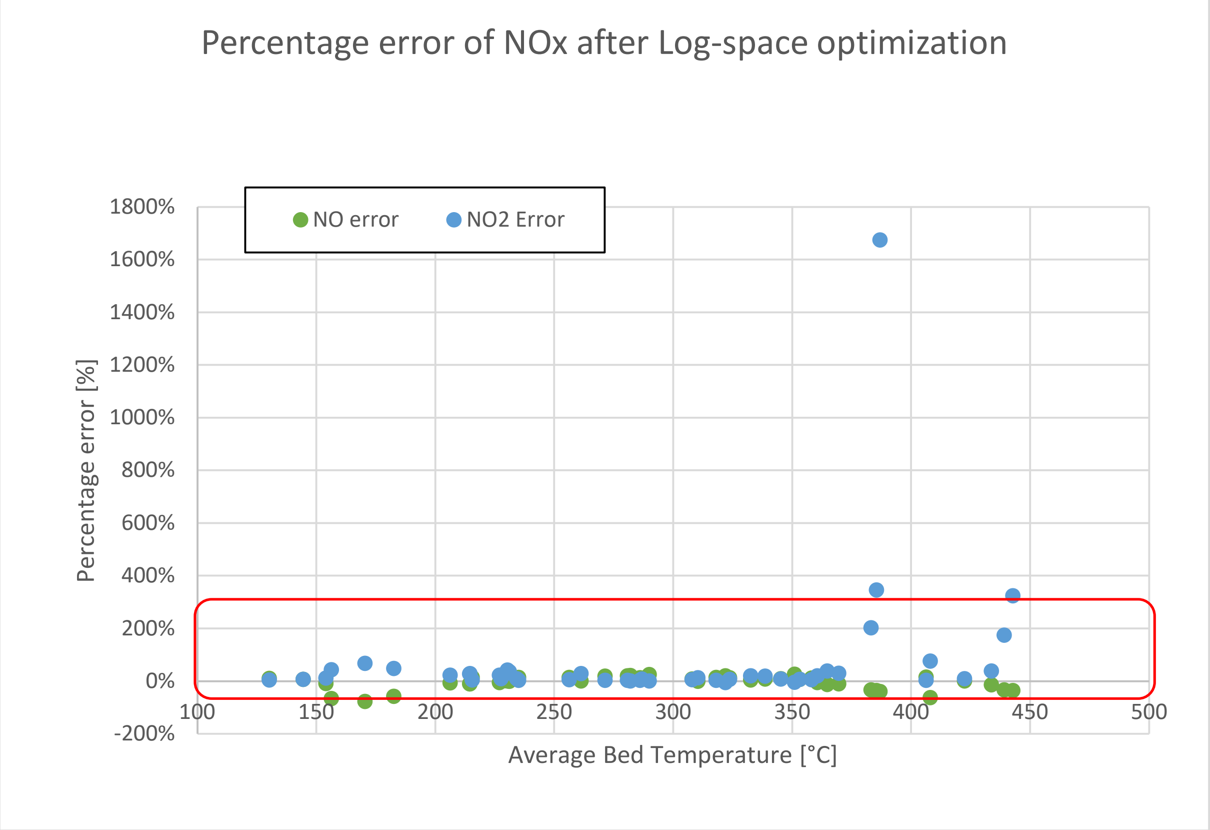

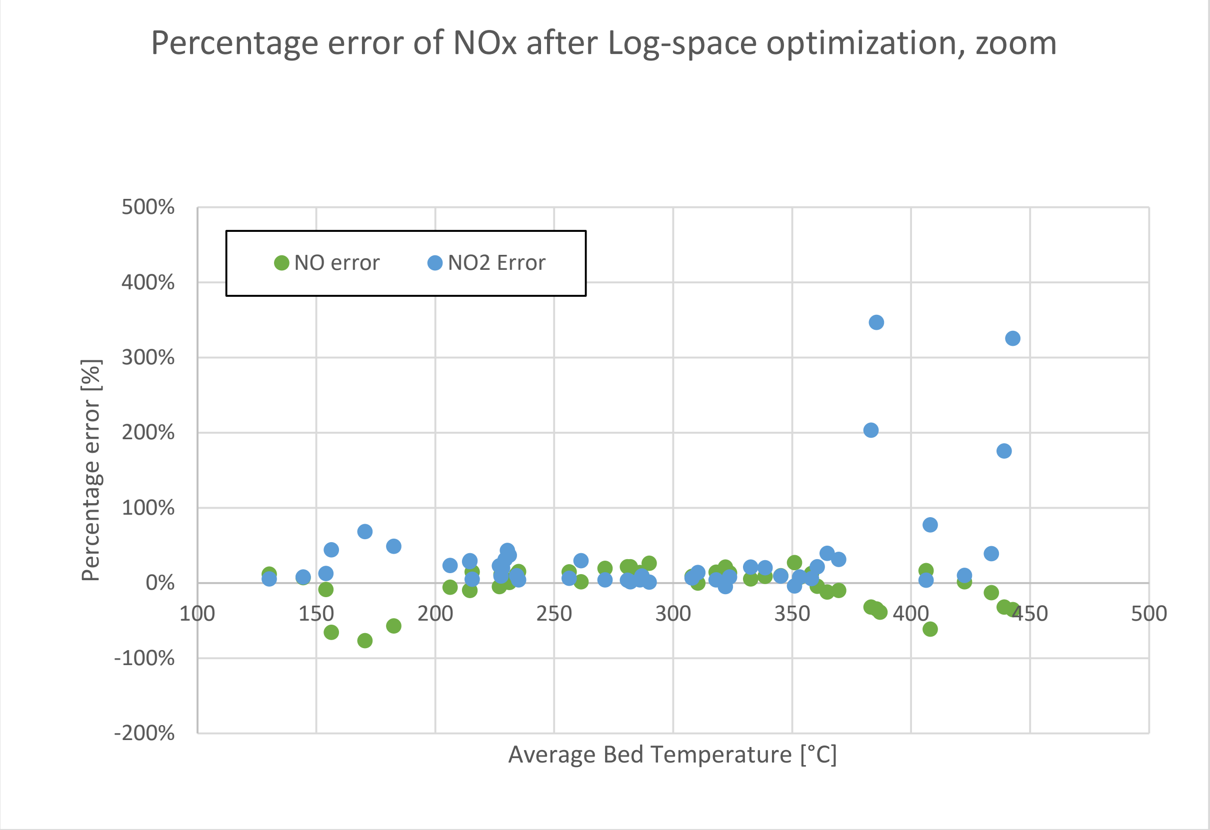

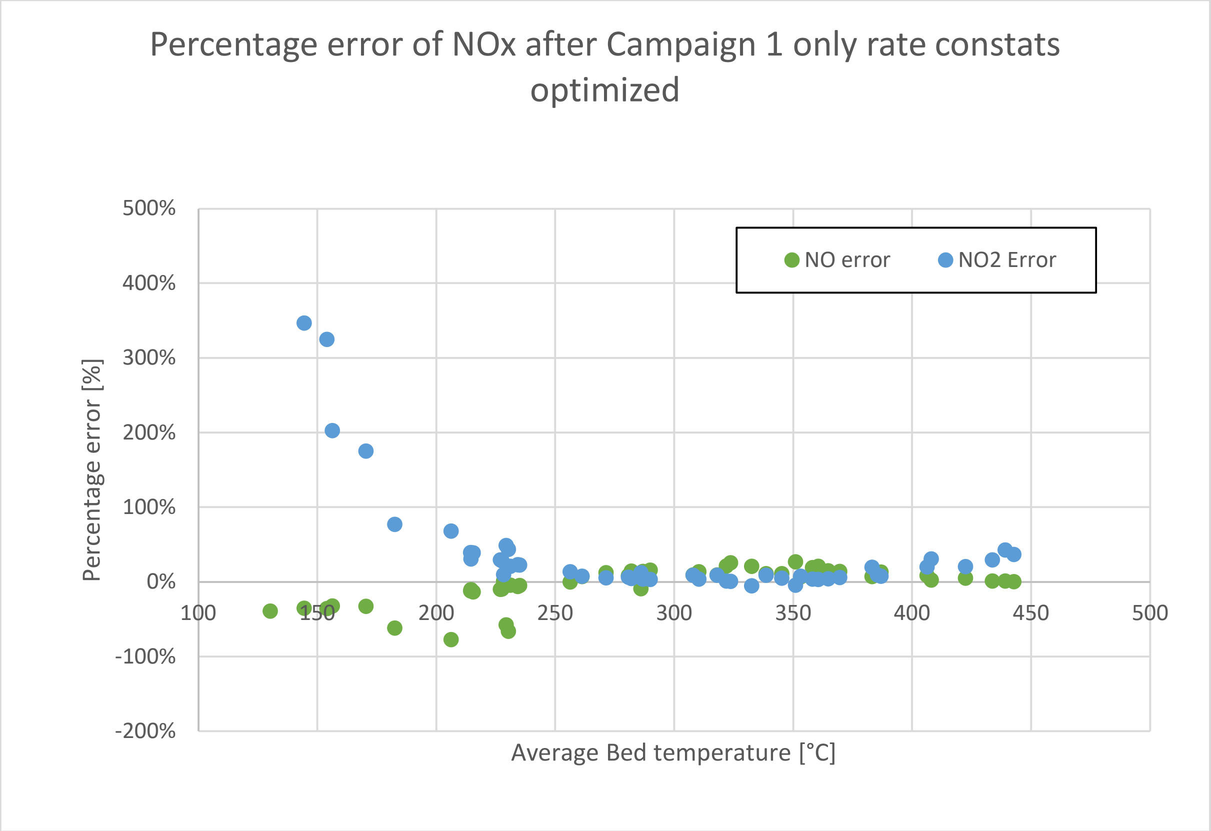
Percentage error of NOx after Campaign 1 only rate constats optimized

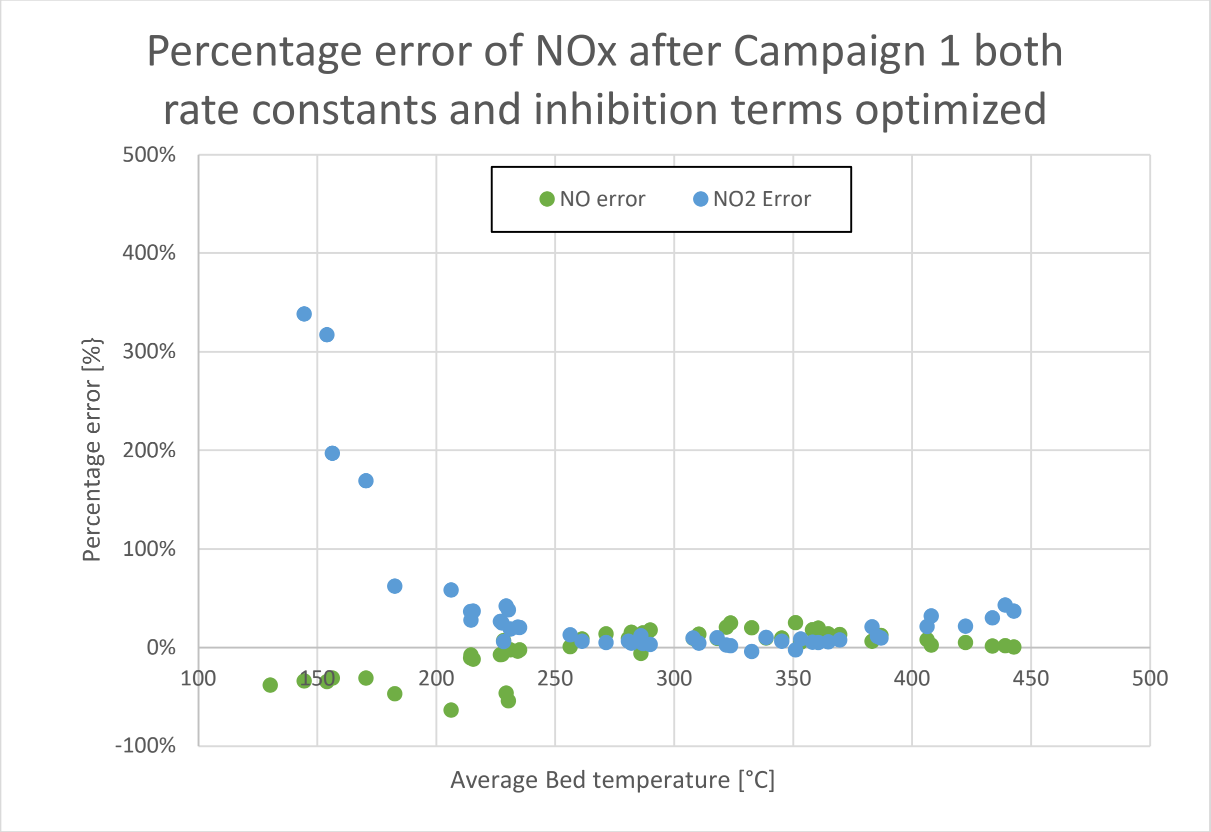
Percentage error of NOx after Campaign 1 both rate constants and inhibition terms optimized

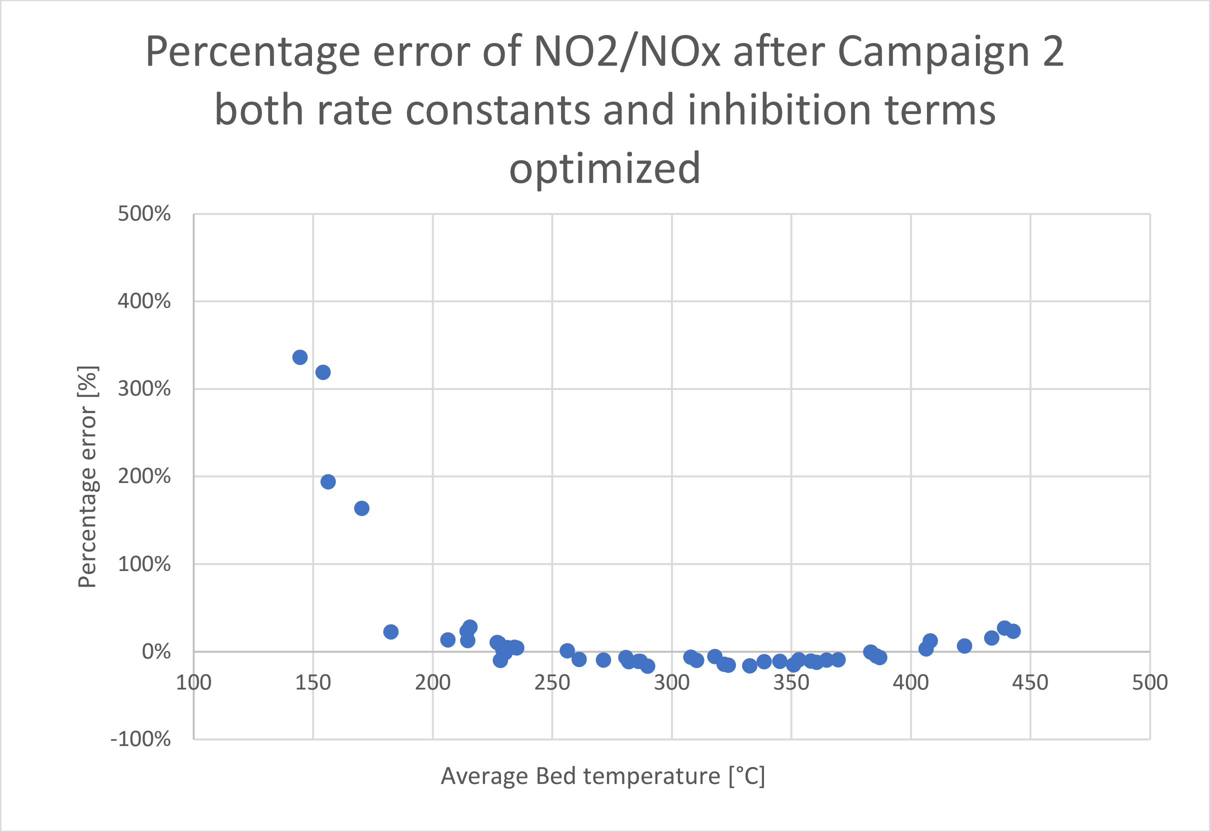
Percentage error of NO2/NOx after Campaign 2 both rate constants and inhibition terms optimized
500%
400%
300%
200%
100%
0%
-100%
Percentage error [%]
100
150
200
250
300
350
400
450
500
Average Bed temperature [°C]

The following pages show the graphs of the driving cycles with the parameters resulting from optimisation campaign 1, which show the best correlation.

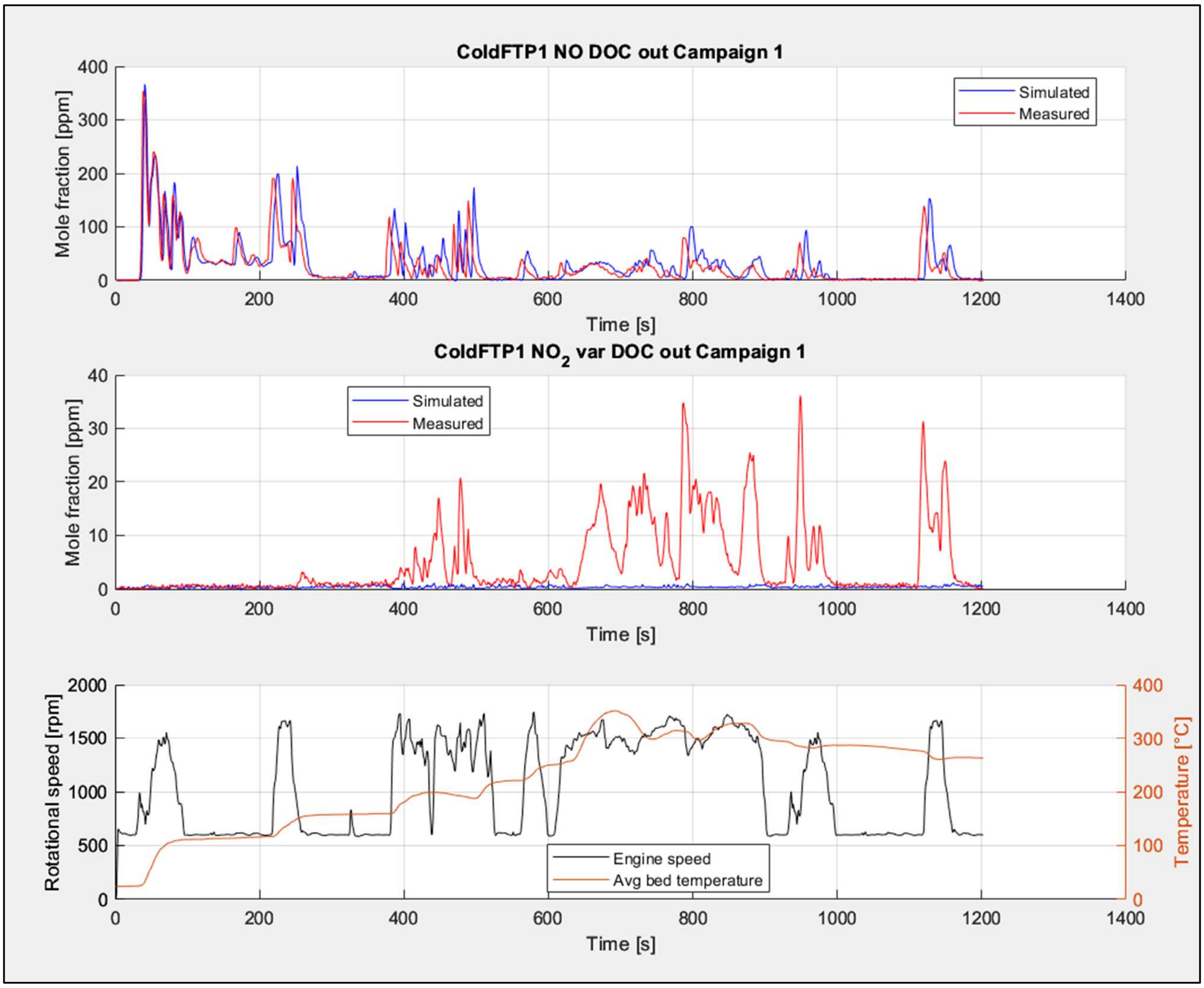

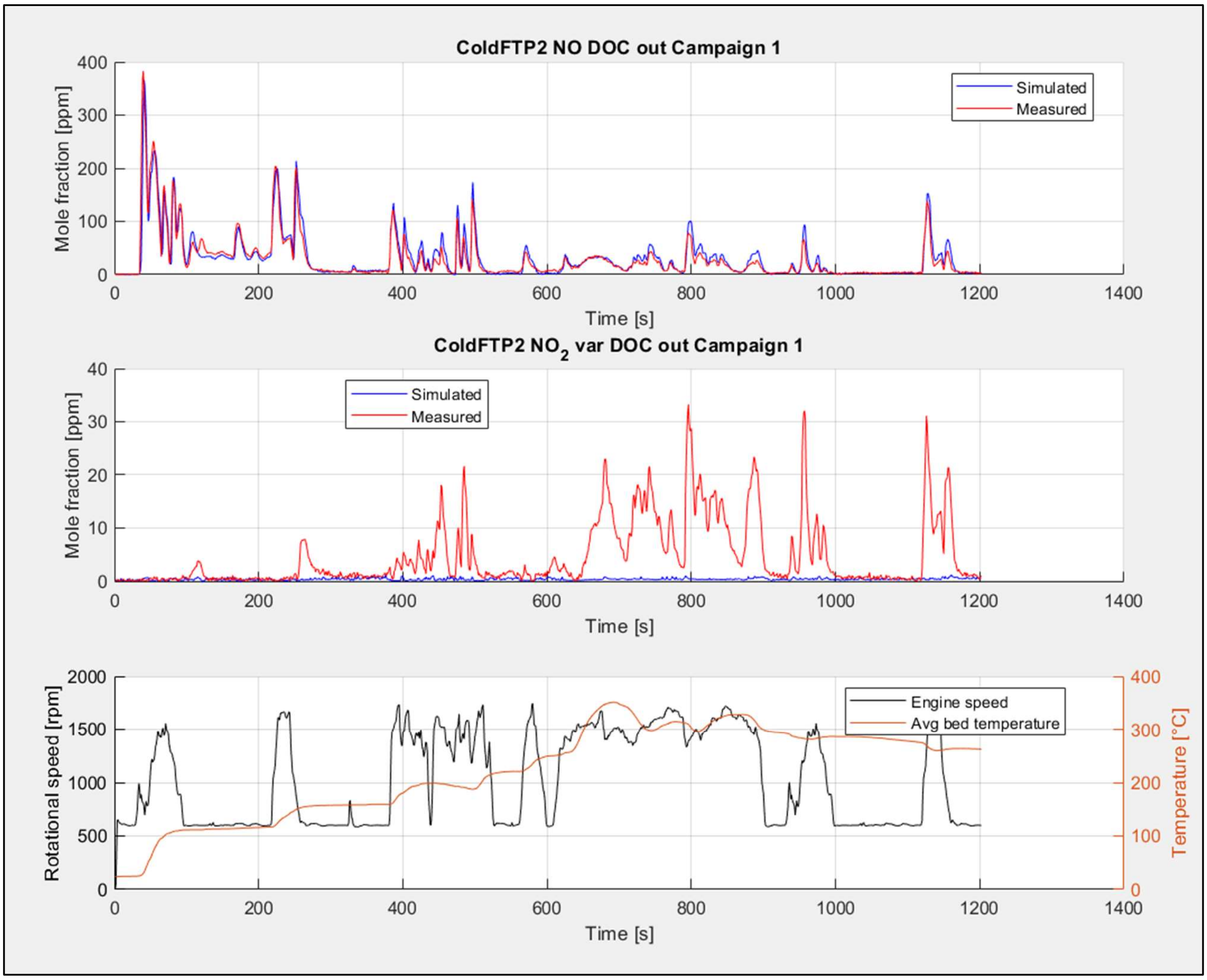
ColdFTP2 NO DOC out Campaign 1
Mole fraction [ppm]
Time [s]
Simulated
Measured
ColdFTP2 NO$_2$ var DOC out Campaign 1
Mole fraction [ppm]
Time [s]
Simulated
Measured
Rotational speed [rpm]
Temperature [°C]
Time [s]
Engine speed
Avg bed temperature
0
100
200
300
400
0
10
20
30
40
0
500
1000
1500
2000
0
200
400
600
800
1000
1200
1400

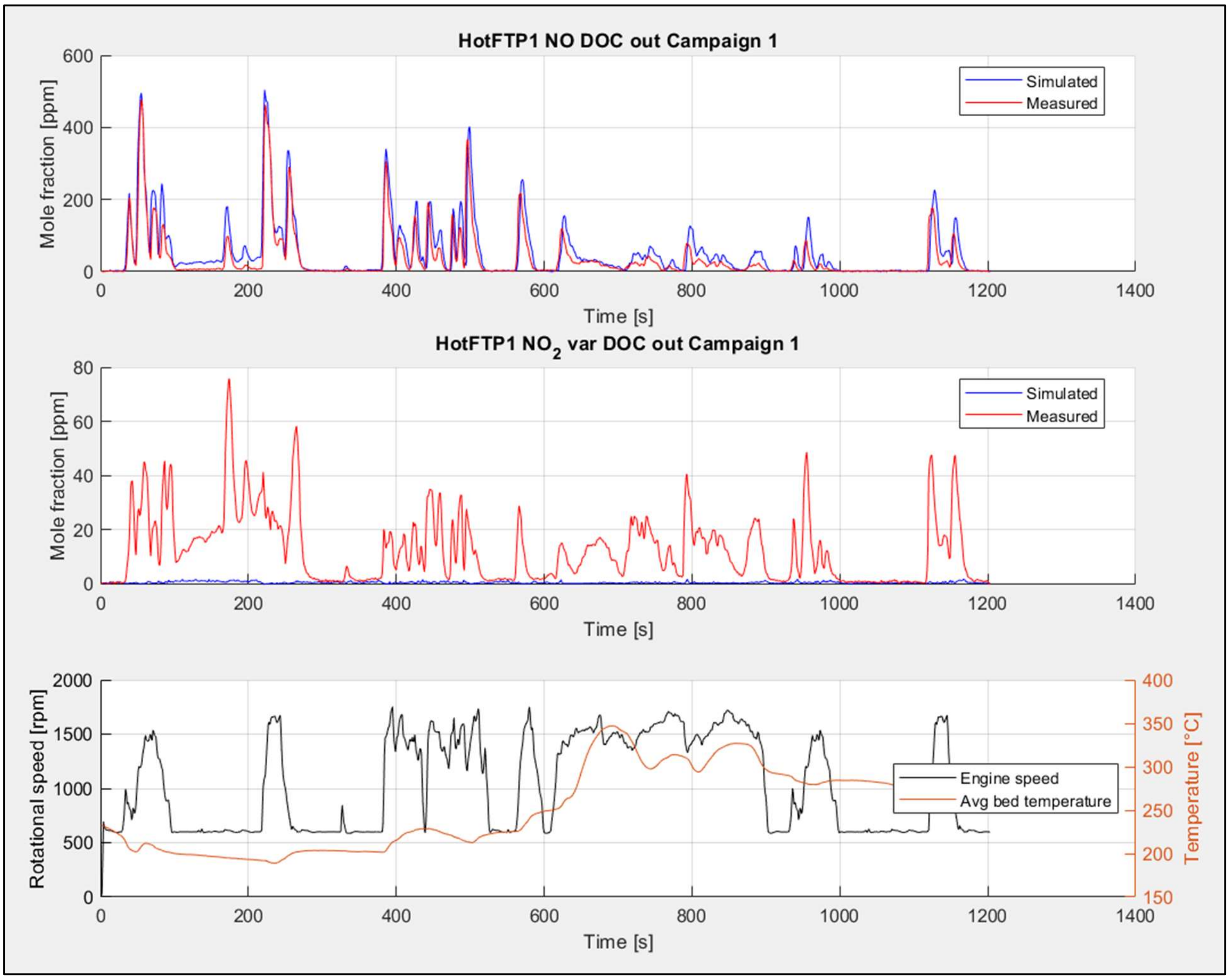
HotFTP1 NO DOC out Campaign 1
Mole fraction [ppm]
Time [s]
Simulated
Measured
HotFTP1 $NO_2$ var DOC out Campaign 1
Mole fraction [ppm]
Time [s]
Simulated
Measured
Rotational speed [rpm]
Temperature [°C]
Time [s]
Engine speed
Avg bed temperature
0
200
400
600
800
1000
1200
1400
0
20
40
60
80
0
500
1000
1500
2000
150
200
250
300
350
400

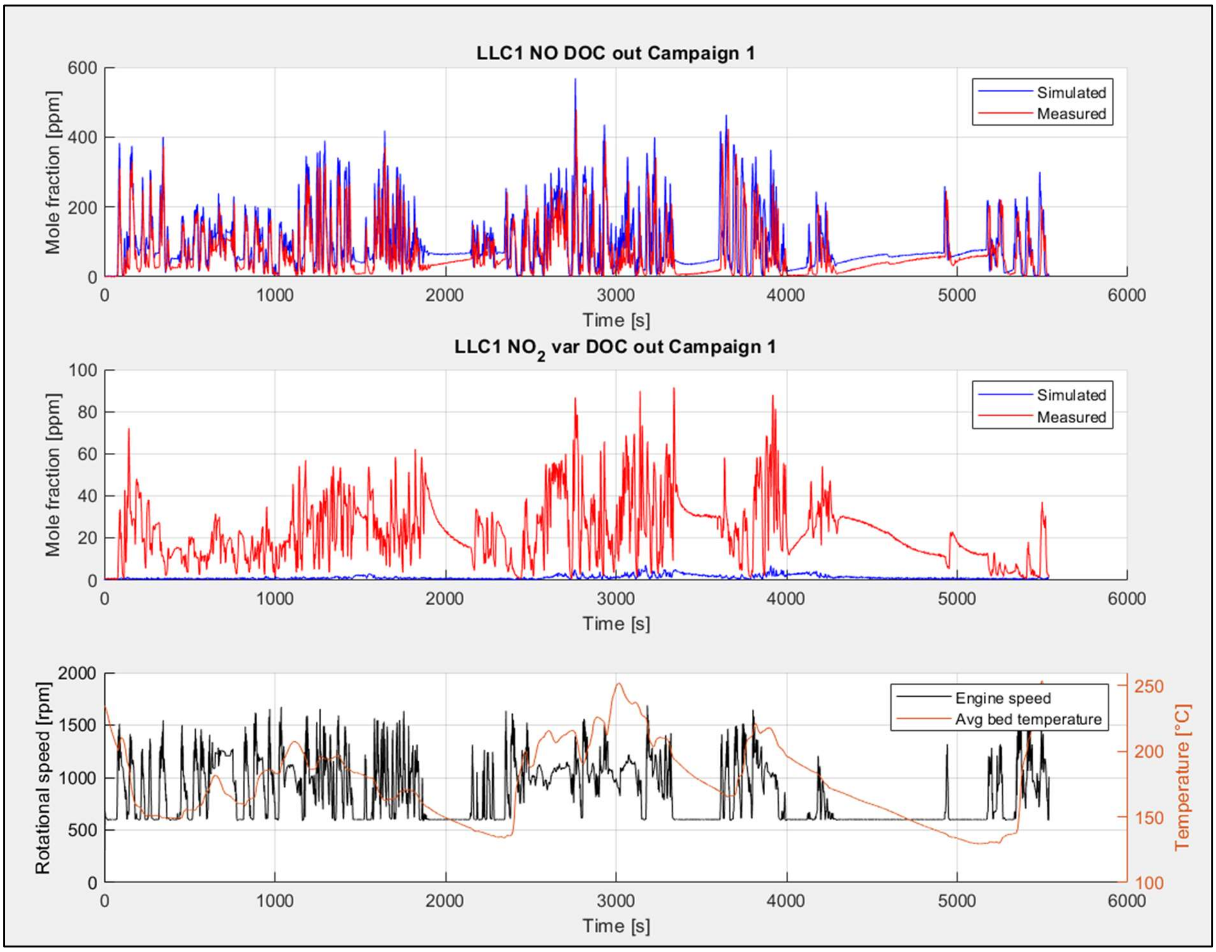
LLC1 NO DOC out Campaign 1
Mole fraction [ppm]
0
200
400
600
Time [s]
0
1000
2000
3000
4000
5000
6000
Simulated
Measured
LLC1 $NO_2$ var DOC out Campaign 1
Mole fraction [ppm]
0
20
40
60
80
100
Time [s]
Simulated
Measured
Rotational speed [rpm]
0
500
1000
1500
2000
Temperature [°C]
100
150
200
250
Time [s]
Engine speed
Avg bed temperature

# Nomenclature

| | |
|---|---|
| A | Face area [m$^2$] |
| $A_{ai}, E_{ai}$ | Inhibition terms |
| $A_i$ | Pre-exponent multiplier |
| $a_j$ | Active site density for reaction j [mol-site/m$^3$] |
| $c_r$ | Total concentration at 1 atm [mol/m$^3$] |
| $c_{s,i}$ | Molar concertation of trace species at catalyst surface [mol/m$^3$] |
| $D_{i,m}$ | Binary diffusion coefficient of species i in the mixture [m$^2$/s] |
| $D_{i,m}$ | Hydraulic diameter [m] |
| $E_i$ | Activation energy |
| $G_i$ | Inhibition function of species i |
| $K_i$ | Adsorption constant for species i [m$^3$/mol] |
| $K_{eq}$ | Equilibrium constant for NO oxidation |
| $k_i$ | Rate constates [varies] |
| $k_{m,i}$ | Mass transfer coefficient for species i [mol/(m$^2$ s)] |
| $\dot{m}$ | Mass flow rate [kg/s] |
| $M_i$ | Molar mass of the species I [kg/mol] |
| m | Stoichiometric coefficient |
| n | Stoichiometric coefficient |
| R | Gas constant [J/kg K] |
| $r_j$ | Rate of reaction j [mol/(mol-site s)] |
| $S$ | Surface area per volume reactor [1/m] |
| $s_{ij}$ | Stoichiometric coefficient of species i in reaction j |
| T | Temperature [K] |
| Sh | Sherwood number for mass transfer |
| $x_{g,i}$ | Mass fraction of species i in bulk gas phase |
| $x_{s,i}$ | Mass fraction of species i in gas at catalytic surface |
| $y_i$ | Mole fraction of species i |
| z | Axial position [m] |
| $\rho_{gas}$ | Average gas density |
| $\Sigma_i$ | Diffusion volume of species i |